Alma Mater Studiorum-Università di Bologna

SCUOLA DI SCIENZE

Dipartimento di Chimica Industriale "Toso Montanari"

Corso di Laurea Magistrale in

Chimica Industriale

Classe LM-71 - Scienze e Tecnologie della Chimica Industriale

Synthesis of Heteroleptic Zinc Complexes for *imaging* in living cells

Tesi di laurea sperimentale

CANDIDATO

Roberta Tabone

RELATORE

Prof.ssa Letizia Sambri

CORRELATORE

Dr.ssa Claudia Bizzarri

Anno Accademico 2018-2019

Acknowledgments

The achievements obtained in this thesis and the drafting of the work itself would not have been the same without the precious help of Dr. Bizzarri, my research supervisor, although this mere definition does not quite do justice to the relevance of the role she played.

Thanks to her patient dedication, motivation, remarks and constructive criticisms, she proved to be a phenomenal guide, playing a considerable impact on my academic career, as well as an excellent example at a personal level. Through the humbleness and the untamed enthusiast so ever-present in her work, she encouraged me to always strive for the better and to believe in myself, showing me how hard work and determination are key to success. I could not have wished for a greatest mentor.

I would also like to thank Prof. Letizia Sambri for her advice and guidance during the time of my internship and my thesis, and Prof. Stefan Bräse for hosting me in his research group.

Last but not least, I would like to thank my family and my friends, for supporting and helping me during my studies.

Table of contents

1-Introduction 1

1.1-Cancer: an overview 1

1.1.1-Cancer: prevention 3

1.1.2- Cancer: importance of early diagnosis 3

1.2- Imaging 4

1.2.1- Imaging strategies 5

1.2.2- Optical imaging 7

1.3- Fluorescence imaging 7

1.3.1- Intrinsic limitations 11

1.3.1.1-Light interaction with tissue 11

1.3.2-Near-infrared advantages 12

1.4-Near-infrared dyes 13

1.4.1-Cyanine dyes 14

1.4.2-Squaraine derivatives 15

1.4.3-Phthalocyanines and porphyrin derivatives 16

1.4.4-BODIPY 17

1.5-Dipyrrins: overall backdrop 18

1.5.1-Dipyrrins: structure 19

1.5.2-Dipyrrins: metal complexes 19

1.6-Heteroleptic bis(dipyrrinato)metal complexes 21

1.7- Bis(dipyrrinato) Zinc (II) complexes 24

1.8- State of the art and previous work 24

2- Aim of the thesis 26

3-Results and Discussion 27

3.1- Functionalization of dipyrrins 29

3.1.1-Synthesis of plain dipyrrins 30

3.1.1.1-Functionalization in Meso 30

3.1.1.2 Functionalization in position 2 and 8 32

3.2- Synthesis of π-expanded dipyrrins 33

3.3- Synthesis of dipyrrins with water soluble groups. 35
3.3.1-Synthesis of dipyrrins with glycolic chain 35
*3.3.1.1 Synthesis of aldehyde **2f*** 37
3.3.2-Synthesis of dipyrrins with sulfonate group. 38
3.3.2.2 Synthesis of substituted alkynes. 40
*3.3.2.2.1-Alkyne-functionalized dipyrrins **3b-c*** 40
3.3.2.2.2 Synthesis of 4-(phenylethynyl)-benzaldehyde 43
3.4- Synthesis of Zn-complexes. 45
3.4.1- Synthesis of heteroleptic complexes 46
*3.4.2- Synthesis of homoleptic complexes **6b*** 47
3.5-Photophysics 49
3.5.1-Previous work 49
*3.5.2-Excitation and emission spectra of the new complexes **6a-f*** 52
3.6-Biocompatibility 58
3.6.1- In Vitro Cytotoxicity and cell Viability assays 58
3.6.2- MTT assay: general framework 60
*3.6.3- MTT assay of complexes **9a-d*** 62
*3.6.4- MTT assay of complexes **6a-f*** 64

4- Conclusion and outlook 67

5-Experimental section 68
4.1-Materials and Methods 68
4.2 -Commercially available starting materials 71
*4.2.1- 1H-Pyrrole **(1)*** 71
4.2.2- Aldehydes 71
4.3 -Synthesis of precursors and intermediates. 73
4.4- Synthesis of plain dipyrrins. 79
4.5-Synthesis of π-expanded dipyrrins. 83
4.6- Synthesis of dipyrrins with glycolic chain 85
4.7- Synthesis of Zn-complexes 87

6-Bibliography 92

- List of Abbreviations

DNA	DeoxyriboNucleicAcid
IARC	Internation Agency Research on Cancer
PET	Positron Emission Tomography
SPECT	Single Photon Emission Tomography
MRI	Magnetic Resonance Imaging
IR	Infrared
NIR	Near-infrared
UV	Ultra-Violet
Vis	Visible Light
Hb	Haemoglobin
HbO_2	Oxyhaemoglobin
PS	Photosensitizers
PDT	Photodynamic Therapy
BODIPY	4,4'-difluoro-4''-bora-3a,4'''a-diaza-*s*-indacene
HOMO	Highest occupied molecular orbital
LUMO	Lowest unoccupied molecular orbital
DCM	Dichloromethane
DMF	*N, N*-dimethylformamide
MeOH	Methanol
CY	Cyclohexane
°C	Grad Celsius
g	Gramm
h	Hour
L	Liter

M	Molarities in mol/L
m/z	Masse to charge ratio
mg	Milligramm
min	Minute
mL	Milliliter
mmol	Millimol
mol	Mol
MS	Mass spectroscopy
HRMS	High Resolution Mass Spectroscopy
MALDI	Matrix-Assisted Laser Desorption/Ionization
m/z	Masse to charge ratio
λ	Wavelenght
Φ	Photoluminescence Quantum Yield
τ	Luminescence Lifetime
R.T.	Room temperature (25 °C)
S_0	Singlet ground state
TLC	Thin layer chromatography
Rac	Racemic
NMR	Nuclear Magnetic Resonance
S_N	Substitution Nucleophilic
MTT	*(3-(4,5-dimethylthiazol-2-yl)-2'-5'-diphenyltetrazolium bromide*

1-Introduction

1.1-Cancer: an overview

A neoplasm or a tumour is a mass of tissue that grows exponentially and differently from normal tissue. The malignant manifestation of a tumour is called “cancer”, from the Greek *καρκινος*, term coined by Hippocrates.

The prevailing theory formulated in the middle of the last century interprets cancer as a set of about 200 diseases characterized by abnormal cell growth (see Figure 1), released by the body's normal control mechanisms. The transformation process of a normal cell into a neoplastic cell takes place through various stages with accumulation of genetic, functional and morphological anomalies.

The molecular structure of the tumours, in its constant variations, represents the research field, in which the greatest hopes for future clinical therapies are placed. Proliferation (cellular division) is a physiological process that takes place in almost all tissues and in countless circumstances: normally there is a balance between proliferation and programmed cell death (apoptosis). The mutations in the DNA that lead to cancer lead to destruction of these orderly processes: this results in uncontrolled cell division and tumour formation. The cancer event requires more than one mutation against different classes of genes, in particular in those genes that control cell division, cell death and repair processes of the DNA.

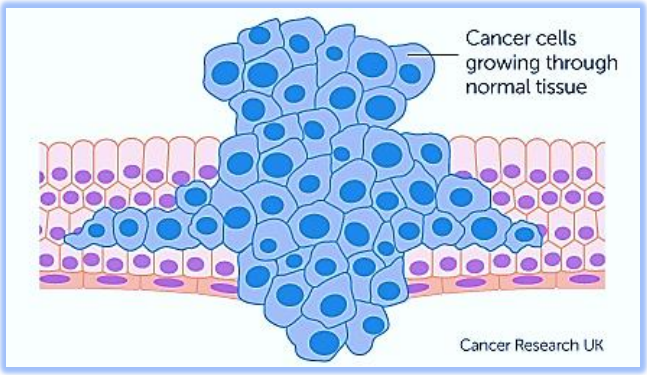

Figure 1: Growth of cancer cells across normal tissues[1]

Our body is able, through processes of repair and activation of the immune system, to block the processes of transformation but, when this capacity is lost, the cell is transformed, through various stages, into a cell tumour.[2]

Cancer is the second leading cause of death in both more and less economically developed countries (after ischaemic death disease and stroke). Based on data from the Global Cancer Observatory (GLOBOCAN) 2018,[3] produced by the IARC,[4] it was estimated about 18 million of new cancer and 9.6 million death in 2018.

A tumour can affect most any part of the body and has many atomic and molecular subtypes that each requires specific management strategies. Lung, breast, colorectum, prostate, stomach, oesophagus and liver cancer are the most common types of cancer in men and women[3] (Figure 2).

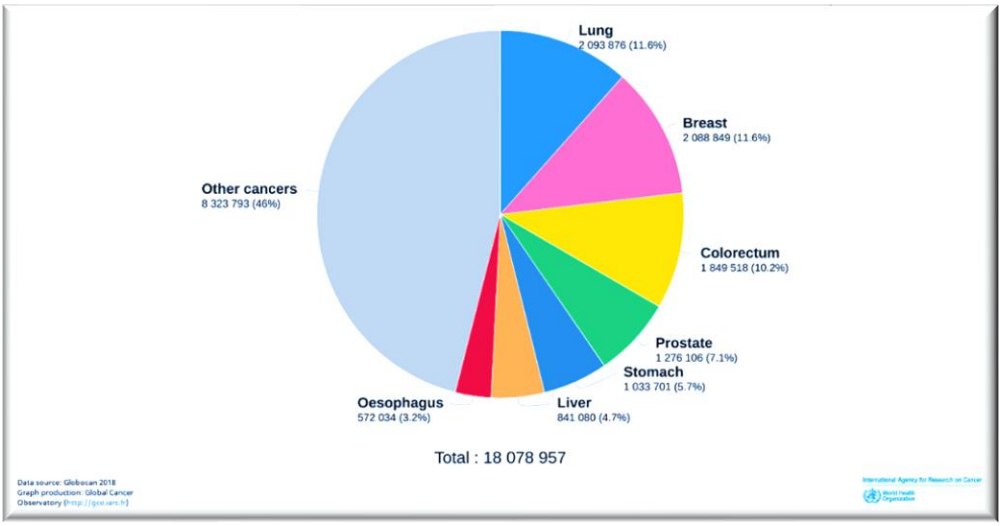

***Figure 2**: Estimated worldwide number of new cancer cases in 2018 (all cancers, both sexes and all ages)* [3].

The burden is expected to grow worldwide, due to the growth and aging of the population, particularly in less developed countries, in which about 82 % of the world's population resides. Based on projections, devised by the "World Health Organization", cancer deaths will continue to rise with an estimated 11.4 million dying in 2040.[5]

1.1.1-Cancer: prevention

The occurrence of cancer is growing because of the increasing prevalence of established risk factors such as smoking, overweight, physical inactivity and changing reproductive patterns associated with urbanization and economic development.

As stated by GLOBOCAN, between 30-50 % of all cancer cases are preventable. National policies and programmes should be implemented to raise awareness, to reduce exposure to cancer risk factors and to ensure that people are provided with the information and support they need to adopt healthy lifestyle. Prevention, in fact, offers the most cost-effective long-term strategy for the control of cancer.

1.1.2- Cancer: importance of early diagnosis

A prompt cancer diagnosis generally increases the chances for successful treatment by focusing on detecting symptomatic patients in a timely manner. Often, however, especially in particularly settings of lower resources and vulnerable populations, there is a delay in accessing cancer care and this results in a late-stage identification of tumour. The consequences of delayed or inaccessible cancer treatment are the following: a) lower probability of survival, b) greater treatment morbidity and c) higher costs of care, resulting in unavoidable deaths and cancer disability.

Early diagnosis improves cancer outcomes by aiding at the earliest possible stage and it is therefore an important public health strategy in all settings.

Screening, instead, is defined as the presumptive identification of unrecognized disease in an apparently healthy asymptomatic population by means of tests, examinations or other procedures that can be applied rapidly and easily to the target population.

A deadly disease, so overbearing and dreaded, could be reduced by implementing evidence- based strategies for prevention and timely detection.

It is therefore imperative to improve cancer diagnostic methods in early or even pre-syndrome stage.

1.2- Imaging

As early detection is crucial in order to improve survival rates and reduces the morbidity associated with radical resections due to the late presentation of the cancer, many tools have been developed.

The Society of Nuclear Medicine (SNM) and its Molecular Imaging Centre of Excellence (MICoE) have adopted an official definition of molecular imaging:[6] ‘‘Medical imaging is the visualization, characterization, and measurement of biological processes at the molecular and cellular levels in humans and other living systems”.

Medical imaging consists of processes of creating visual representations of the inside of a body for clinical analysis and medical intervention, as well as the visual representation of the function of certain organs or tissues (physiology). It reveals the internal structures hidden by the skin and bones, as well as diagnose and treat diseases, also creating a database of normal anatomy and physiology to allow the identification of anomalies.

Traditionally, the primary role of medical imaging has been to help medical diagnosis through the visualization of the presence, location, and extent of pathologies, because molecular imaging techniques are capable of providing functional information at the cellular level.[6]

This powerful diagnostic instrument is often perceived to designate the set of techniques that produce non-invasively images of the internal appearance of the body and it can be seen as the solution to inverse mathematical problems: this means that the cause (the properties of living tissue) is deduced from the effect (the observed signal).
The term "non-invasive" is used to indicate a procedure in which no instrument is introduced into a patient's body, as in the case of most of the used imaging techniques.

While anatomical imaging plays a major role in medical imaging for diagnosis, surgical guidance/follow-up and treatment monitoring, the rapidly evolving field of molecular imaging promises improvements in specificity and quantitation screening and early diagnosis, focused and personalized therapy.[7]

The main advantage of *in vivo* molecular imaging is the ability to characterize diseased tissues without invasive biopsies or surgical procedures. In addition, it can be used to measure the response to therapy.

1.2.1- Imaging strategies

Several diagnostic imaging technologies developed over the past three decades have had a profound impact on clinical medicine. Although scientific imaging systems are primarily used for displaying anatomical, physiological and metabolic parameters, experimental animal systems are additionally being developed to image at cellular and molecular level *in vivo.*[8]

The existing different diagnostic imaging modalities, such as: computed tomography (CT), positron emission tomography (PET), single photon emission computed tomography (SPECT), magnetic resonance imaging (MRI), ultrasound (US) and optical imaging (OI), differ in five main aspects:[9]

1. Resolution
2. Depth penetration
3. Energy expanded for image generation
4. Availability of injectable
5. Existence of biocompatible molecular probes and respective detection threshold

The energy source, in particular, stands out in three main typologies: ionizing and non-ionizing radiations and RM-based (magnetic field and radiofrequencies).

In Table 1 are summarized the major advantage of the abovementioned techniques, categorized by the energy source that provide the imaging technology.

Table 1:*Different molecular imaging modalities: advantages and disadvantages*

Energy source imaging technology	***Favourable properties***	***Drawbacks***	***Probe typology***
• *Nuclear (ionizing radiations)*			
-PET	*High sensitivity (~10^{-13}mol/L)* *Metabolic-dynamic information*	*Low-spatial resolution (1÷2mm)*	*Positron-emitting radionuclides*
-SPECT	*High sensitivity (~10^{-14} mol/L)* *Metabolic-dynamic information*	*Low-spatial resolution (1÷2mm)*	*γ-emitting radionuclides*
• *RM-based (magnetic field +radiofrequencies)*	*High spatial resolution (50 μm)* *Metabolic-dynamic information*	*Low sensitivity*	*Free MR, paramagnetic or superparamagnetic contrast materials*
• *Optical (non-ionizing radiations)*	*Capability of differentiating a variety probe*	*Low tissue penetration improved by resort to NIR*	*Bioluminescent or fluorescent materials*

1.2.2- Optical imaging

Optical imaging requires the use of light photons to obtain detailed images of organs and tissues as well as smaller structures, including cells and molecules.[10] Since the energy source, which includes visible, ultraviolet and infrared light, are non-ionizing radiations, this imaging technique reduces significantly patient exposure to harmful radiations without causing the damage that can occur with ionizing radiation used in some other imaging techniques. For this reason, optical imaging can be used for lengthy and repeated procedures over time to monitor the progression of disease or the results of treatment. The aforementioned technique is particularly useful for visualizing soft tissues that can be easily distinguished from one another due to the wide variety of ways different tissues absorb and scatter light. Because it can obtain images of structures across a wide range of sizes and types, optical imaging can be combined with other imaging techniques, such as MRI or X-rays, to provide enhanced information. Moreover, optical imaging takes advantage of the various colours of light in order to see and measure many different properties of an organ or tissue at the same time. Other imaging techniques are limited to just one or two measurements.

A plethora of optical-based molecular imaging techniques are used in preclinical research for evaluating molecular targets of contrast agents and/or of therapeutics as well as characterizing, such as: *Endoscopy, Optical Coherence Tomography (OCT), Photoacoustic Imaging, Raman Spectroscopy, Super- resolution Microscopy, Terahertz Tomography and Diffuse Optical Tomography*.

The main disadvantage of Optical Imaging is the lack of penetration dept, especially at visible wavelengths, depending on tissue related light absorption and scattering

1.3- Fluorescence imaging

Ergo, optical imaging techniques are emerging as promising non-invasive, real-time and high-resolution modalities for the cancer detection. Among those, fluorescence imaging has been appreciated in biological sciences and immense attention has been dedicated to its development, owing to its extraordinary contrast and specificity (See Figure 3). Nevertheless, the information derived from this type of systems can be

regarded as an important complement to microscopy studies performed on cell cultures and tissue slices because it provides informations about specific biological processes in fully integrated living systems.[11]

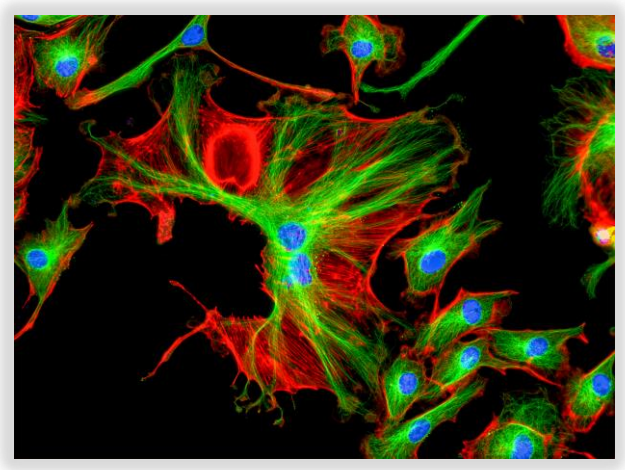

***Figure 3**: Fluorescence Microscope Image of Bovine Pulmonary Artery Endothelial Cells.*[12]

Policard first reported in 1924 that the necrotic centre of an experimental rat sarcoma showed a red fluorescence from endogenous porphyrins, when excited by ultraviolet light[13]. From this starting point, many new applications have emerged with different varieties of fluorophores and fluorescence proteins.[14]

Fluorescence is a type of luminescence that occurs in chemical systems.

When a molecule absorbs a photon (blue arrow in Figure 4), the singlet ground state (S_0) is promoted to a singlet excited state and then, several processes occur with varying probabilities,[15] illustrated in Jablonski diagram (Figure 4).

The first thing happens is relaxation to the lowest vibrionic energy level of the first excited state (S_1) through internal conversion or vibrionic relaxation pathways (black wavy line in Figure 4). The excess energy is converted into heat. Being the spin of electron still paired with the ground state, the excited molecule may return to ground state with concomitant emission of a photon. This process is called fluorescence (green arrow in Figure 4) and it is a spin-allowed process, therefore it is quick

(nanosecond timescale). The emitted photon is generally lower in energy, in respect to the absorbed photons, which corresponds to a longer wavelength. Thus, the emission spectrum appears often as the mirror image of the absorption spectrum.[11,15] At the same time, some electrons in the excited singlet state can move to a lower energy excited triplet state via intersystem crossing. The latter event ultimately results in emitting a photon through phosphorescence (red arrow in Figure 4).

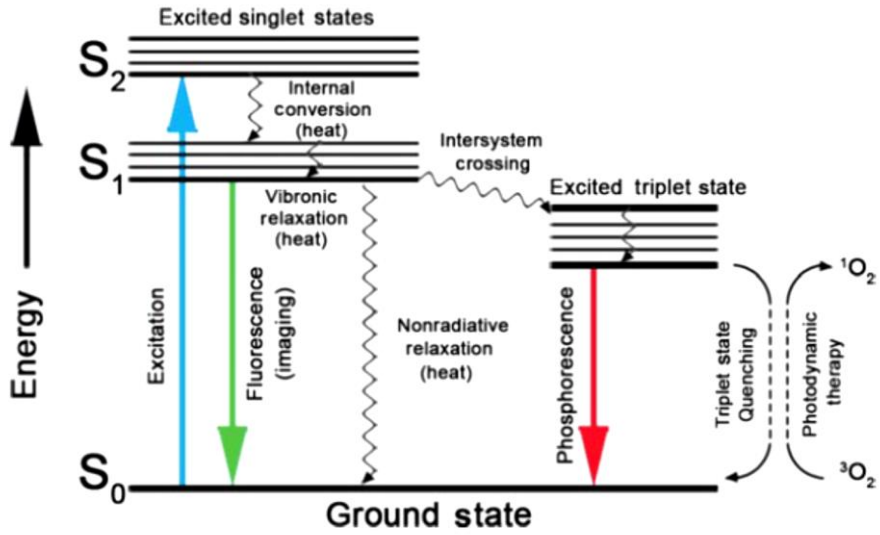

***Figure 4**: Jablonski diagram: energy level diagram for a photoluminescence system*[16].

Moreover, as shown in Figure 4, triplet oxygen, the ground state of oxygen molecule, is a very effective quencher for fluorophores in the excited triplet state. For this reason, it is able to be excited to reactive singlet state (right-hand dotted line in Figure 4), producing phototoxic effect to living cells. This, is the guiding principle used in photothermal and photodynamic therapy.[17]

Figure 5 illustrates the salient differences between *in vitro*, *ex vivo* and *in vivo* fluorescence from biological applications relating in the specific to brain imaging.[18] High resolution, high sensitivity and high specificity images can be rendered down to sub-micron resolution in vitro study cellular and sub-cellular molecular process.

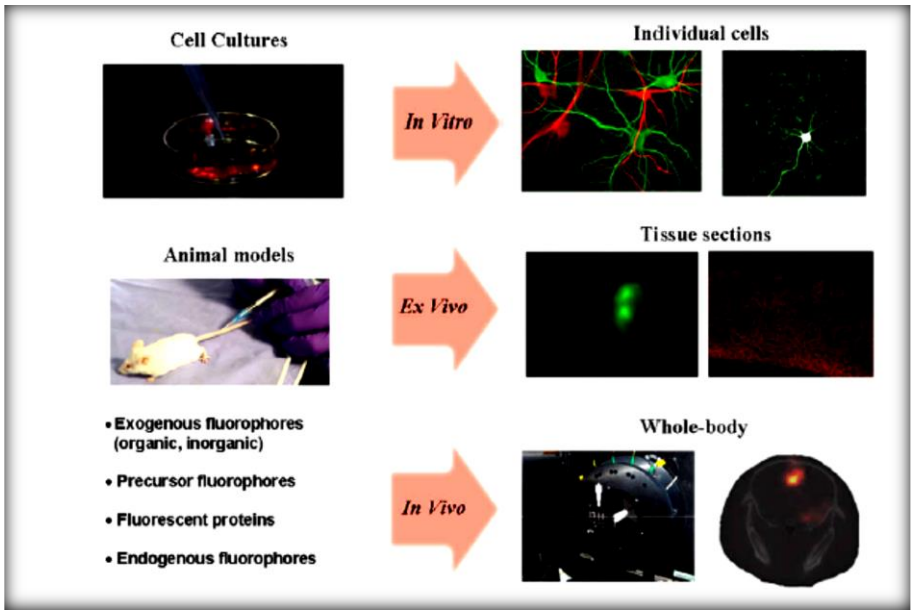

Figure 5: *Illustration showing different fluorescence imaging paths used in the scope of pre-clinical study.*[19]

The top-right part of the figure shows two-photon microscopy images of mouse hippocampal neuron and glial cells transfected with fluorophore. Animal models can be used for *ex vivo* studies of tissue slice as well as for whole-body *in vivo* studies. *Ex-vivo* slices shown (middle-right images) correspond to brain tissue with glioma cells highlighted with fluorescence from the fluorogenic probe. The *in vivo* whole-body image (lower-right in the figure) corresponds to a fluorescence tomography image associated with porphyrin contrast from a brain tumour model.

Though in essence the underlying technological and biological principles appear to be the same, imaging in each of these regimes imposes unique challenges requiring significantly different approaches to system design.

In this work, the focus has been on *"in vitro"* imaging and it is extremely important to realize that there are intrinsic limits on the biological information that can be extracted from even the most carefully designed *in vitro* imaging instrument.

1.3.1- Intrinsic limitations

Although the potential use of *in vitro* fluorescence imaging in biological studies is incredibly high, there are inherent drawbacks. In part these restrictions are due to the interaction of light with microscopic components of tissue. In addition, it is challenging to guarantee that biomarkers of interest have a detectable level of optical contrast, which is generated specifically enough to deliver useful objective information.[20]

1.3.1.1-Light interaction with tissue

Even if the basic principle behind fluorescence imaging is similar to that used in fluorescence microscopy techniques, when living body are examined, the desired information is typically associated with biochemical events occurring deep within the tissue. Considering body tissues as a bulk medium, light propagation through such a medium implicates processes of refractions, reflection, absorption and scattering.[21] Scattering of light in tissue has the most pronounced effect on light intensity and directionality, this implies that photons, being part of the detected signals, have undergone multiple scattering events in the process of irradiance of the excitation light into the body and radiance of the emission out the body.

Besides scattering, absorption of light quanta is most relevant for the loss of light intensity with the penetration depth. Microscopic components within tissue, from small molecules (like sugars, fatty acids, amino acids, nucleotides, ions, water) and macromolecules (proteins, phospholipids, RNA, DNA, polysaccharides) to larger structures such as organelles and cell membranes, altogether absorb light in the ultraviolet (UV) through the visible (VIS) wavelength range. Absorption by tissue components in this wavelength range limits effective light penetration to a few hundred microns. However, significantly larger depths can be probed using light in the far-red or near-infrared wavelength range.

1.3.2-Near-infrared advantages

As shown in Figure 6, haemoglobin (Hb), oxyhaemoglobin (HbO_2) and water, the major absorbers of visible and infrared light, have their lowest absorption coefficient in the near-infrared (abbreviated as NIR) region around 670-900 nm.

Since the absorption of these chromophores is at least one order of magnitude lower than in the VIS part of the spectrum, this potentially allows detectable signals to be measured through several centimetres of tissue.

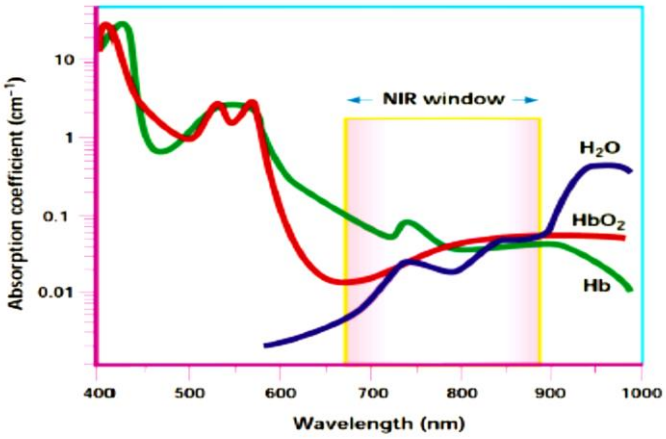

***Figure 6**: NIR window generally suited for in vivo imaging because of minimal light absorption by haemoglobin (<650 nm) and water (>900 nm).*[22]

In the NIR part of the electromagnetic spectrum, elastic scattering of photons dominates over absorption, making multiple scattering the main mechanism for light propagation.[11]

This phenomenon is so significant because the average photons have an equal probability for travelling in any direction after having penetrated less than 1 mm of tissue and in this way the light transport in tissue can be modelled as a simple isotropic diffusive process with reasonable precision.

In the fluorescence process, scattering acts on both the excitation light and the fluorescence emission travelling back to the tissue detection area. This introduces an intrinsic blurring in fluorescence images, an aftermath that is amplified for fluorescent targets that are further away from the illumination and detection area. Another

important consequence of scattering is that it amplifies the effect of the wavelength-varying absorption spectrum of tissue chromophores, causing the shape and peak position of detected fluorescence spectra to vary depending on the path lengths traversed by light in tissue.[23]

Whenever tissue absorbs light, there is a chance that fluorescent light will be emitted. There is in fact a relationship of excitation and emission wavelengths to tissue autofluorescence. It should be considered the presence of a wide variety molecules present in living tissue that can act as a biochemical sources of autofluorescence,[24,25] such as tryptophan, NADH, collagen, elastin and flavins. Because the main excitation peaks for the natural fluorophores are usually in the visible part of the spectrum, their impact on far-red and NIR fluorescence imaging is often negligible. Nonetheless, fluorescence signs from the molecular probe of interest can still be corrupted especially when the probe is weakly fluorescing or sparsely distributed. The non-specific signal from autofluorescence can either mask delivered signals or be erroneously attributed, leading to an inability to discriminate the tissue of interest or to a severe overestimation of the probe's fluorescence activity.

It has been demonstrated that autofluorescence from biological fluorophores can interfere strongly with probes incorporating short wavelengths emitters, but do not strongly hinder in the NIR.[26]

1.4-Near-infrared dyes

Satisfactory cancer NIR fluorescence imaging requires excellent NIR probes with superior chemical and photophysical properties. An ideal NIR probe must function in the NIR spectral range, with large Stoke shifts for minimum interference between absorption and emission spectra, high molar absorption coefficient and quantum yield for intense fluorescence, sufficient chemical and photostability in solvents, buffers or biological detection, good water solubility to avoid dye aggregation in aqueous environment and last but not least, low toxicity. Additionally, a qualified NIR probe should have suitable chemical functionality allowing available conjugation with specific ligands for targeting purpose.

Current NIR probes include two categories: inorganic and organic molecule. Inorganic NIR contrast molecules mainly associated with quantum dots (QDs) and other nanoparticles.[27–30]

Compared to inorganic probes, organic NIR fluorescent dyes are very attractive candidate for imaging because they exhibit feasible conjugation with various kinds of specific molecules such as chemical small molecules, amino acids, proteins, etc. Moreover, owing to the affordability for covalent or non-covalent combination with cancer-targeted organic and biological molecules, NIR dyes are intensely sought as very promising approach to image cancer specifically and sensitively.[31]

Organic dyes which are active in the NIR region have attracted ongoing attention in biomedical applications although a few have received approval from the *Food and Drug Administration*[32] *(FDA).* Advantages include minimal interfering absorption and fluorescence from biological samples, inexpensive laser diode excitation, reduced scattering and enhanced tissue penetration depth. However, there are only a few NIR dyes that are readily available due to the limitations of conventional dyes, such as poor hydrophilicity and photo-stability, low quantum yield, insufficient stability and low detection sensitivity in biological system, etc.

Significant progress has been made on the recent development of NIR dyes, including cyanine dyes, squaraine, phthalocyanines, porphyrin derivatives and 4,4'-difluoro-4''-bora-3a,4'''a-diaza-*s*-indacene molecule, from here on abbreviated as BODIPY, with highly improved chemical and photostability, high fluorescence intensity and long fluorescent time.

1.4.1-Cyanine dyes

Cyanine dyes, also called as polymethine cyanine dyes, are small organic molecules with two aromatic nitrogen-containing heterocycles linked by a polymethine bridge (see Figure 7).

Since their discovery, these fluorescent compounds have found numerous technical applications, including their use as photographic sensitizers,[33] nonlinear optical materials[34] and fluorescent probes for biomolecular imaging.[35–37]

Indocyanine Green (ICG), for instance, has been approved by FDA in 1985 for evaluating blood flow and clearance.[38]

Nowadays, some cyanine dyes are among most important NIR fluorescent dyes with high molar absorptivity coefficient (often reaching 200,000 mol^{-1} cm^{-1} L), excitation bands in the range 600-900 nm and fluorescence quantum yields.[19,39]

However, many cyanine dyes suffer from poor photostability, low quantum yields, undesired aggregation and mild fluorescence in aqueous solution. With the continues developments of these compounds, significant progress has been made to overcome these limitations.[36,40–42,43]

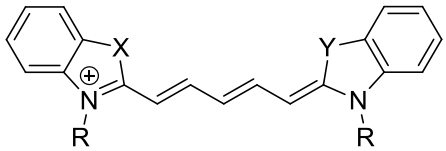

Abs max (nm) >700
Emis max(nm)>800
ε ($mol^{-1}cm^{-1}L$)>200,000

X,Y=O,S,$C(CH_3)_2$ or $C=CH_2$
n=0-4
R= $(CH_2)_xSO_3^-$

***Figure 7**: Basic structure of Cyanine Dyes and relatives photophysical features*

1.4.2-Squaraine derivatives

Squaraine, often called Squarylium dyes, consist of an oxocyclobutenolate core with aromatic or heterocyclic components at both ends of the molecule (Figure 8).

These compounds exhibit excellent physical-chemical properties, such as extremely intense absorption bands, high molar absorptivity and good photoconductivity.[44–46] Nevertheless, due to their large and planar hydrophobic π-conjugated structures, increasing the water solubility of conventional squaraines remains an important challenge. There are only very few NIR squaraines that emit at wavelengths above 800 nm in aqueous solution.[47–49]

With the aim of improving hydrophilicity, Suzuki *et al.,*[50] Nakazumi *et al.,*[51] Gassensmith *et al.,*[52] have introduced a water-soluble moiety into a squaraine framework.

Because of their photophysical characteristics, both in their free form and after linkage to proteins, the Squarylium dyes are a subject of particular interest and represent a potential versatile fluorescent scaffold for constructing various types of highly stable near-IR imaging probes.

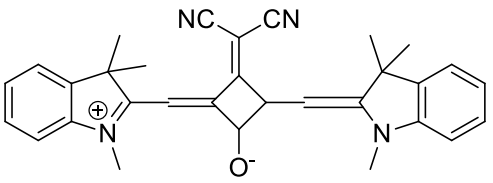

Abs max (nm): 650-800
Emis max(nm) >800
ε ($mol^{-1}cm^{-1}L$) >100,000-300,000

Figure 8*: Basic structure of Squaraine derivatives and relatives photophysical features*

1.4.3-Phthalocyanines and porphyrin derivatives

Phthalocyanines are two-dimensional 18π-electron aromatic porphyrin derivatives consisting of four bridged benzo-fused pyrrole subunits linked together through nitrogen atoms (Figure 9). The basic chromophore of phthalocyanine is (4n + 2) π-electrons in its 16-centre ring moiety, rendering π electrons strongly delocalized around their perimeter. For this reason, these compounds are thermally and chemically stable and can support intense electromagnetic radiation.

Interestingly, the two hydrogen atoms of the central cavity can be replaced by several central metals and a variety of substituents can be incorporated,[31] both at the periphery of the macrocycle and at the axial positions, allowing finetuning of the physical properties. Therefore, these unique properties make phthalocyanines and porphyrin derivatives well-known not only for dyes but also for molecular materials used in electronics,[53] optoelectronics,[54] and biomedicine,[16,55]

Despite the long π-π electronic conjugation provides these dyes high photostability and strong absorption bands, most of them show absorption and emission maxima

below 700 nm. Atshuiro *et al.*[56] have demonstrated that the addition of benzene groups or multiple electron-donating substituents shifts the absorption bands from the visible to the NIR spectral region.

Likewise, imaging applications as biosensors phthalocyanines and porphyrin derivatives have also been known as photosensitizers (PS) for photodynamic therapy (PDT) of cancers,[57] since this kind of dyes can be taken up in malignant and dysplastic tissues and generate singlet oxygen when the tumour area is exposed to light.[16,17,58,59]

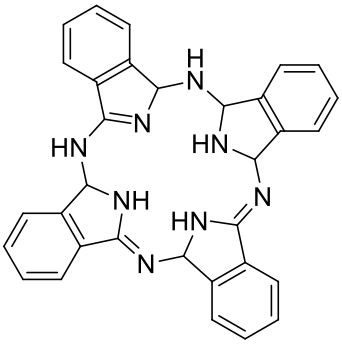

Abs max (nm): 650-800
Emis max(nm):700-1000
ε ($mol^{-1}cm^{-1}L$)>100,000

***Figure 9**: Basic structure of phthalocyanine and relatives photophysical features*

1.4.4-BODIPY

Fluorophores based on the 4,4'-difluoro-4''-bora-3a,4'''a-diaza-s-indacene molecules are commonly designated as BODIPY fluorophores (Figure 10). BODIPY dyes were first discovered in 1968 by Triebs and Kreuzer.[60] Even in this pivotal work the fluorescence of this type of complexes was recognized as their most important property.

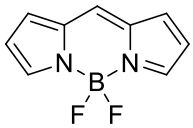

Abs max (nm): 650-800
Emissmax(nm) >700
ε($mol^{-1}cm^{-1}L$)>200,000

***Figure 10**: Basic structure of BODIPY and relatives photophysical features*

These dyes tend to be strongly UV-Vis absorbing molecules, emitting relatively sharp fluorescence with high quantum yield and excellent thermal and photostability.[61] These attractive characteristics have led these compounds to become highly popular for application as laser dyes, molecular photonic wires, chemosensors, fluorescent switches, electron transfer reagents and bioprobes.[62–69]

Most BODIPY dyes emit from yellow to deep-red emission with relatively short fluorescence emission maxima (around 500 nm) and low extinction coefficients (around 80,000 M^{-1} cm^{-1} L). The increasing attention paid to these compounds is due to their useful and tuneable photophysical properties. Thus, the latter can be tight by modification of the pyrrole core, leading to potential frameworks suitable for different applications. [67,68]

Different approach for shifting absorption and emission spectrum to NIR region have been attempted in recent years. For example, Donoru and colleagues,[72] have synthesised BODIPY polymeric and copolymeric at the meso position cores which was in the near-infrared emission. Studies have shown that modification of the pyrrole core can obtain BODIPY-based probes with high molar absorption coefficient (ε_{max}>8.8) and high fluorescence quantum yield (Φ~1.0) even in water. [73–75]

Moreover, these fluorophores present an interesting and rich functionalization chemistry but, at the same time, it is very difficult introduce moieties in the BODIPY core because of the lack of straightforward methods.[67]

BODIPY are nothing more than boron-difluoride complexes of dipyrrins. But the intriguing properties of 4,4'-difluoro-4''-bora-3a,4'''a-diaza-*s*-indacene molecules have made them the most commercially important examples of dipyrrinato complexes.

1.5-Dipyrrins: overall backdrop

Studies in the area of dipyrrin chemistry have been mostly geared towards the synthesis of porphyrins. This is due to the historical application of dipyrrins: its chemistry dates to the time of Hans Fischer[76] who employed these molecules as precursors to naturally porphyrin. Formation of charge-neutral chelated complexes with a variety of metal cations has been the source of most new avenues of dipyrrin research.

1.5.1-Dipyrrins: structure

Dipyrrins are formally composed of a pyrrole ring and an azafulvene attached to each other at the α position: a dipyrromethane with one more degree of unsaturation (Figure 11). This added degree of unsaturation affords the delocalization of the electron density across the dipyrrins such that structural data shows that the two pyrrolyl units are equivalent when they are identically substituted.

Guidelines for the nomenclature to be used for dipyrrins, and many other oligopyrrolic molecules, were established by IUPAC in 1987 [77] that also recommended numbering scheme for dipyrrin nomenclature as shown in (Figure 11).

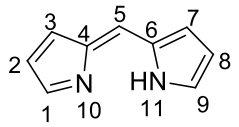

***Figure 11**: Numbering system for dipyrrins*

Publications on the subjects of dipyrrin research date back nearly a century and in this time these molecules have been known by many names: dipyrromethenes, azadipyrromethenes, pyrromethenes, dipyrrylmethenes, diaza-*s*-indacene.

It is occasionally more illustrative to refer to the 1- and 9- positions as the *α* positions, following from historic pyrrole nomenclature, and the 5-position as the *meso* position, a term borrowed from the naming of porphyrins. In fact, the electronic and geometric specifications of dipyrrins can reflect the similarity as hemi-porphyrin.

1.5.2-Dipyrrins: metal complexes

Dipyrrins are known to form isolable stable complexes with a variety of metal ions.[78] Upon deprotonation, the monoanionic dipyrrinato ligand form neutral homoleptic and/or heteroleptic complexes.

Dipyrrin can accept a wide variety of metal ions, including: magnesium (II),[79] calcium (II), [80] manganese (II) and (III),[81] iron (II) and (III),[82] cobalt (II) and (III),[83] nickel (II),[84]

copper (II)[85,86] and zinc(II),[83,84,87–93] to form bis(dipyrrinato) metal (II) and tris(dipyrrinato)metal (III) complexes (Figure 12).

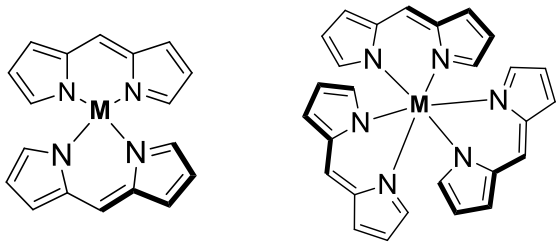

Figure 12: *Structure of bis(dipyrrinato) metal (II) and tris(dypirrinato) metal (III) complexes.*

The coordination geometry of metal complexes of dipyrrins is influenced by the steric interactions between substituents at the 1,9-positions of multiple ligands brought into close proximity by complex formation.[94] These steric requirements force tetrahedral or octahedral coordination geometry in homoleptic complexes (bearing two or more identical ligands on a metal centre), meanwhile heteroleptic complexes (those connecting two or more different ligands on metal centre) of dipyrrins facilitate formation of square-planar coordination geometry.
Even if, especially for metal(II) ions, square planarity is usually the preferred geometry, the steric interactions between 1,9-substituents of dipyrrins, even those as small as hydrogen atoms, were found to distort the geometry of coordination about the metal ions, inducing the adoption of a pseudo-tetrahedral coordination geometry.

The complexation process of dipyrrins has recently been studied using several spectroscopic techniques. Absorption, spectroscopy, calorimetry and ^{1}H-NMR spectroscopy were used to prove the existence of heteroleptic dipyrrinato metal complexes as intermediates in the complexation of metal ions by dipyrrins to form homoleptic complexes.
Studies have shown that homoleptic complexes are generally formed when 0.4 equivalents of the metal salt are used in the complexation reaction.[85] Instead, heteroleptic complexes are more likely to be formed in the presence of stoichiometric amounts (or excess) of metal salt, as expected. Acetylacetonate ligands (acac) are

excellent ancillary ligands for heteroleptic dipyrrinato complexes, as the steric hindrance near the metal centre is minimal.[95]

Research revealed that the equilibrium between homoleptic and heteroleptic complexes (see Figure 13) can be shifted toward one kind of structure rather than another by a number of factors including the basicity of the medium[96] and the coordination ability of the salt anion.[97] For example, metal chlorides do not form heteroleptic dipyrrin complexes as readily as metal acetates or acetylacetonates.

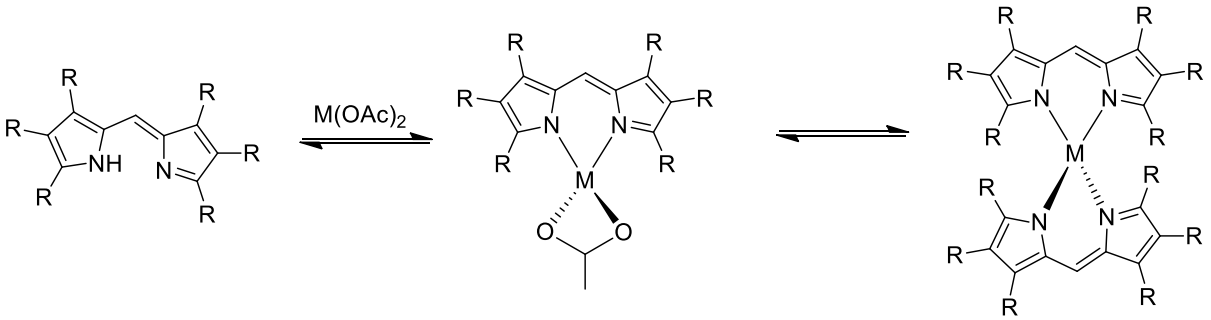

Figure 13: *Formation of homoleptic dypirrinato metal complex through a heteroleptic intermediate*

1.6-Heteroleptic bis(dipyrrinato)metal complexes

Molecules in which two pyrrole rings are linked together with a methane bridge are termed dipyrrins (or dipyrromethenes)and the latter were originally synthesized with the intended use as precursors to macrocyclic tetrapyrroles and strapped porphyrins.[98] Since the discovery of bis(dipyrrinato)metal complexes in 1924,[76] they have been regarded as trivial substances in materials science because they have long been believed to be non-luminescent or weakly luminescent.

This drawback seriously reduces the value of these compounds in many applications. However, Lindsey *et al*.,[99] focused their attention on the steric effect of the peripheral aryl groups, in order to improve fluorescence.

The researchers demonstrated that the introduction of bulky aryl group at the *meso*-position leads to fluorescence enhancement, but, however, quenching in polar solvents remains a serious problem.

Sakamoto and Nishihara[100] proposed a thermal transition/equilibrium from/between the emissive[78] π-π* excited state (**D*-Zn-D** or **D-Zn-D***) to/and non-emissive charge-separated state (**$D^{\cdot+}$-Zn-$D^{\cdot-}$** or -**$D^{\cdot-}$-Zn-$D^{\cdot+}$**), where **D** and **Zn** denote respectively a dipyrrinato ligand and Zn^{2+} ion (see Figure 14). The complex may be regarded as a bichromophoric molecule, in which two dye entities (dipyrrinato ligands in this case) are linked by a Zinc (II) ion.

In homoleptic complexes the two ligands (identified with **D**) are identical, therefore also the electronic structure is the same and nonetheless the HOMO-LUMO energy gap. For this reason, photoexcitation in these kinds of systems often results in the formation of charge-separated state which are generated by one-electron transfer.[101–103] The charge separated state is known to be stabilized in polar solvents.

Homoleptic complex

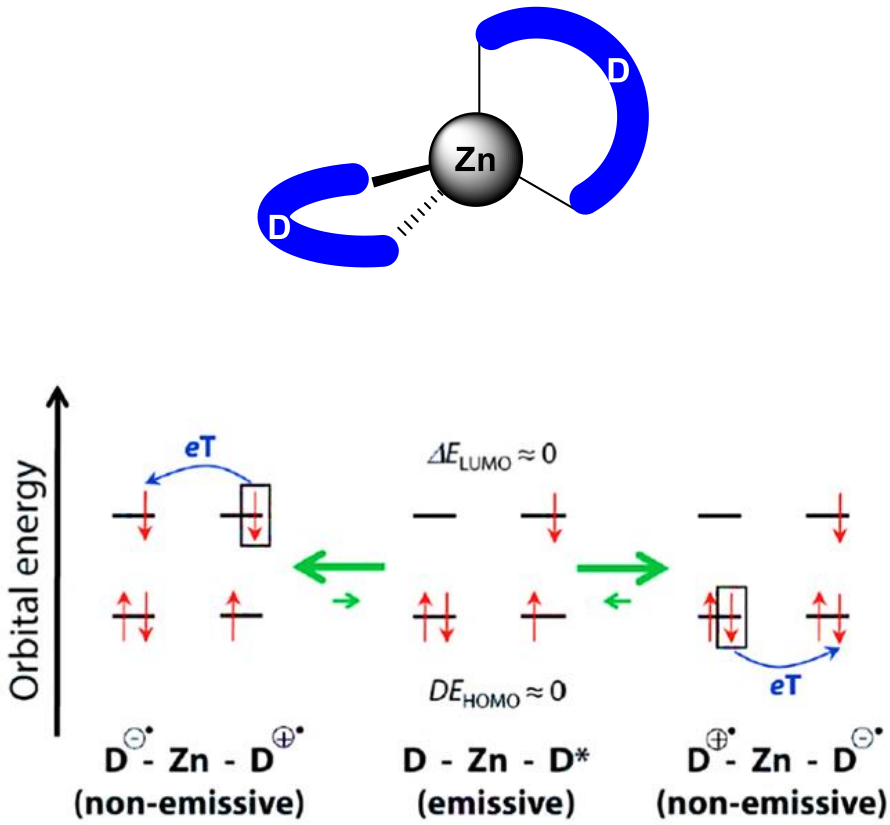

***Figure 14**: Schematic illustration of (Top) homoleptic (Zn)(II) complex, (bottom) plausible thermal equilibrium between emissive and non-emissive state.*[104]

On the other hand, heteroleptic complexes (see Figure 15) contain two different types of dipyrrinato ligand (**D_1** and **D_2**), with drastic difference in their electronic structure. Therefore, the π-expansion localized and HOMO and a LUMO, so quenching separated state are disfavoured compared to the emissive π-π* excited state. Consequently, heteroleptic complexes possess higher quantum yields, and this effect is highlighted in polar solvents.

Heteroleptic complex

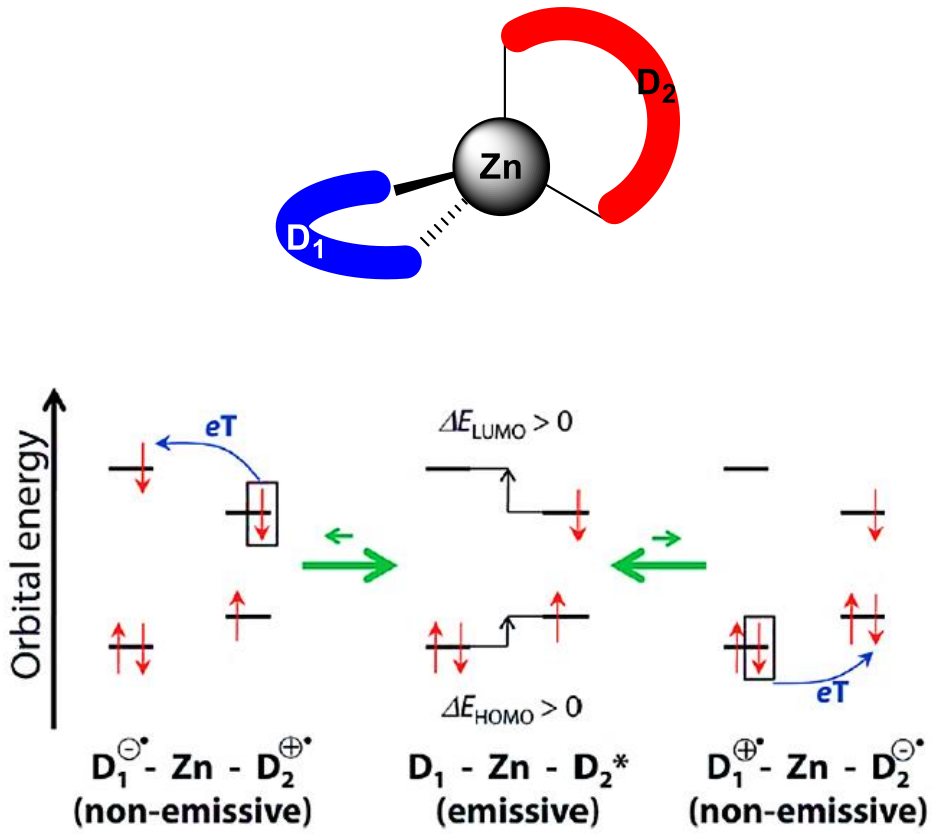

***Figure 15**: Schematic illustration of (Top) heteroleptic (Zn)(II) complex, (bottom) plausible thermal equilibrium between emissive and non-emissive state.*[104]

1.7- Bis(dipyrrinato) Zinc (II) complexes

In the past two decades, fluorescent metal complexes have developed as an essential class of imaging agents, due to their photophysical properties including high fluorescence, large Stokes shifts, long fluorescence lifetimes and good photostability.[55] They were mostly designed as means of sensors or labels, with particular emphasis in second and third-row transition metals as well as lanthanide-based complexes, for *in vitro* and *in vivo* bioimaging applications.[105] However, most of these elements present important limitations, such as: photo- and intrinsic cytotoxicity, unclear relationship between metal complex structure and cellular compartmentalisations, due to the complex variable coordination spheres. These downsides could be overcome by introducing d^{10} metal ion Zn (II) in the design of new metal organic complexes.

Zinc is the second most abundant transition metals and an indispensable trace element in the human body, extensively present in proteins, active in metabolism, gene expression and signal transduction. Zn (II) is an essential metal ion for normal biological processes, with key roles in nervous, immune and reproductive systems, and exhibits a central role in human growth and development.

The need to investigate the versatile function of micronutrient zinc has produced remarkable progress in new tools to screen Zn (II) at intracellular level, such as fluorescence microscopy. For this purpose, many fluorogenic probes chelating intracellular Zn (II) have helped to elucidate its role.

1.8- State of the art and previous work

The starting point of this thesis is the follow-up study of the research previously performed in the research team where this work was done. In particular, the focus of the present study is the development of new luminescent Zinc (II) complexes and their possible activity in cell imaging.

Dmitry Tungulin *et al.*,[106] have successfully prepared eight bis(dipyrrinato) Zn (II) complexes with symmetric and unsymmetrical dipyrrins, obtained by Knoevenagel condensation. All complexes absorb intensely in the region from 450 to 650 nm.

Nonradiative deactivation pathways were minimized, achieving very high Φ values (66%) in a non-polar solvent. They also found that the *meso* substitution of the dipyrromethene systems implies a large difference in steric hindrance within these systems, resulting, therefore, in different emission properties.

The purpose to improve Φ also in polar solvents (for the reason discussed in the section 1.7) have led to a change of course from homoleptic to heteroleptic complexes. In order to perform this, were synthesized three heteroleptic complexes with quite good Φ in dichloromethane and emission in NIR region.[107]

2- Aim of the thesis

This thesis arose from an interest in luminescence heteroleptic bis(dipyrrinato) Zn (II) complexes and their application in *cell imaging*, due to their attractive and fascinating characteristics, already discussed in the introduction.

Among imaging technologies, near-infrared fluorescence imaging has been dedicated immense attention owing to its low absorption and autofluorescence from surrounding organism and tissues in this specific spectral region, which minimize background interference and improve tissue depth penetration.

An ideal near-infrared probe should be equipped with excellence chemical and photophysical properties.

The target of this work is the synthesis of new heteroleptic bis(dipyrrinato) Zn (II) complexes having two main features: the emission in the near-infrared region and water-solubility.

In order to purse these intentions, the low-energy emission was achieved by expansion of π-conjugation of simple dipyrrins using Knoevenagel condensation[106] and tri(ethylene)glycol chain was introduced to increase the water solubility of the final complex.

Photophysical and luminescent properties of the new complexes were investigated and compared with the homoleptic and heteroleptic bis (dipyrrinato) Zn (II) complexes previously synthetized.

Finally, with a view to a potential biological use of these new complexes in biological their biocompatibility was tested using a cell viability assay: *(3-(4,5-dimethylthiazol-2-yl)-2'-5'-diphenyltetrazolium bromide* (MTT) assay.

3-Results and Discussion

In earlier studies performed in the same research group where this work was done, homoleptic Zn (II) complexes containing symmetric and unsymmetrical dipyrrins, were synthesised by functionalization of simple dipyrrins with 2-naphtalencarbaldehyde or 1-mesitaldehyde having as substituents in the *meso* (or 5) position anthracen-9-yl and 2,4,6-trimethylphenyl-1-yl groups.[106]

These compounds absorb intensely in the region going from 450 to 650 nm and they present minimal nonradiative deactivation pathways, achieving very high Φ values (66%) in non-polar solvents.

Based on these observations, the focus of this work was to increase the absorption in the far-red region, tuning the luminescence properties of new bis (dipyrrinato) Zn (II) complexes and, at the same time, to improve their solubility in water or water soluble solvents, in order to make them suitable for biological purposes.

Therefore, in this thesis five new heteroleptic and one new homoleptic Zn (II) complexes (**6a-g**) are presented and investigated, obtained from the functionalization of 1,3,7,9-tetramethyl-dipyrromethene backbones with bulky aryl groups in the *meso* position, α and β-pyrrole position (see Scheme 1).

Bis(dipyrrinato) Zn (II) complexes were synthetized following the general procedure present in literature.[108]

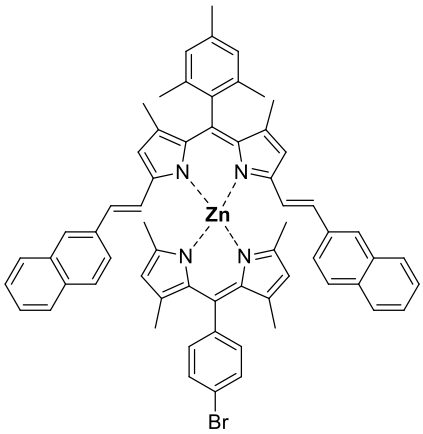

6a

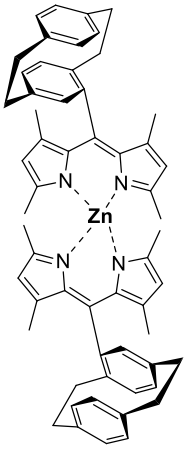

6b

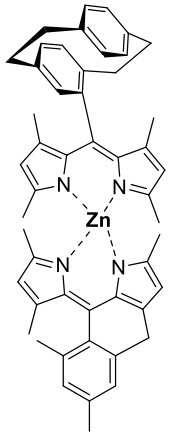

6c

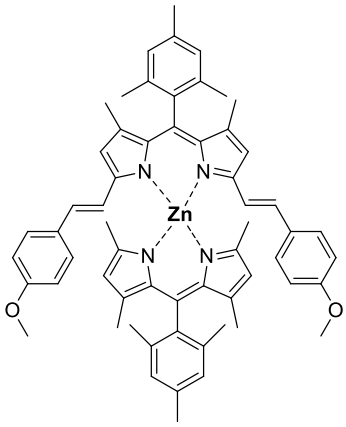

6d

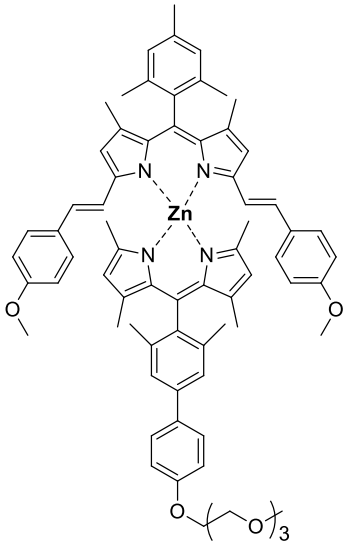

6e

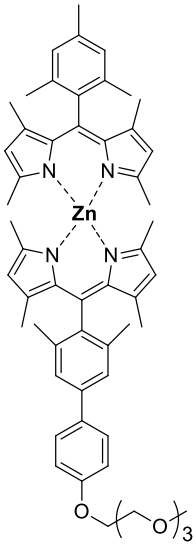

6f

Scheme 1*: Structures of the six new bis(dipyrrinato) Zn (II) complexes investigated in this thesis.*

3.1- Functionalization of dipyrrins

The functionalization of the pyrrole rings is a powerful tool to tailor their application-based properties.

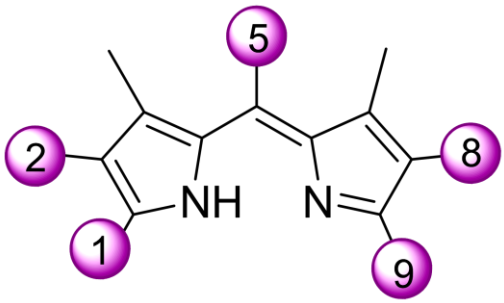

Figure 16*: Chemical structure of the dipyrromethene and the positions that were functionalized in this work.*

As stated above, dipyrrin is a monovalent bidentate ligand bearing two pyrrole units, bridged by an sp^2 carbon atom.[78] A simple dipyrromethene is very attractive because of their accessibility from several synthetic routes and their ability to be modified post synthesis. In this work were functionalized the α positions of the pyrroles (1,9 in dipyrrin, see Figure 16), the β position of the pyrrole (2,8 in Fig. 16) and the *meso* position (5 in Figure 16).

For specific applications, it is aimed to extend the π- conjugation of the dipyrromethene system or to introduce water-soluble groups.

The summaries of the synthetic pathways used in order to obtain functionalized dipyrromethene in different positions and with different groups, are shown hereafter, depending on the targeted properties.

3.1.1-Synthesis of plain dipyrrins

The array of methods generally employed for the synthesis of dipyrrins has recently been expanded. There are some classic methods, like the MacDonald coupling,[109] an acid-catalysed (generally HBr) condensation of a 2-formyl pyrrole with a pyrrole that is unsubstituted in the β position (2-in figure 16) . This procedure is generally suitable for the preparation of asymmetrical dipyrrins or dipyrrins with no substituents at the *meso* position (5-in Figure 16). Yields for this reaction are usually very high but can be limited by purification of the product form the reaction mixture, which is typically achieved by precipitation. Development of reliable methods for the preparation of symmetrical dipyrrins, in particular those substituted with aromatic rings in the 5-position, by oxidation of dipyrromethanes, has been one of the most important advances in dipyrrin chemistry in recent years[110].

3.1.1.1-Functionalization in Meso

At this juncture, Dolphin *et al*.,[111] developed a general procedure, as outlined in Scheme 2, in which the first step of the synthesis involved in a self-condensation of an appropriate pyrrole and a carbonyl precursor, under acidic conditions. The optimal conditions for this reaction require 2.5 equivalent of the precursor pyrrole, 2,4-dimethyl-1*H*-pyrrole, and one equivalent of the aromatic aldehyde. The reaction was carried out under argon atmosphere, at room temperature, in the presence of hydrochloric acid 0.2 M. The second step was the oxidation of the obtained dipyrromethane with 2,3,5,6-Tetrachlorocyclohexa-2,5-diene-1,4-dione (p-Chloranil), that affords to the corresponding dipyrrins. Although this technique is highly successful for the synthesis of dipyrrins, some limitations have been encountered: oxidation may generate a consumption of the starting material (the conversion of the pyrrole is never total since it is in excess respect to the carbonyl precursor), without yielding the appropriate pyrrole. Indeed, yields for such reaction are around 50 %, probably also due to the fact that precipitation is not the best method to purify the product and it proved necessary the purification *via* column chromatography.

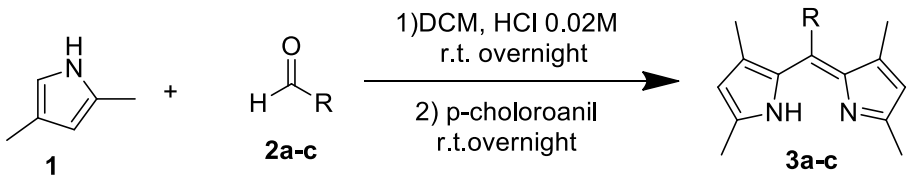

a: 4-Bromo-phenyl
b: Mesithyl
c: rac-4-Formyl[2.2]paracyclophane

Scheme 2**: Synthetic scheme to obtain simple plain dipyrrins **3a-c.

One of the most attractive features of this reaction is the high purity of the product and also the scalability of the procedure.

The obtained crude products **3a**, **3b**,**3c** (Figure 17) were purified *via* column chromatography in alumina, using gradient eluent made of dichloromethane/methanol (max. 1% MeOH) for the compounds **3a** and **3b**, and only dichloromethane for the compound **3c**. The structures were confirmed by ^{1}H-NMR.

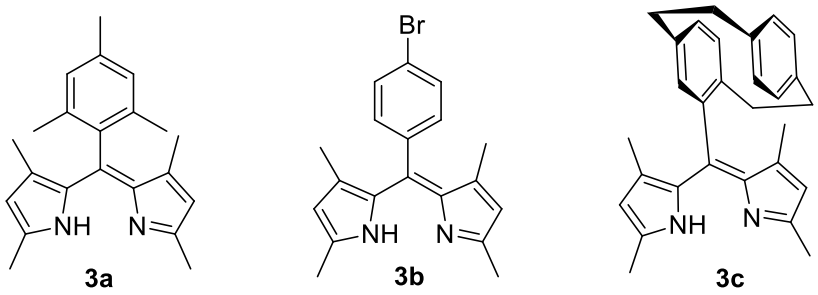

Figure 17: Plain dipyrrins **3a**,**3b**,**3c**

The products **3a-c** were obtained with different yields, between 50-67% (see Table 2).

***Table 2:** Name, type of aldehyde and yield of plain dipyrrins*

Sample	Aldehyde	Yield
3a	Mesithylaldehyde	50-67%
3b	4-bromo-phenylaldehyde	50-68%
3c	rac-4-Formyl [2.2] paracyclophane	50%

3.1.1.2 Functionalization in position 2 and 8

Dipyrromethenes can undergo an electrophilic substitution at the position 2 and 8 (see Figure 16). The introduction of heavy atoms, such as iodine, on the molecular skeleton has multiple effects: it alters the excited state populations, inducing the “heavy-atom effect[15] and, since it is a good-leaving group, iodo-substituted organic compounds are recognised as valuable synthons or precursor for further functionalization *via* cross-coupling reactions.

The basic source of iodine is the iodide anion (I^-), but since this species is a weak nucleophile, the iodination involves the use of an oxidant, such as iodic acid, for the transformation *in situ* of inactive iodide to an active iodonium species (I^+) that acts as electrophile.

Di-iodination of both pyrrole rings is achievable using a iodine source.[112]

According to the general procedure,[61] 1 equivalent of (2Z)-2-[(3,5-dimethyl-1*H*-pyrrol-2-yl)-mesityl-methylene]-3,5-dimethyl-pyrrole (**3a**) was solved in a mixture of chloroform and methanol and then was put to react with 2 equivalent of iodine and 2 equivalent of iodic acid. The reaction was carried out for 1.5 hours at 0 °C (See Scheme 3). The crude residue was recrystallized from dichloromethane/methanol at -30 °C.

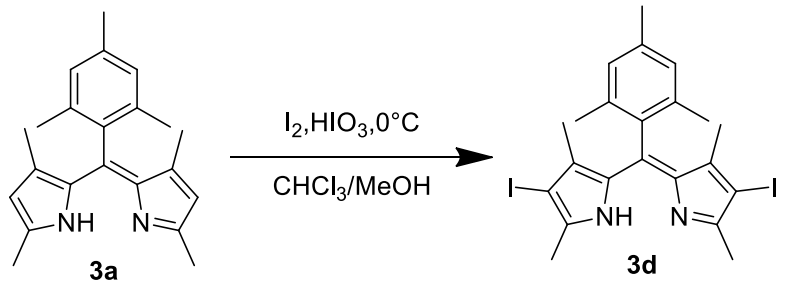

Scheme 3**: Synthetic procedure for dipyrrins **3d

The product was obtained with a high yield, 87%, in agreement with the values found in literature[112] and its structure was confirmed by ^{1}H-NMR spectra.

3.2- Synthesis of π-expanded dipyrrins

In order to increase achieve red and near-IR emission, the π-conjugation in dipyrromethene ligands was expanded using a Knoevenagel condensation.[61,113] This reaction takes its name from German chemist Emil Knoevenagel, who first described this reaction in 1896 and it is widely used for C=C bond formation.[114] It is based on a nucleophilic addition of a compound, after deprotonation of its active hydrogen, to the carbonyl moiety of an aldehyde (or ketone) followed by the removal of water.[115] In this case, the active hydrogens are those of the methyl groups in α position to the nitrogen of the pyrrole rings that undergo a condensation with the aldehyde (See Scheme 4).
Π-expanded dipyrrins **4a-b** and **4c-d** were synthesised by condensation of 3,4-dimethoxybenzaldehyde (**2d**) and naphthalene-2-carbaldehyde (**2e**) respectively with plain dipyrrins **3a**.

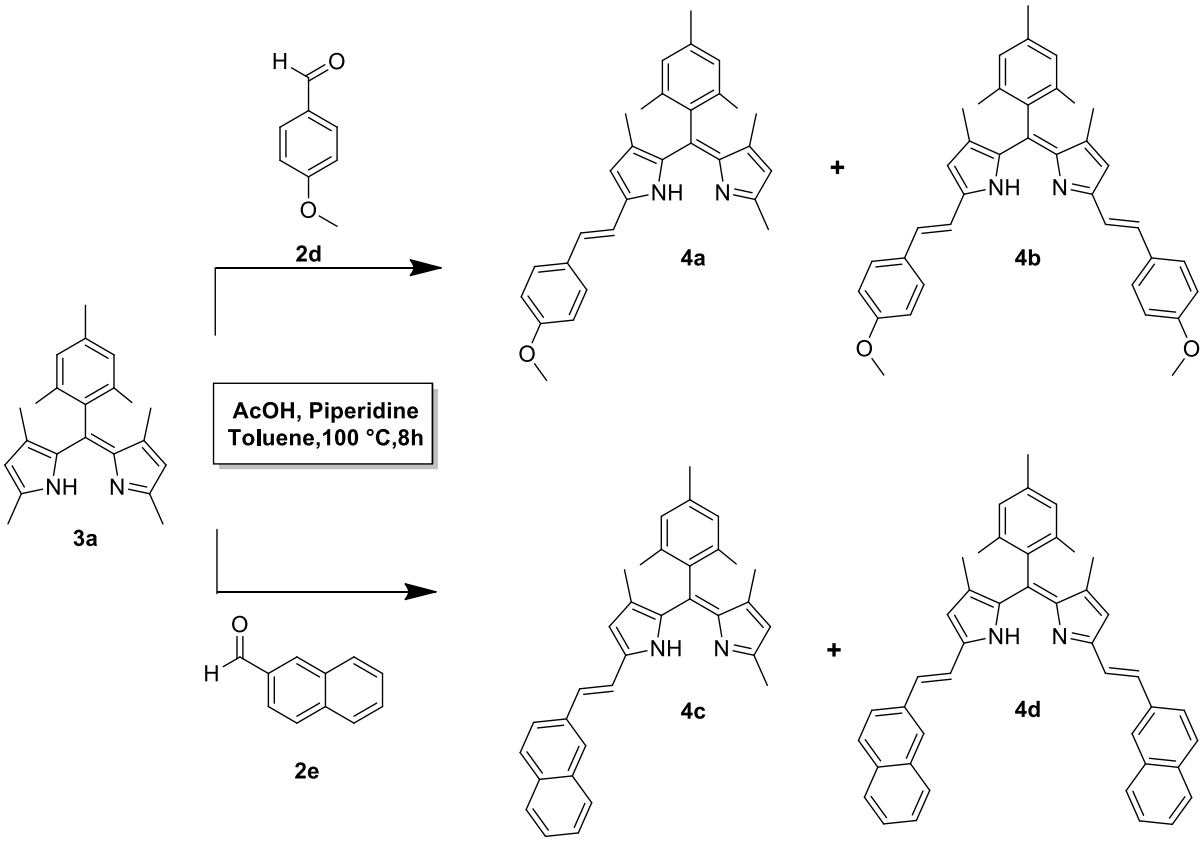

***Scheme 4**: Synthetic scheme for the functionalization of plain dipyrrins **3a** via Knoevenagel condensation to obtain dipyrrins **4a-d**.*

The reaction is endothermic and for this reason was carried out at 100 °C. This high temperature is necessary because water, which is formed as a side product, can be eliminated via distillation. In order to repristinate the volume of toluene that might as well evaporate from the reaction, a Dean-Stark apparatus was used. The reaction was catalysed by an organic base such as piperidine (500 μL) and was left stirring overnight at room temperature.

In each Knoevenagel condensation we performed, as it was observed in previous studies,[106] the starting dipyrrin was completely converted in 8 hours, however, beside the difunctionalized product, the monosubstituted ligand was always formed, regardless of the number of aldehyde equivalents used for the reaction (see Scheme 4).

As shown in Scheme 4, in this reaction were formed two different products: the unsymmetrical ligand, i.e. the π-expanded dipyrrins mono-functionalized only in 1-position **4a** and **4c** and the symmetrical ligand, which is the π-expanded dipyrrins bi-functionalized, in both 1 and 9-positions **4b** and **4d** (see Scheme 4).

In the Table below (Table 3) are reported the corresponding yields.

Π-expanded dipyrrin	**Substitution**	**Yield**
4a	Unsymmetrical	70 %
4b	Symmetrical	30%
4c	Unsymmetrical	60%
4d	Symmetrical	40%

Table 3: Compound, substitution and yield of dipyrrins **4a-d.**

The non-trivial and more tedious step was the purification of the crude product: the mono and bi-functionalized dipyrrins, despite being two different compounds, are very

similar. In fact, during the purification, performed *via* column chromatography, the bands of the dipyrrins **4a** and **4b** were really close, and it was very difficult to separate the two pure products. Analogously, this also applied for dipyrrin **4c** and **4d**.

3.3- Synthesis of dipyrrins with water soluble groups.

In order to improve the solubility of the final zinc complex in water or water miscible solvents, the introduction of functional groups such as triethylene glycol methyl ether and sulfonate was performed. Hereafter, the first strategy is discussed in paragraph *3.2.1* and the strategy for the introduction of the sulfonate group in paragraph *3.2.2*

3.3.1-Synthesis of dipyrrins with glycolic chain

One strategy adopted to increase aqueous solubility is the introduction of water-solubilizing functional groups such as glycolic chains.[116] To obtain this kind of dipyrrins, two different synthetic pathways were chosen (see Scheme 5). As shown below, the aldehyde **2f** was used in two different reactions.

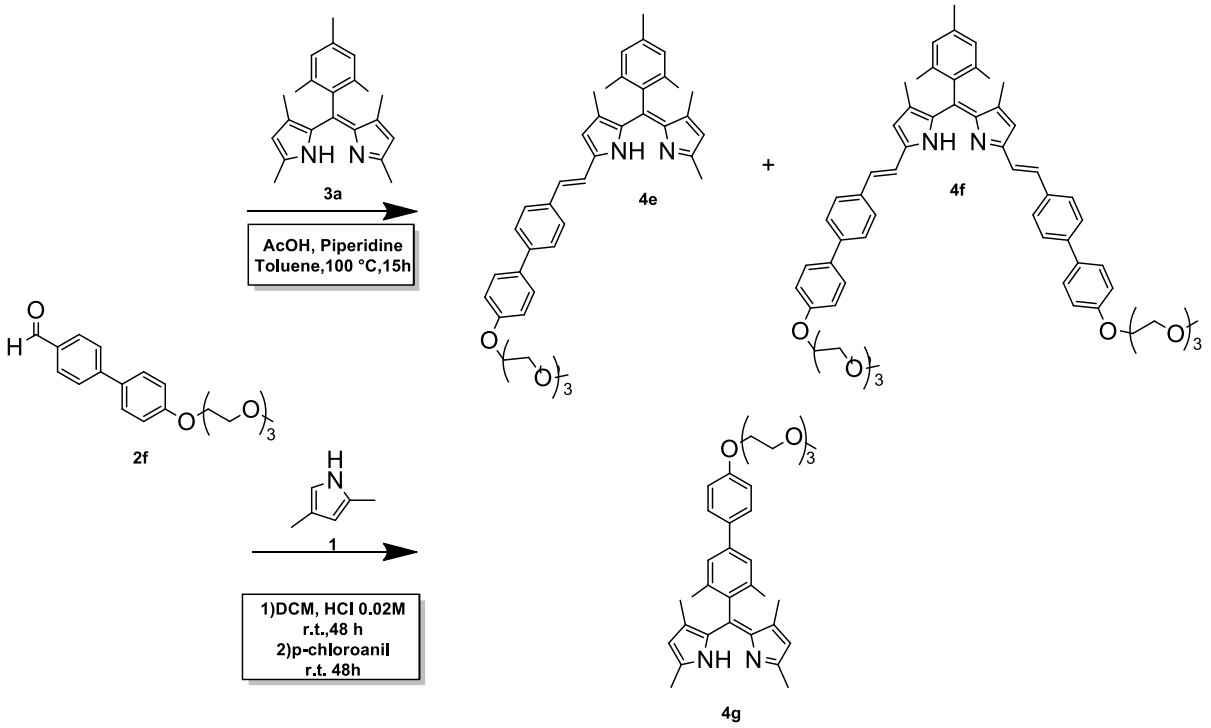

***Scheme 5**: Synthetic scheme to obtain dipyrrins **4e-g** with glycolic chain.*

Part of this was used in a Knoevenagel reaction[117] with the dipyrrins (**3b**) in order to obtain dipyrrins **4e-f** (Scheme 5- top). The reaction was performed following the same conditions discussed previously (see 3.2), except for a longer reaction time: after 8 hours of stirring at 100 °C there was still starting material (**3b**), for this reason the reaction was carried out for additional 7 hours. The crude residue was purified *via* column chromatography, using dichloromethane with 1% of methanol as eluent and 0.2 % of triethylamine. The product **4f** was obtained with 35% of yield.

For the synthesis of compound **4g** the reaction between the aldehyde **2f** and 2,4-dimethyl-1*H*-pyrrole was performed using the same conditions described in (3.1.1.1.), except, also in this case, for the reaction time. The first step of the synthesis has requested 48 hours, in order to obtain the complete conversion of the starting material, while the second step, the addition of the p-chloranil, has taken 24 hours to afford the corresponding dipyrrin **4g.** The product **4g** was obtained with 45 % of yield.

*3.3.1.1 Synthesis of aldehyde **2f***

The aldehyde **2f** is not commercially available, therefore, was synthetized in laboratory, through a multi-step synthesis (see Scheme 6).

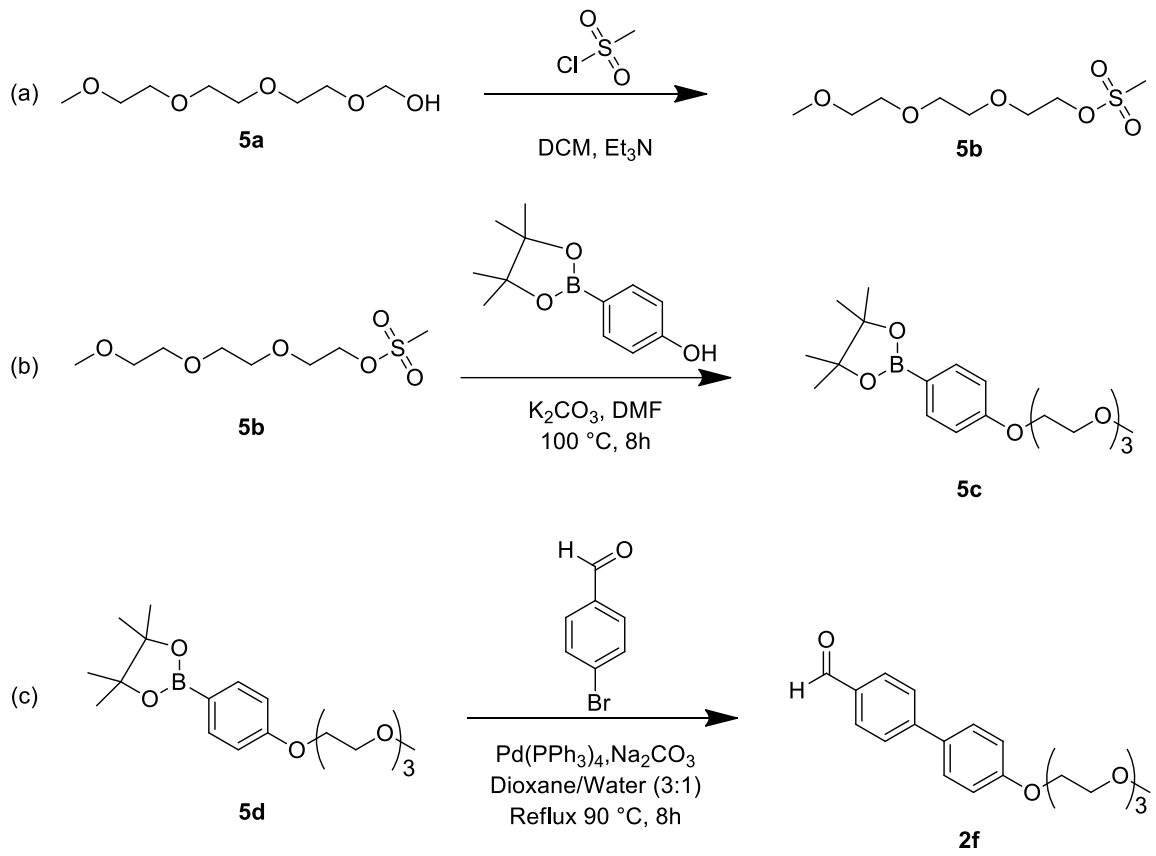

***Scheme 6**: Schematic multi-step synthesis to obtain aldehyde **2f**.*

The first step **(a)** is the activation of the 2-[2'-(2''-methoxyethoxy) ethoxy] ethanol (**5a**). The hydroxyl group is not a good leaving group, and so, to ensure that it can be substituted with another group, it must be activated. Among the various strategies employed to achieve that, can be used specific reactive, such as methane-sulfonyl chloride. This last acts as electrophile, expelling a chloride ion, following a mechanism S_N2, giving the methane-sulfonic acid 2-[2'-(2''-methoxyethoxy) ethoxy] ethyl ester (**5b**) with 78 % of yield.

The second step **(b)** is another nucleophilic substitution S_N2, between **5b** and 4-(4',4'',5,5'-tetramethyl-1,3,2-dioxaborolan-2''-yl) phenol in order to obtain **5c** with 46 % of yield.

The third and last step **(c)**, is the reaction between **5d** and 4-bromobenzaldehyde **2b** in order to obtain the corresponding aldehyde. As depicted in Scheme 6, the aldehyde **2f** was obtained *via* a Suzuki Cross Coupling.[118] The first publication dates back to 1979 for work of Akira Suzuki,[119] who shared the 2010 Nobel Prize in Chemistry with Richard F. Heck and Ei-ichi Negishi for their effort for discovery and development of palladium-catalysed cross coupling in organic synthesis.[120]

In the specific reaction illustrated in Scheme 6, the coupling partners are a boronic acid **5d** and an organohalide, 4-bromobenzaldehyde **2b**, in order to obtain the aldehyde **2f**.

The Suzuki Cross-Coupling takes place in presence of a catalyst, a palladium complex, such as tetrakis(triphenylphosphine)palladium $Pd(PPh_3)_4$ and a base (in this case: Na_2CO_3).[121] This last has multiple roles in the reaction: it activates the organoboron compound, forming the boron-ate complex as well as facilitates the *transmetalation* step, and moreover it accelerates the *reductive elimination* step by reaction of the alkoxide with the palladium complex[122]. Since this reaction requires anaerobic conditions, it was carried out under argon atmosphere and the solvent mixture 1,4 dioxane/water (5:1) was degassed through the "Freeze-pump thaw cycling".[123]

The reaction was refluxed for 6 hours at 80 °C. The crude residue was purified *via* column chromatography in silica, using a gradient eluent made of dichloromethane and 1% of methanol. The product **2f** was obtained with 87 % of yield.

3.3.2-Synthesis of dipyrrins with sulfonate group.

The second strategy used to increase the solubility of the final zinc complexes in water or water miscible solvents was the introduction of the sulfonate group. Sulfonates are derivative of sulfonic acids and have the general chemical formula of $R\text{-}SO_3^-$.
Their C-S bond is quite strong and does not undergo hydrolysis.

A convenient introduction of this functional group in a molecule is the alkyne-azide cycloaddition with an azido-alkyl-sulfonate, previously prepared from 1,4-butansultone, as indicated in Scheme 7.

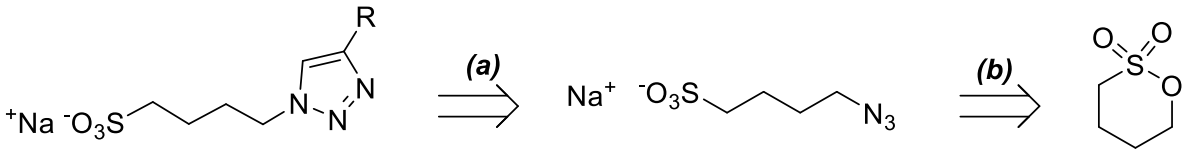

***Scheme 7**. Retrosynthetic pathway for the synthesis of 1,2,3-triazole heterocycle with sulfonate functionalization. (a) Alkyne-azide cycloaddition between 4-azido-butanesulfone and an alkyne; (b) Nucleophilic substitution of sodium azide in 1,4-butanesulfone.*

Beside the trivial synthesis of the 1,2,3-trizoles, these heterocyclic moieties have drawn attention of the chemists, pharmacologists, microbiologists, owing to its indomitable biological potential[124]. Among heterocyclic compounds, triazole nucleus is one of the most important, well-known heterocycles, considered as a privileged structure in medicinal chemistry[125]. While earlier methods for preparing these molecules often required harsh condition[126], in 2002 Medal, Sharpless and Fokin, developed mild and direct methods for accessing 1,4-disubstituted 1,2,3 triazoles in one step, with a copper- catalysed azide alkyne cycloaddition (CuAAC).[127,128]

Moreover, a method to form also the corresponding 1,5 disubstituted 1,2,3 triazoles was found with the ruthenium-catalyzed azide alkyne reaction (RuAAC).[129]

The aforementioned reactions require an azide and an alkyne. In contrast to the CuAAC reaction, which is limited to terminal alkynes, the RuAAC reaction was found to tolerate internal alkynes, providing access also to 1,4,5-trisubstituted 1,2,3-triazoles.[130,131]

In order to obtain dipyrrins functionalised with a triple-bond, several synthetic pathways were followed, involving the cross-coupling reaction named after the Nobel Prize winner, Sonogashira.

3.3.2.2 Synthesis of substituted alkynes.

Since the target compound was a substituted alkyne (internal or terminal), numerous Sonogashira cross-coupling reactions were performed. The reaction name arises from the discovery in 1975, by Sonogashira, Tohda and Hagihara of a palladium catalysed C-C bond formation process between a terminal sp hybridized carbon of an alkyne with a sp^2 carbon of an aryl or vinyl halide (or triflate).[132]

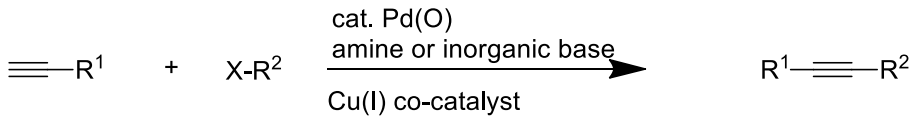

R^1: Aryl, Alkyl, SiR_3
R^2: Aryl, Vinyl
X: I, Br, Cl, Otf

***Scheme 8**: General synthetic scheme for a Sonogashira Cross-Coupling*

The reaction is generally carried at room temperature, using a palladium source such as $PdCl_2(PPh_3)_2$ as catalyst, combined with a co-catalytic amount of CuI in basic solvent (e.g. amine, such as trimethylamine or diisopropylamine) [133](see Scheme 8).

*3.3.2.2.1-Alkyne-functionalized dipyrrins **3b-c***

The meso-functionalised dipyrrin **3b** was used in two different Sonogashira cross-coupling reactions with two different substrates: trimethylsilylacetylene (Scheme 9) and ethynylbenzene (Scheme 10).

The reaction requires anhydrous and anaerobic conditions, therefore the syntheses were carried out under argon atmosphere, using dry diisopropylamine (DIPA) as solvent, which acts also as nucleophilic base.

The reaction performed with trimethylsilyl acetylene (4 equiv.) as alkyne, didn't lead to success (see Scheme 9). The reaction was carried out at room temperature, but, even if it was left stirring for 48 hours, no product was formed.

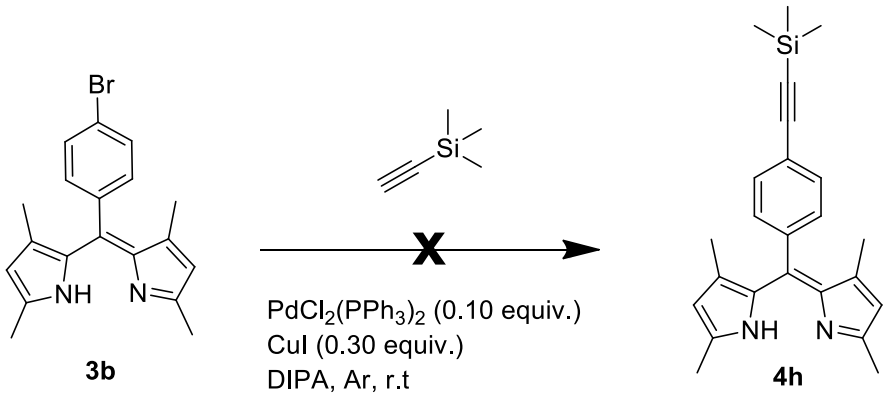

***Scheme 9**: Sonogashira Coupling with trimethylsilyl acetylene as alkyne*

One possible cause of the unsuccessful reaction could have been the alkyne used, since the reagent was very old. However, when ethynylbenzene was used instead, the reaction did not lead to any product either.

The reaction (see Scheme 10) was first carried out at room temperature, however, after 24 hours there was no conversion of the starting material yet. Thus, the temperature was increased to 80°C. The high temperature is possible in reaction shown in Scheme 10 since the ethynylbenzene has a boiling temperature of 143°C while trimethylsilylacetylene evaporates already at 53°C. After 10 hours of stirring at 80 °C, one new spot apperead on TLC. For this reason the crude residue was purified *via* column chromatography packed with silica, using dichloromethane and cyclohexane (50:50) as eluent.

Unfortunately, the ^{1}H-NMR spectra of the purified showed signals that did not corresponding with the target compound.

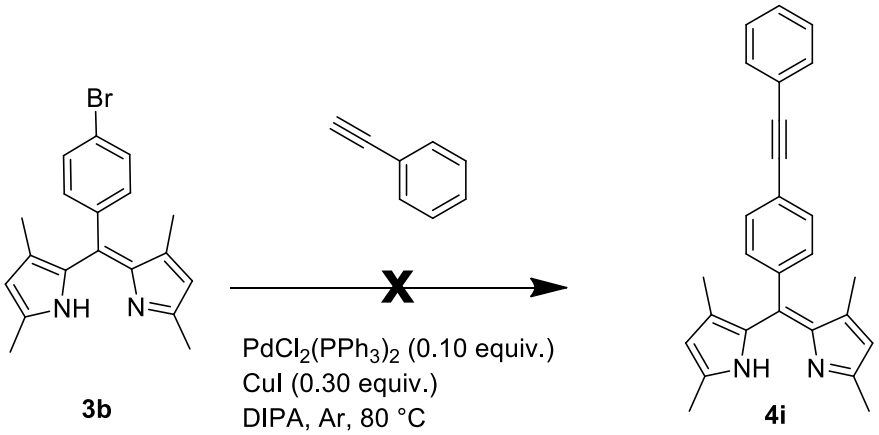

***Scheme 10**: Sonogashira Coupling* with *ethynylbenzene*

In view of the failure of the precedent Sonogashira couplings listed above, another strategy was used in order to introduce the triple bond in the dipyrromethene structure. This time was chosen to functionalize the 2 and 9-position of dipyrrin, therefore was performed a Sonogashira cross-coupling with the bis-iodo functionalized dipyrrins **3d** (See Scheme 11).

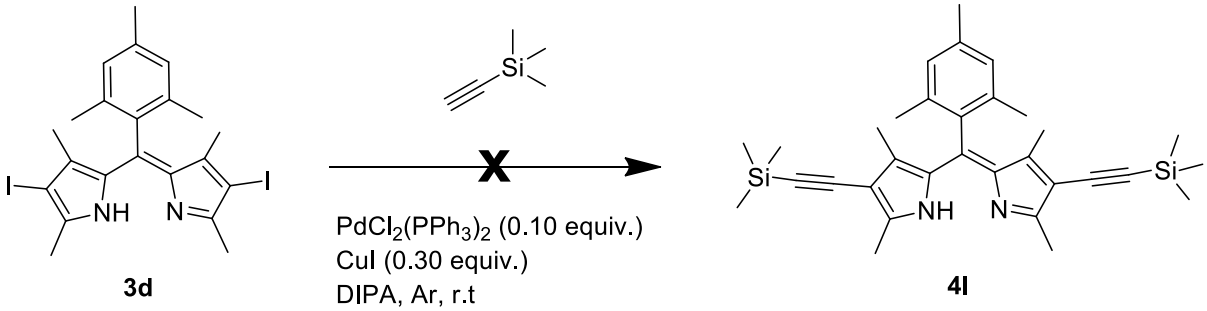

Scheme 11**: Sonogashira Coupling with dipyrrins **3d

The reaction was conducted using the same conditions and the same equivalents mentioned above, but also in this case no product was formed. It might be possible that the dipyrromethene, being a chelating ligand, coordinates the palladium catalyst deactivating its catalytic activity. The inhibition of the catalyst might be then responsible for the unsuccessful cross-coupling reaction directly on the dipyrrin.

3.3.2.2.2 Synthesis of 4-(phenylethynyl)-benzaldehyde

As mentioned above, the speculated problem during the reaction was related to the inhibition of the catalyst and possibly simultaneous damage of the dipyrrins under these conditions. A different attempt to achieve alkyne-functionalized dipyrrins was performed *via* functionalization of an aldehyde, which serves then in the condensation with the pyrrole. In particular, a Sonogashira cross-coupling reaction was performed between ethynylbenzene and 4-bromobenzaldehyde (see **Scheme 12**).

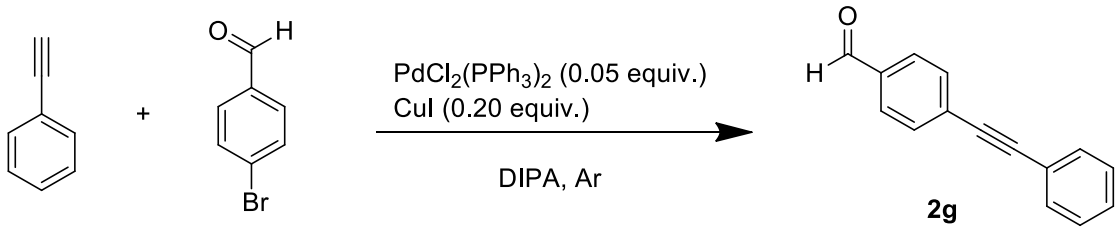

Scheme 12**: Synthetic scheme to obtain aldehyde **2g

The reaction was carried out under argon atmosphere at room temperature for 12 hours and then was heated at 80 °C for 9 hours. The crude residue was purified *via* column chromatography, packed with silica, using as eluent mixture dichloromethane: cyclohexane (70:30).

Part of the product, *4- (2´phenyl-ethynyl)-benzaldehyde,* confirmed by ^{1}H-NMR analysis was subsequently employed in the reaction with the 2,4-dimethyl-1*H*-pyrrole, (see Scheme 13) following the same procedure adopted in the synthesis of dipyrrins **3a-c.**

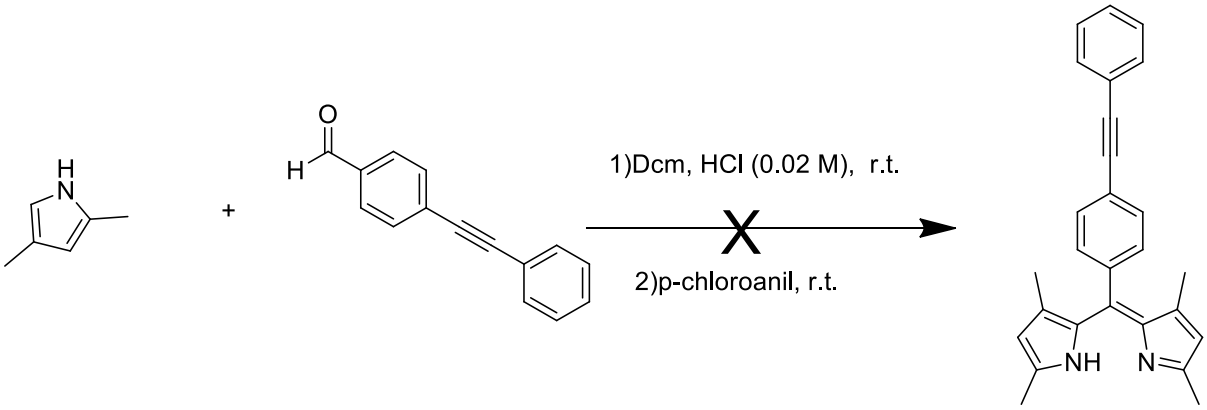

***Scheme 13**: Synthesis of dipyrrin with 4-(2 phenyl-ethynyl)-benzaldehyde*

The crude residue was firstly purified *via* column chromatography using as eluent ethyl acetate. The obtained compound was analysed by ^{1}H-NMR, but the signals did not match with those of the target structure.

The *4- (2´phenyl-ethynyl)-benzaldehyde,* was used in a ruthenium- catalysed azide alkyne reaction (RuAAC) (see Scheme 14).

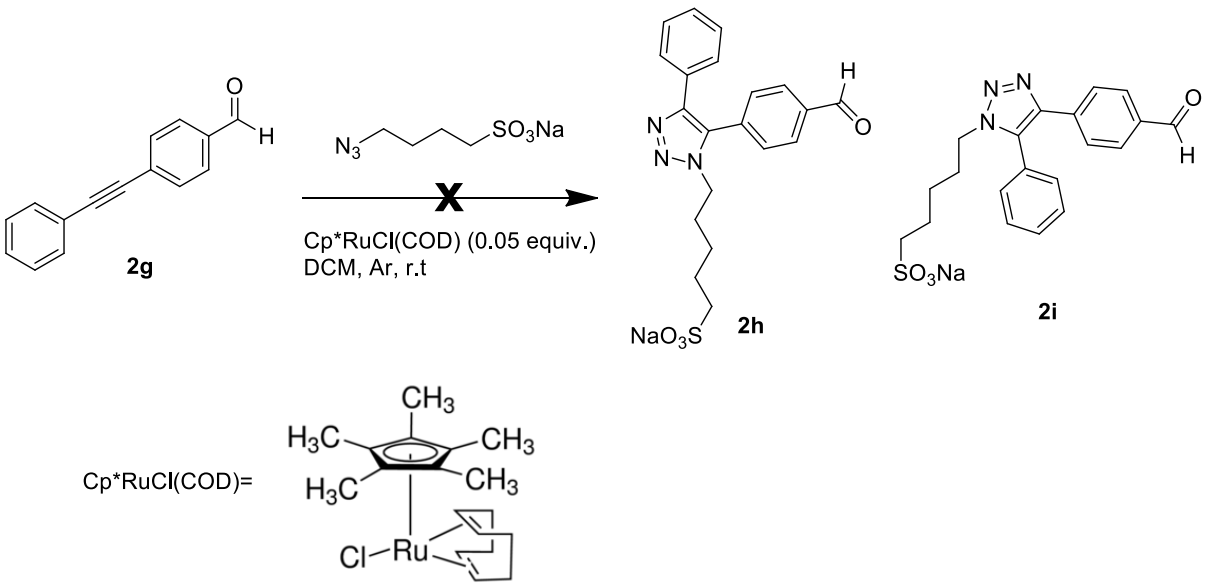

***Scheme 14**: Synthetic scheme of RuAAC*

As indicated above, the click reaction was performed between the aldehyde **2g** and the azide. As catalyst was employed 2.5 % of Chloro (pentamethylcyclopentadienyl) (cyclooctadiene) ruthenium (II), Cp*RuCl (COD). The reaction was carried out under argon atmosphere and was left stirring at room temperature for 48 hours. No product was formed.

3.4- Synthesis of Zn-complexes.

As already mentioned in the introduction, pyrrolic nitrogen atoms in dipyrrins are able to coordinate metals ions[134] and form isolable complexes. Upon deprotonation, dipyrrinato ligands generally form neutral complexes, homoleptic when the metal coordinates identical ligands, heteroleptic when the metal core is chelated by different ligands. Was chosen zinc as metal ion and were synthesized bis (dipyrrinato) zinc (II) complexes.

Zn (II) complexes usually are tetracoordinated and have a tetrahedral geometry. This is due to the fact that zinc (II) is a late transition metal with full *d* valence electrons and a charge of 2+, which means that a stable 18-electron complex can be formed through 4-coordination number with two monoanionic chelating ligands. In bis(dipyrrinato) Zn (II) complexes, the central zinc atom is tetracoordinated with two nitrogen atoms from each ligand, filling the coordination sphere.

The synthetic route to prepare this kind of complexes is very simple, according to the procedure already described in literature[106] (see scheme 15).

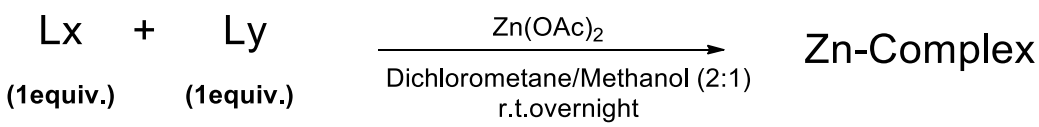

Scheme 15*: General scheme to obtain bis(dipyrrinato) Zn (II) Complexes*

3.4.1- Synthesis of heteroleptic complexes

For the heteroleptic complexes, two different kind of dipyrrins, one equivalent each, previously functionalized, were dissolved in a 2:1 mixture of dichloromethane/methanol. Then zinc diacetate was added, and the reaction was carried at room temperature overnight (See Scheme 16).

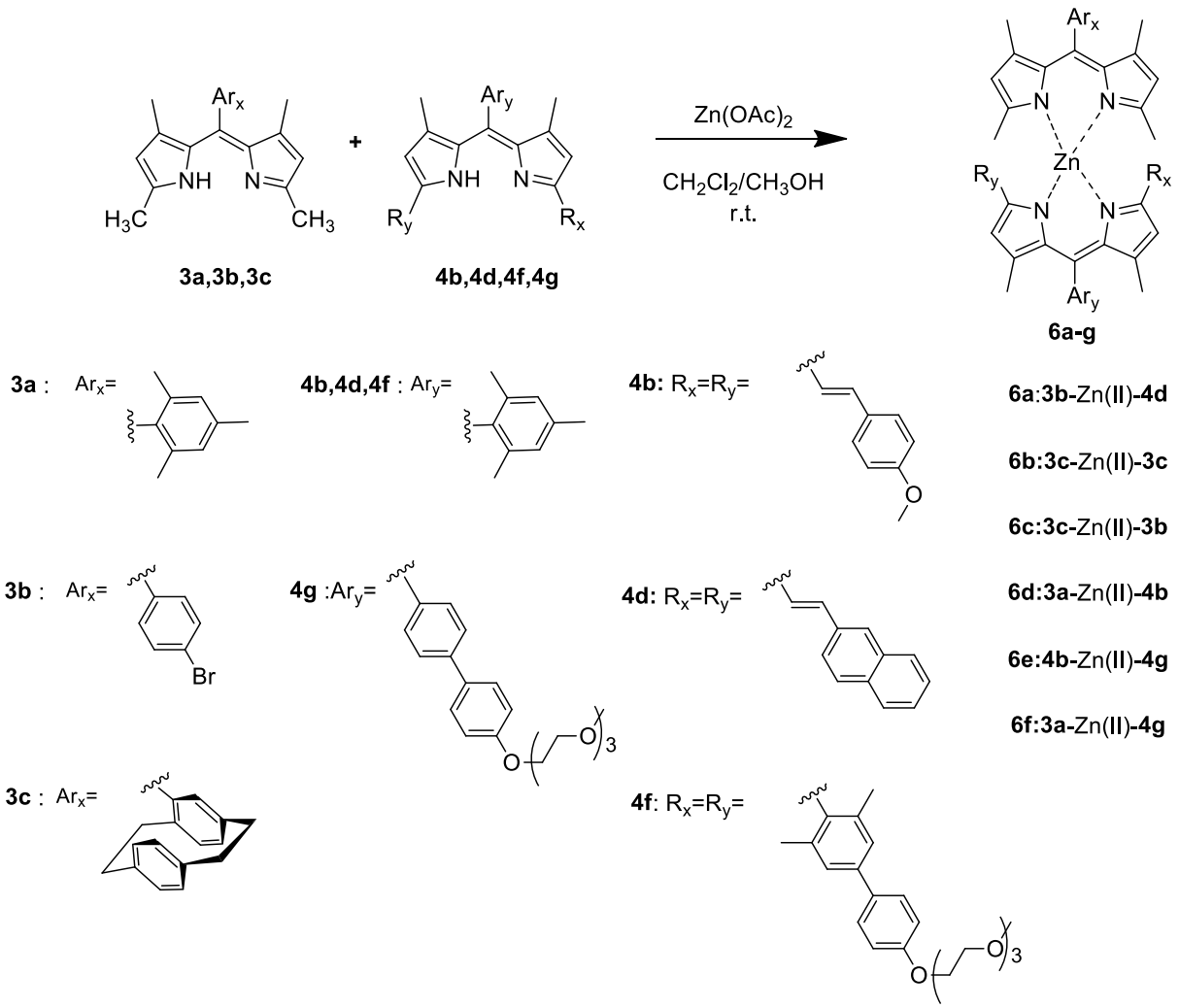

***Scheme 16**: Synthesis of heteroleptic Zn (II) complexes*

Simple dipyrrins **3a-c**, π-expanded dipyrrins **4b-c** and dipyrrins with glycolic chain **4f-g**, were employed in order to obtain complexes with different properties.

Even if the two different kind of dipyrrins were reacted in stoichiometric ratio, the reaction gave rise to the formation of three complexes: one heteroleptic and two homoleptic. For this reason, the crude residue was purified by flash chromatography on alumina, using dichloromethane as eluent.

The yields of the final complexes were low, ranging from 10 to 30 %.

All complexes were analysed with ^{1}H-NMR, ^{13}C-NMR and high-resolution mass.

*3.4.2- Synthesis of homoleptic complexes **6b***

Although this work has focused on heteroleptic complexes, one homoleptic complex was synthesised with dipyrrins **3c**, as it has never been reported in literature so far (see Scheme 17).

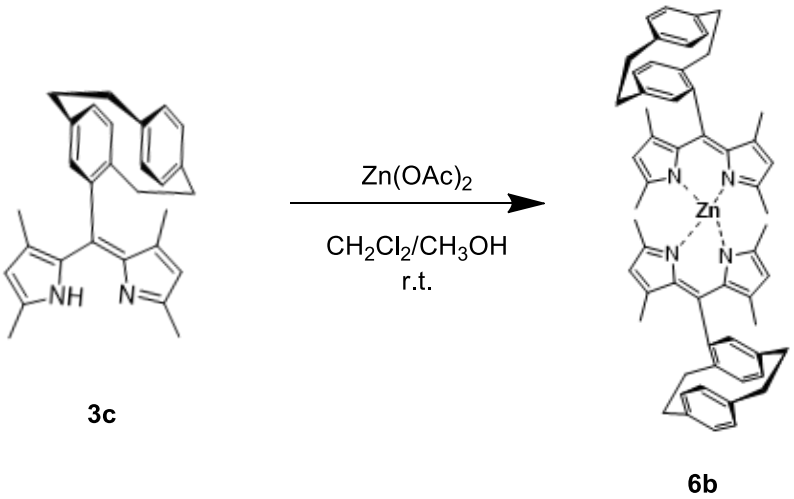

Scheme 17**: Synthesis of homoleptic Zn (II) complex **6b

To form the complex **6b**, two equivalents of the dipyrrin **3c** were reacted with one equivalent of zinc diacetate in a 2:1 mixture of dichloromethane/methanol. The reaction was carried out at room temperature. To promote a slow crystallization, the new complex was purified by recrystallization in cyclohexane.

The ^{1}H-NMR spectra of the complex **6b** shows only broad peak, difficult to understand. It is supposed that the dipyrrin **3c**, since it was synthetized from the *(rac)-4-Formyl [2.2] paracylophane,* bearing planar chirality, is a mixture of different diastereoisomers. Therefore, being a mixture of different molecules, the peaks are broad and difficult to integrate. The structure of the complex **6b** was confirmed by high resolution mass.

3.5-Photophysics

3.5.1-Previous work

In order to explain the choices of substituents and functionalization of bis(dipyrrinato) zinc complexes prepared and analysed in this study, an overview of the different complexes synthetized and characterized in Claudia Bizzarri's team where this work was done[107,135] is given. These respective structures are reported below (See Figure 18) and their photophysical data will briefly discussed and compared with those of the new complexes.

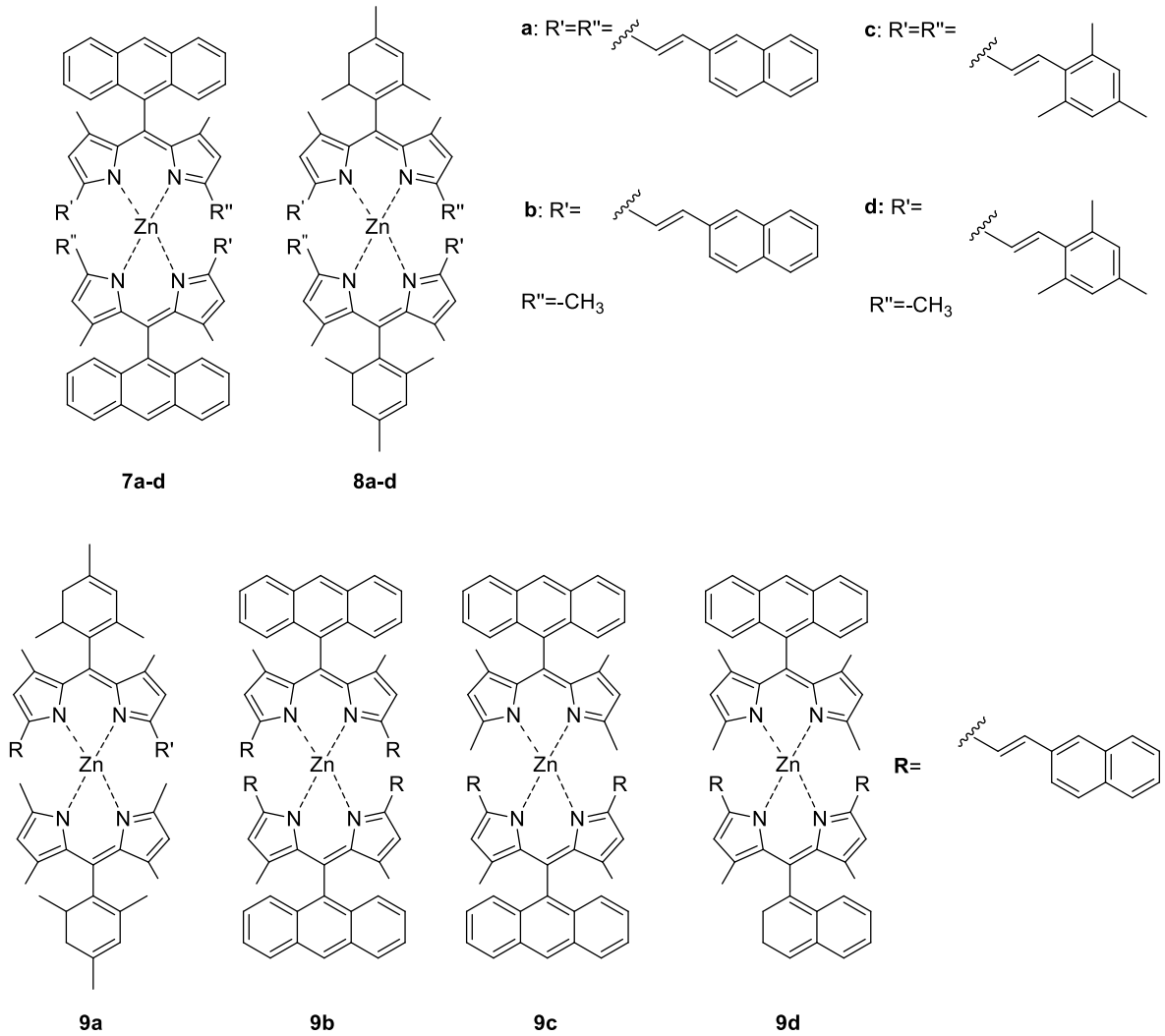

***Figure 18**: Structures of the twelve bis(dipyrrinato) zinc (II) complexes that were investigated previously in the research team where this work was done.*

The measurements were carried out in cyclohexane or dichloromethane (spectroscopic grade) at room temperature.

A summary of the spectroscopic properties, including photoluminescence quantum yields Φ and excited- state lifetimes τ, is shown in Table 4.

Complex	λem[a]/nm	Φ[a], [c]	τ[a]/ns
7a	649	0.09 (0.009) [b]	4.3
7b	582	0.09 (0.003) [b]	4.6
7c	615	0.21 (0.004) [b]	5.0
7d	564	0.16 (0.004) [b]	4.1
8a	649	0.25 (0.004) [b]	4.1
8b	574	0.58 (0.005) [b]	4.7
8c	603	0.37 (0.005) [b]	4.7
8d	559	0.66 (0.003) [b]	4.1
9a	633(685) [d]	0.53 (0.35) [b]	4.39
9b	644(692) [d]	0.05 (n.a.) [b]	3.92
9c	639(694) [d]	0.18 (n.a.) [b]	1.72(63.9%),5.84(36,1%) [e]
9d	637(693) [d]	0.08 (n.a) [b]	1.52(89.5%),8.53(10.5%) [e]

Table 4: [a] Measured in cyclohexane. [b] Measured in dichloromethane. [c] Quantum yields were determined by the reference method, using as reference $Ru(bpy)_3Cl_2$ in air-equilibrated water (Φ = 0.028). [d] Emission relative maxima of shoulder emission. [e] Percentage values obtained by biexponential fitting.

As already discussed in paragraph 1.6, homoleptic complexes contain two identical chromophores units, thereby a photoinduced charge transfer from one ligand to the second one breaks the symmetry of the excited state[106].

Especially in polar solvents, the lowest singlet excited state of such complexes is a non-emissive charge separated state (CT)[15] and its population opens nonradiative deactivation pathways.

Since the photophysics of the homoleptic bis(dipyrrinato) Zn (II) complexes **7a-d** and **8a-d**, might be affected by the population of a CT state in polar solvent (for example CH_2Cl_2), their luminescence properties were investigated in cyclohexane.

Complexes **7a-d**, with anthracenyl substituents in meso position show noteworthy quantum yields values (0.09«Φ«0.16). Although these values are not excellent, in respect to the zinc complex with plain ligands,[111] the increase of the luminescence is about 10 times.

But the most outstanding values are provided by the complexes **8a-d** with ever-growing value of photoluminescence quantum yields, especially for complexes **8b** and **8d**, respectively, a value of Φ equal to 0.58 and a value of Φ equal to 0.66. This actually attests what was reported by Lindsey *et al.*[136] about the steric effect of the peripheral aryl group in *meso* position.

At the time, the researchers had demonstrated that the replacement of the phenyl group of bis(dipyrrinato) zinc (II) complex with a 2,6 dimethyl phenyl group, in *meso* position, transform the molecule from a weak emitter into highly fluorescent chromophore. This is confirmed by the data obtained by Claudia Bizzarri and co-workers[106] and shown in Table 4: the replacement of the antracen-9-yl with the 2,4,6-trimetylphen-1-yl in *meso* position, results in an improvement of fluorescence. As expected, for all complexes **7a-d**, **8a-d**, the emission intensity in polar solvent, such as dichloromethane, is totally quenched (Φ <0.01), due to the formation of a charge-separated state.

Regarding the emission maxima, it is in the far-red region for complexes **1a** and **2a**, while red emission was observed for complexes **1c** and **2c**. Thus, this observation led to the synthetic strategy to increase the conjugation in dipyrrins by symmetric functionalization, in order to shift the emission in the NIR region.

The luminescent properties of complexes **9a-d,**[107] were evaluated in cyclohexane and in dichloromethane.

This shift to a lower energy state with a longer wavelength is referred to a *Bathochromic Shift* (also called *red shift*) caused by a positive solvatochromism.

In this series of complexes, the complex **9a** shows high Φ in both solvents: respectively 0.53 in cyclohexane and 0.35 in dichloromethane, proving therefore that that heteroleptic complexes do not undergo significant quenching in polar solvent, unlike their respective homoleptic counterparts.

The fluorescence has a single exponential decay with excited state lifetimes that are in the range of 4ns to 5ns for the series **7a-d**,**8a-d** and **9a-b** meanwhile for the series **9c-d** ranges the decays are biexponential.

*3.5.2-Excitation and emission spectra of the new complexes **6a-f***

Below the spectra and photochemical data of the new complexes are reported. A summary of spectroscopic properties, including emission maxima and excited-state lifetimes, is shown in Table 5.

-Complex 6a

The excitation and emission profiles of the heteroleptic complex **6a** are shown in Figure 19.

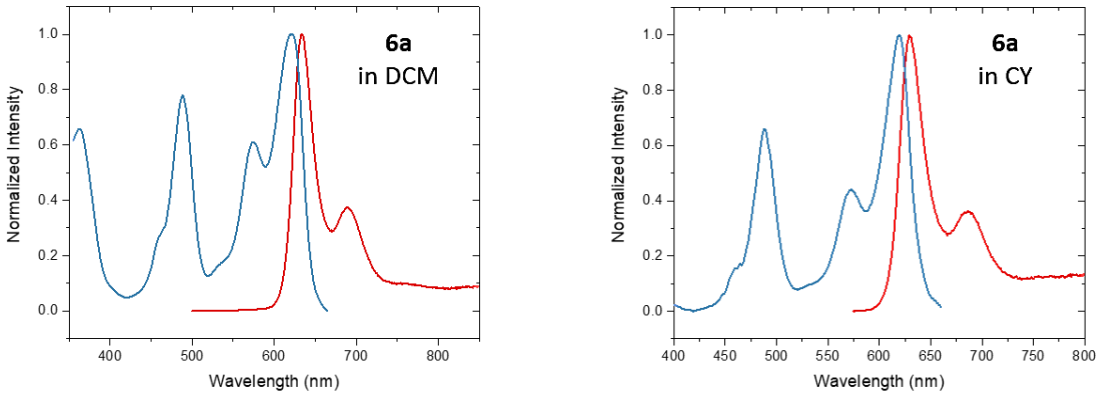

Figure 19: Emission (red line) and excitation spectra (blue line) of complex **6a** in dichloromethane (DCM, left) and in cyclohexane (CY, right)

Complex **6a** has a ligand centred emission with a maximum at 632 nm and a relative maximum at 690 nm in dichloromethane. In cyclohexane, the emission profile is very similar although it is slightly red-shifted (645 nm and 695 nm).

The emission maxima of the complex present a very small Stokes shift, as expected for fluorescent chromophores with a localized excited state.

The excitation spectrum shows the same bands appearing in the absorption spectrum and the two different ligands in the heteroleptic complex are easily spotted. The profile from 450 to 500 nm is due to the plain dipyrrin **3b** while the one from 510 to 650 nm is due to the functionalized dipyrrin ligand **4d**.

Noteworthy, in the emission spectra in Figure 19, there is only an emission band, due to the functionalized ligand, confirming an energy transfer from the higher excited state of the plain dipyrrin to the lower lying excited state of the functionalized ligand.

The latter emits in the NIR region: the emission maxima are 640 nm and 632 nm, respectively in cyclohexane and dichloromethane. This hypsocromic shift in a more polar solvent (DCM) occurs, probably due to a destabilization of the LUMO, increasing the HOMO-LUMO energy gap of the complex **6a**.

The presence of an heavy atom, such as Br, as substituents of the aromatic molecule, present in dipyrrin **3b**, can result in fluorescence quenching (*internal heavy atom effect)*[15] because of the increased probabiliity of intesystem crossing. However, it is resonable to assume that the effect is minimal, since the complex **6a** show high fluorescence upon illumination. Anyway, a quantitative analysis can not be done at this stage, as the fluorescence quantum yield could not be measured.

-Complexes 6b, 6c

The excitation and emission profiles of complexes **6b-c** are shown in Figure 20.

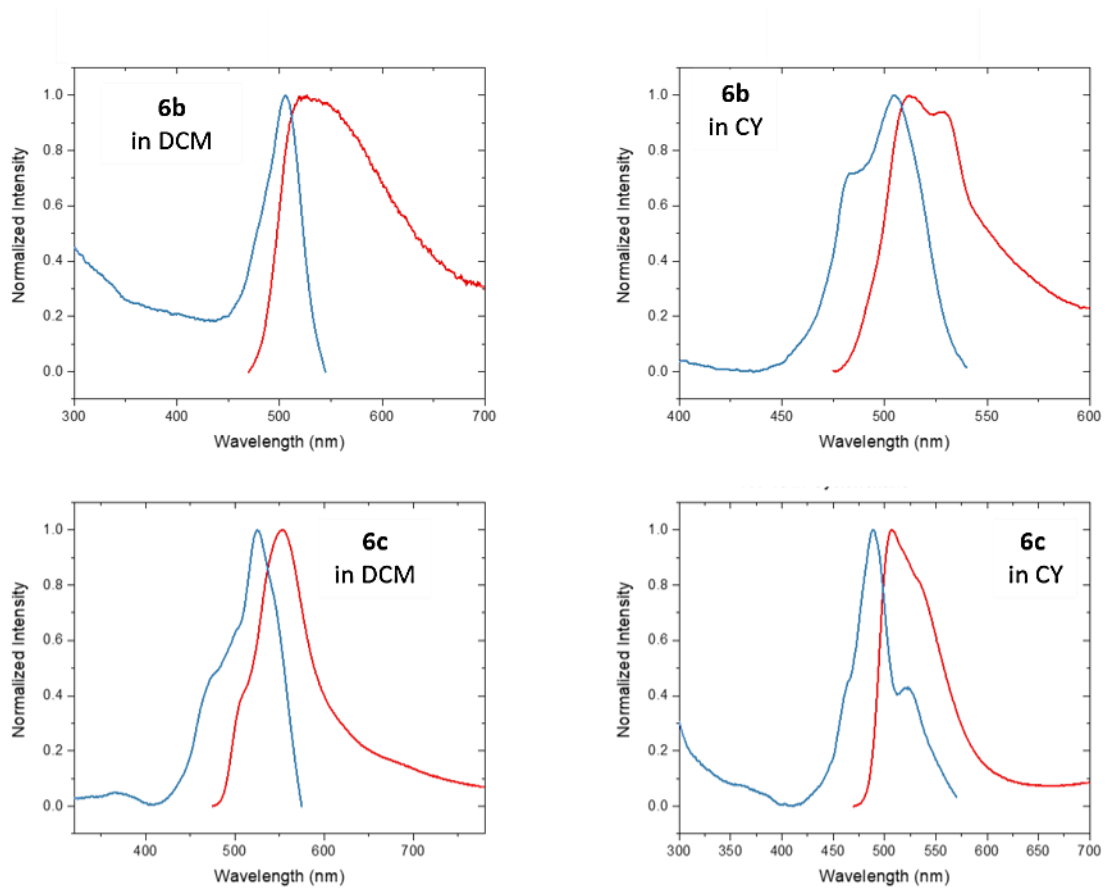

Figure 20: Emission (red line) and excitation spectra (blue line) of complex **6b (top)** and **6c (bottom)** in dichloromethane (left) and in cyclohexane (Right).

Complex **6b** shows one excitation band (λ_{exc} ~ 500 nm in both solvent) and one broad emission band (λ_{em} = 513 nm in CY and 527 nm in DCM), with small Stoke Shift. Complex **6c**, meanwhile**,** shows two excitation band, even if the first one looks like a shoulder of the second band, with relative maxima at 525 nm in dichloromethane (the maximum of the shoulder is difficult to individuate) and 475 nm and 525 nm in cyclohexane. This is probably due to the very similar structure of the dipyrrins **3a** and **3c**, having then a very similar photophysics.

The emission profile of complex **6c** is composed of one emission band (λ_{em} = 508 nm in CY and 510 nm in DCM). Also, for the abovementioned complex, the excitation and emission profile present a small Stoke shift.

This comparison born with the intent to underline the difference between the homoleptic complex **6b**, formed by two identical dipyrrins (**3c**) and the heteroleptic complex **6c**, formed by dipyrrins **3a** and **3c**.

Though at first glance the spectra may look the same, however the emission maxima in both solvents are different. Moreover, both complexes show bathochromic shifts (see Table 5).

Even if the structure of the ligand forming the complex **6c** are different, at the same time dipyrrins **3a** and **3c** are both plain dipyrrins, neither of them benefits of a π-expansion, thereby it is difficult to predict which ligand emits emits before the other one and whose could be perform an energy transfer.

Moreover it is not known if there is a thermal equilibrium due to the fact that the energy state od the plain dipyrrins **3a** and **3c** are so close that there could be a *"back-energy transfer"*.

The excited state lifetime is really small for complex **6b** (≤1 ns both in cyclohexane and in dichloromethane), while is greater but not very high for complex **6c** (2.4 ns in cyclohexane and 3.1 ns in dichloromethane.

-Complexes 6e, 6f

The excitation and emission profiles of complexes **6e-f** are shown in Figure 21.

The complexes **6e** and **6f** have in common one ligand, the dipyrrin **4g** with glycolic chain in *para* position to the phenyl in *meso*, whereas the second ligand of **6e** is the π-expanded dipyrrin **4b**, and the plain dipyrrin **3a** is the second ligand for complex **6f**. Obviously this difference has a signficant impact on emission spectra (see Figure 21).

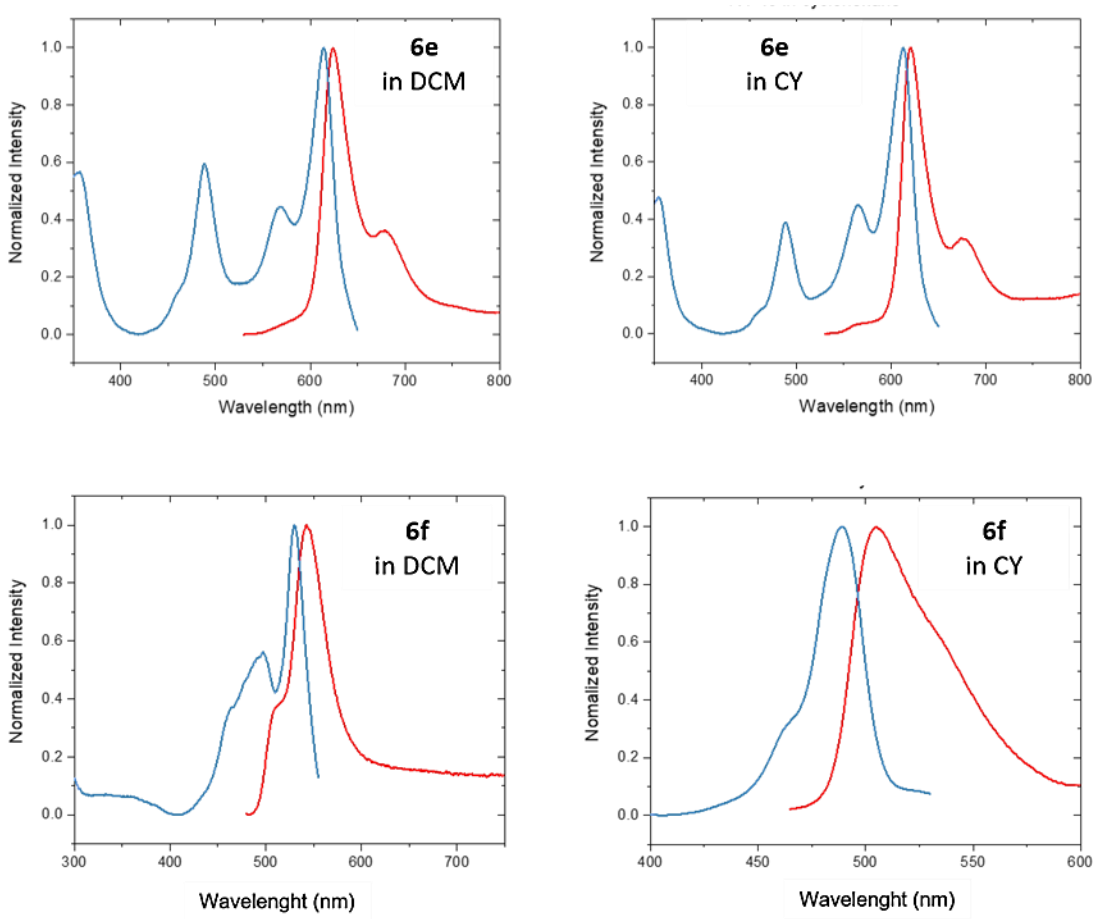

***Figure 21**: Emission (red line) and excitation spectra (blue line) of complex **6e (top)** and **6f** (bottom) in dichloromethane (left) and in cyclohexane (right)*

The excitation profile of complex **6e** exhibits two different band, (λ_{exc} ~ 490 nm and 600 nm in both solvent) albeit the emission profile (both in dichloromethane and cyclohexane) shows only one band, relative to the intraligand emission of dipyrrin **4b**, that emits in red (λ_{em} = 622 nm in cyclohexane and 625 nm in dichloromethane). The disappearance of the emission of dipyrrin **4g** is a proof of the energy transfer from the plain dipyrrin **4g** to the π-expanded dipyrrin **4b**.

As regard the complex **6f**, it is formed by two plain dipyrrins: the glycolic chain of dipyrrins **4g** do not alter the HOMO-LUMO gap significantly, and for this reason the electronic structures of dipyrrins **3a** and **4g** are quite similar. For this reason, as shown in Figure 21, the complex **6f** is characterized by a single excitation band (the shoulder in the spectra in cyclohexane disappear in dichloromethane) and a single emission band.

The excited state lifetime is really small for complex **6f** (1.9 ns in cyclohexane and ≤1 ns in dichloromethane) consistent with the values of the homoleptic complex made of the plain dipyrrin **3a** (2.4 ns in cyclohexane),[111] while for complex **6e is** 3.8 ns in cyclohexane and 3.1 ns in dichloromethane.

Hereafter the emission profiles (Figure 22) and the relative summary spectroscopic properties at room temperature (Table 5) of the new complexes **6a-f** (Figure 22) are reported.

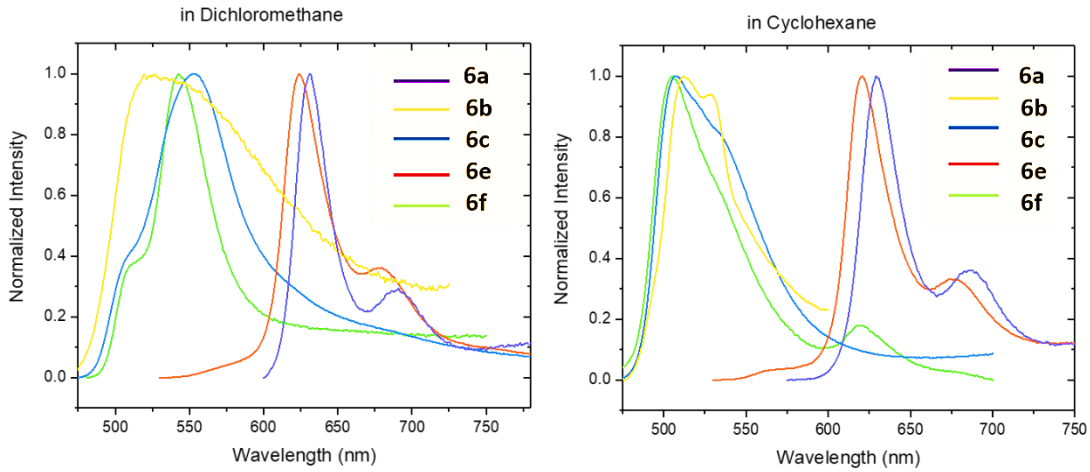

Figure 22: *Emission spectra of complex* ***6a-f*** *in dichloromethane (left) and in cyclohexane (right).*

Complex	λ_{em}[a]/nm	τ[a]/ns
6a	640(632) [b]	3.9/ (3.7) [b]
6b	512(527) [b]	≤1/ (≤1) [b]
6c	508(511) [b]	2.4/ (3.1) [b]
6e	622(625) [b]	3.8/ (3.1) [b]
6f	506(514) [b]	1.9/ (≤1) [b]

Table 5: [a] Measured in cyclohexane. [b] Measured in dichloromethane.

3.6-Biocompatibility

3.6.1- In Vitro Cytotoxicity and cell Viability assays

Though fluorescent probes are popular tools in analytical applications, most challenges arise with the increase in complexity for a multicellular organism.
An aspect not to be underestimated when preparing new compounds having as purpose biological applications, is biocompatibility. For any newly developed molecular marker, which has to be used in biological applications, the first step is the study of its cytotoxicity, in order to ensure that the cells remain healthy after incubation with the probe.

Viability levels and/or proliferation rates of cells are good indicators of cell health. *In vitro* cell viability and cytotoxicity assays with cultured cells are based on various cell functions.
Application of these assays has been of interest over recent years because they are rapid, inexpensive and they are also useful for testing large number of samples. However they have some disadvantages, due to their unsophisticated technology, not enough advanced yet to replace animal tests.[137]

A broad spectrum of cytotoxicity and cell viability assays is currently used in the fields of toxicology and pharmacology for drug screening,[138] such as: dye exclusion assays, colorimetric assays, fluorometric assays and luminometric assays. The choice of the most appropriate method among these assays as well as considering different parameters like specificity and availability in the laboratory when the study is performed, are very important for obtaining accurate and reliable results.

In particular, colorimetric assays may be carried out on different types of cells, whether adherent or suspended cell lines, are easy to perform and comparably economical.

The principle of colorimetric assays is the measurements of a biochemical marker: specific reagents develop a colour in response to the viability of cells, allowing the colorimetric measurement of cell viability *via* spectrophotometer.

There are different types of colorimetric assays, such as:

- ***MTT* assay***: (3-(4,5-dimethylthiazol-2-yl)-2'-5'-diphenyltetrazolium bromide* assay, based on the determination of mitochondrial function of cells.[139]
- **MTS assay**: *(5-(3-carboxymethoxyphenyl)-2-(4,5'-dimethyl-thiazoly)-3'-(4'-sulphophenyl) tetrazolium inner salt* assay, also based on mitochondrial activity cells, used for onsite toxicological assessments.[140]
- ***XTT* assay:** *(2,3-bis (2'-methoxy-4-nitro-5-sulphophenyl)-5'-carboxanilide-2''H-tetrazolium, monosodium salt)*, first described by Scudiero et al.,[141] used to assay cell proliferation as response to different growth factors, based on mitochondrial function of cells.
- ***WST-1 assay:*** *(2-(4-iodophenyl)-3-(4'-nitrophenyl)-5 (2,'4''-disulfophenyl)-2''H tetrazolium monosodium salt assay,* designed to measure the relative proliferation rates of cells in culture, based on the metabolic activity of cells.[142]
- ***WST-8 assay:*** *(2-2'-methoxy-4nitrophenyl-)-3(4'-nitrophenyl)-5-(2'',4''-disulfophenyl)-2'''H tetrazolium, monosodium salt* assay*,* used for cell proliferation assays as well as cytotoxicity assays.[143]
- ***LDH* assay:** *Lactate dehydrogenase* assay, an indicator of irreversible cell death*,* that measure the cytosolic lactate dehydrogenase (LDH)[144] enzyme, quantitatively, releases from damaged cells.
- ***SBR assay****: Sulforhodamine B* assay, first described by Skehan, provide a sensitive index of cellular protein, with very high reproducibility and good linearity with cell number.[145]
- ***NRU assay:*** *Neutral red uptake* assay, developed by Borenfreund[146] is a good marker of lysosomal damage, speed and simple.
- ***CVS assay:*** *Crystal violet* assay, a quick and reliable screening method, suitable for the examination of the impact of compounds on cell survival and growth inhibition.

In order to evaluate the cell viability of the new complexes in this work, the *MTT assay* was performed.

3.6.2- MTT assay: general framework

MTT assay is an enzyme-based assay, first described by Mosmann.[139]

The *(3-(4,5-dimethylthiazol-2-yl)-2'-5'-diphenyltetrazolium bromide (MTT)* salt, a yellow tetrazole derivative is reduced to purple *(E,Z)-5-(4-5''-dimethylthiazol-2-yl)-1,3-diphenylformazan (formazan)* (see Scheme 18) only in the metabolically active (that means living) cells by mitochondrial dehydrogenases,[139] predominantly succinate dehydrogenase.[147,148]

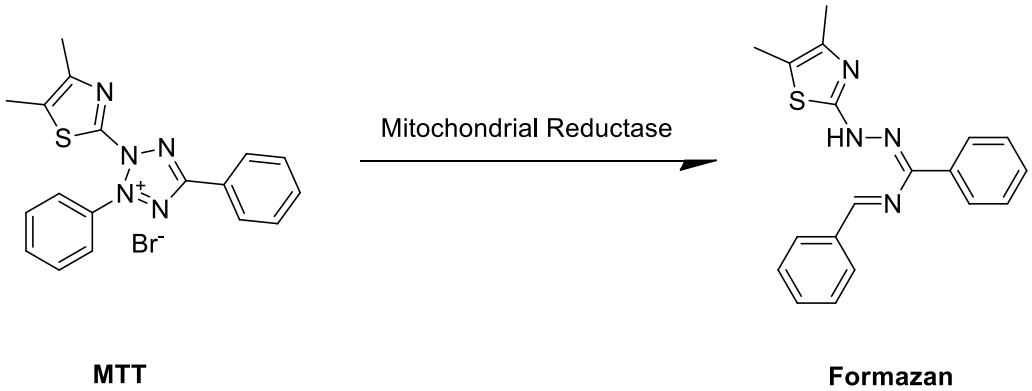

Scheme 18*: Reduction of MTT in formazan*

The total amount of formazan produced upon MTT reduction, after solubilization (usually in dimethyl sulfoxide or ethanol), is measured on spectrophotometers (multiwell scanning) and it is directly proportional to the number of viable cells in the culture, because only living cells have intact mitochondria and cell membrane that can catalyse the reaction.

However, the test has some limitations. At high cell densities, the amount of MTT is not linear with cell number because cell lines could have large intra-assay (variations in results within a dataset of data) and inter-assay variations (change in precision). Moreover, several studies have recently show that the reduction of tetrazolium salts is related not only with mitochondria reductase, but also with many intracellular reductase.[148] Furthermore, research has indicated that intracellularly reduced nicotinamide adenine dinucleotide (NADH) is the main electron donor in MTT

reduction,[149,150] therefore a high NADH concentration may lead to inaccurate MTT assay results.

The cells used in this study were the *HeLa* cells[140] (see Figure 23).

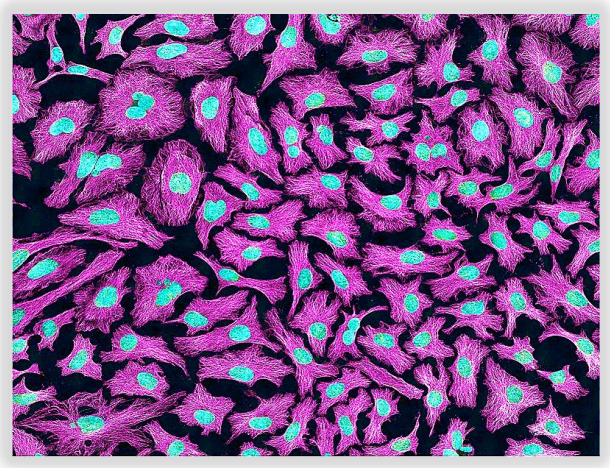

Figure 23*: Multiphoton fluorescence image of Hela Cells with cytoskeletal microtubules (magenta) and DNA (cyan)*[140]

The name *HeLa* was derived from the first two letters of Henrietta Lacks, a patient who died of cervical cancer on October 1951. The line of cells from Lacks's cancerous cervical tumour was taken without her knowledge or consensus, which was a common practice at the time. [151] Cell biologist George Otto Grey, found that they could be kept alive,[152] and developed a cell line, belonging to a strain that has been continuously cultured since 1951. Compared to other human cells, HeLa cells were (and still are) the only cells to survive in vitro. As such, they are often regarded as the first (and thus far, only) immortal human cells ever cultured.[153]

MTT assay was carried out on *Hela* Cells, cultivated with bis(dipyrrinato) Zn (II) complexes **9a-d** and **6a-f** in three different concentrations: 1 µM, 2.5 µM, and 5 µM. Cell viability was monitored after 72 hours of incubation at 37°C, 5% CO_2.

*3.6.3- MTT assay of complexes **9a-d***

In table 6 are reported the values of cell viability, expressed in percentage of the complexes **9a-d.**

The results demonstrate that the cells treated with this series of complexes, at the lowest concentration (1 µM), show a very high survival rate: around 98% and 99 % for complexes, respectively, **9a** and **9d,** about 102 % and 104 % for complexes, respectively, **9b** and **9c**. These last two values, more than one hundred per cent, indicate the reproduction of the cells, probably because placed in a vital and favourable environment to them.

The survival rate of the cells treated with the complexes having a concentration equal to 2.5 µM decreases, but at the same time remains more than fifty per cent: less than 80 % for complexes **9a** and **9d**, around 96% for complex **9c** and more than 100% for complex **9b.**

Compounds	**Survival rate (%)**		
	at 1 µM	**at 2.5 µM**	**at 5 µM**
9a	97.6 ± 1.2	70.7 ± 2.4	40.1 ± 28.4
9b	102.3 ± 1.3	101.5 ± 1.3	101.4 ± 2.3
9c	104.1 ± 0.4	95.7 ± 3.5	91.8 ± 0.3
9d	99.4 ± 2.1	77.2 ± 0.1	74.1 ± 4.5

Table 6: *Percentage values of cell viability and relative standard deviation of complexes **9a-d** at different concentrations.*

At very high concentration (5 µM), a drastic decrease is observed for complex **9a**, the cell viability in fact goes down to 40 %. While for the complexes **9b**, **9c** and **9d** the difference with the values obtained at 2.5 µM is not so neat.

As reported in the Table 6, there is a generic trend: with increasing concentration of the complexes, from 1 µM to 2.5 and 5 µM, the cell viability and therefore the percentage of cells that survive, decrease. In some cases, this reduction is minimal, for example for complex **9b**, where there is almost 100% of cell survival even at higher concentration, or for complex **9c**, whereas for complexes **9a** and **9d**, this diminution is more pronounced.

The results obtained were used to construct a graph of cell viability percentage against complexes **9a-d** concentrations.

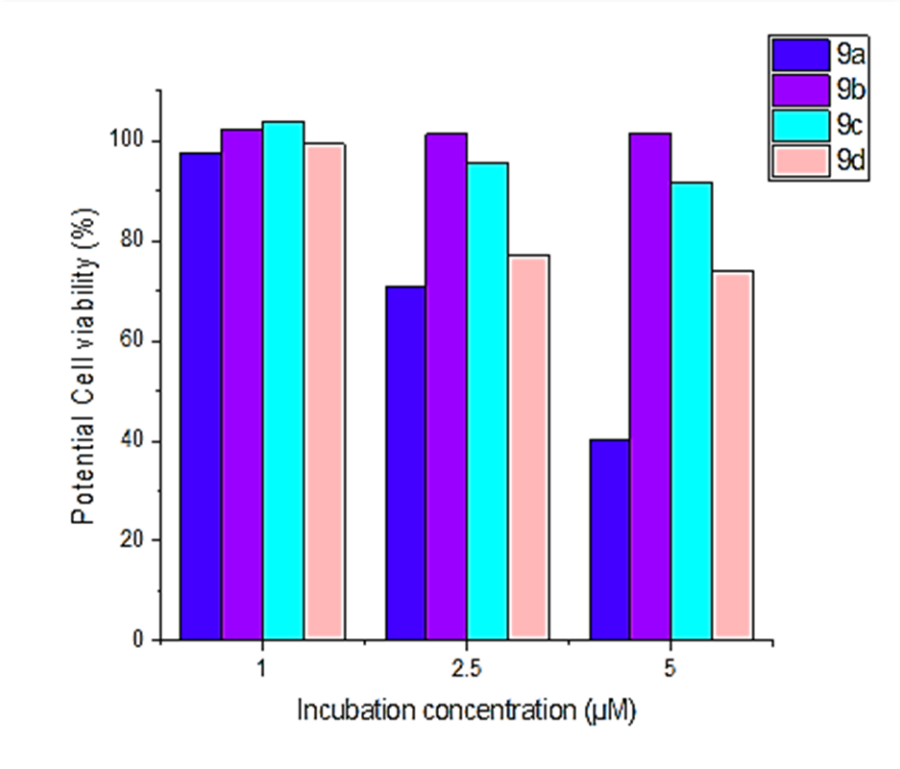

***Figure 24**: Bar graph of potential cell viability (%) of complexes **9a-d** at different concentration.*

*3.6.4- MTT assay of complexes **6a-f***

In Table 7 are reported the values of cell viability, expressed in percentage of the complexes **6a-f.**

In this data set no values of cell viability is equal or greater than 100%, the value nearest to one hundred per cent is that of the complex **6d**, with a survival rate cell of approximately 95 %.

However, the potential cell viability of the cells treated with this series of complexes, at the lowest concentration (1 µM), is high: superior to 80 % for complexes **6a**, **6e** and **6f** and around 74% for complex **6b**.

Compounds	**Survival rate (%)**		
	at 1 µM	**at 2.5 µM**	**at 5 µM**
6a	88.5 ± .2	78.1 ± 3.1	75.9 ± 2.8
6b	73.9 ± 1.3	59.4 ± 1.3	49.3 ± 2.3
6d	94.6 ± 3.5	81.4 ± 2.1	78.8 ± 2.9
6e	84.9 ± 3.9	76.4 ± 1.6	75.4 ± 4.1
6f	83.1± 1.6	70.1 ± 4.1	61.1 ± 7.5

***Table 7**: Percentage values of cell viability and relative standard deviation of complexes **6a-f** at different concentrations.*

As shown in Table 7, the percentage of cells surviving incubated with complexes at concentration of 2.5 µM is about 10% less than those obtained at 1 µM, but, despite this, the values are quite high: ~ 78% for complex **6a** and **6e**, ~ 60 % for complex **6b,** ~70 % for complex **6f** and around 82 % for complex **6d**.

Even in the passage from 2.5 µM to 1 µM, it follows a decrease of 10 % of the survival rate of the cells.

The general tendency adopted by complexes **9a-d**, is also evident in the series **6a-f**: an enhancement of the concentration of the complexes, from 1 µM to 2.5 and 5 µM, resulting in a diminution of the cell viability and therefore of the percentage of surviving cells. But in this case the decrement is constant (about ten per cent) and less marked (see Table 7).

The results obtained were used to construct a graph of cell viability percentage against complexes **6a-f** concentrations.

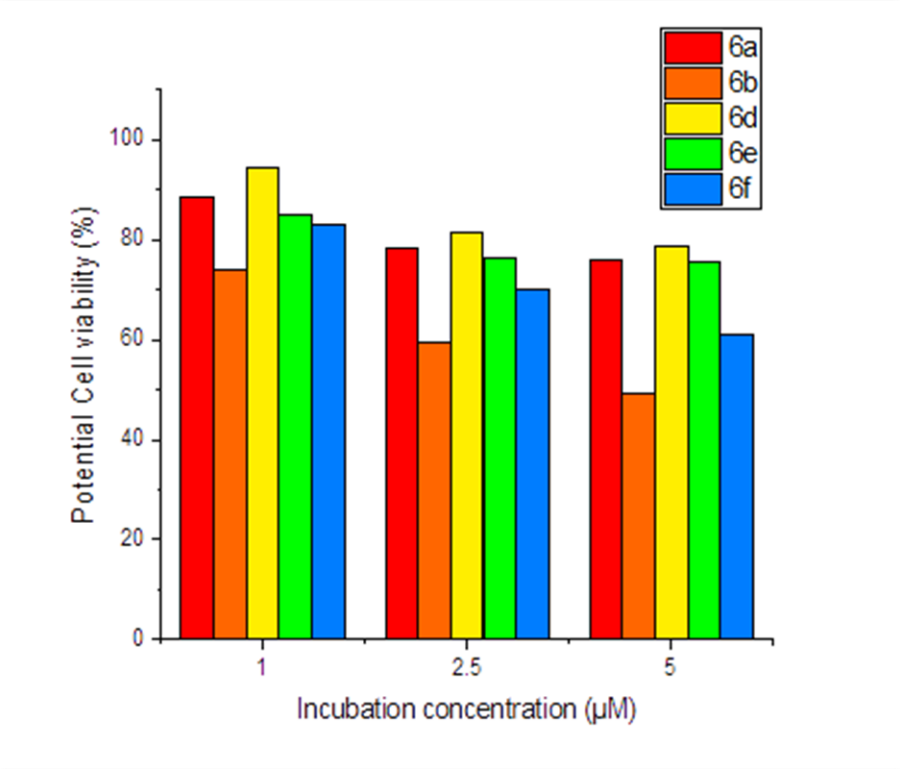

***Figure 25**: Bar graph of potential cell viability (%) of complexes **6a-f** at different concentrations*

To have an overall view of the results obtained with complexes **6a-f** and **9a-d**, the cell viability percentages were plotted against the incubation concentrations and shown in Figure 26.

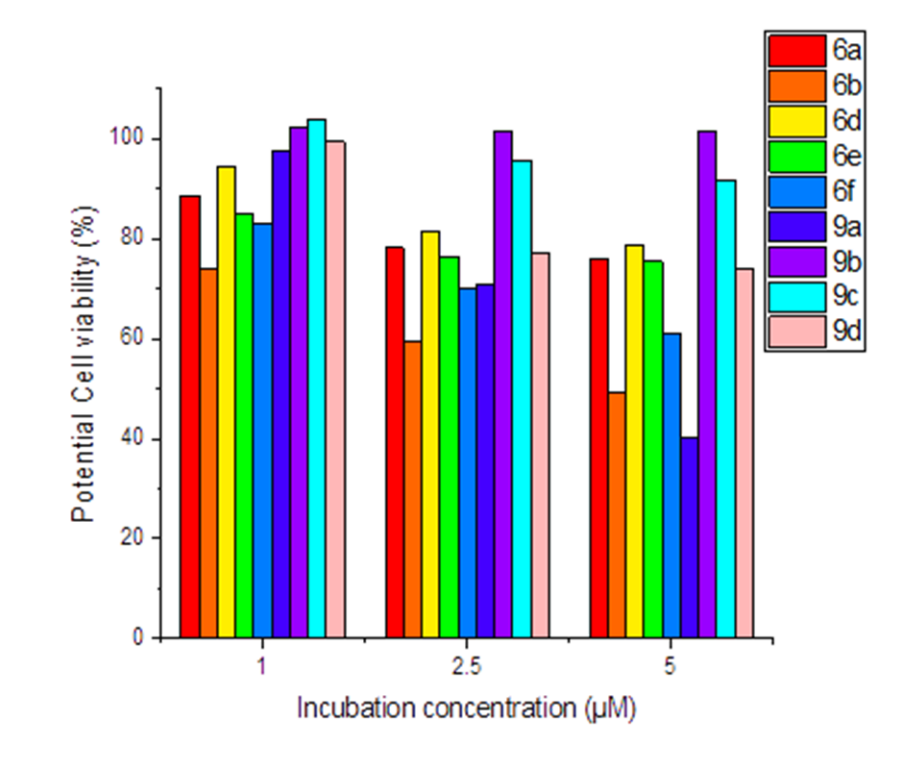

***Figure 26**: Bar graph of potential cell viability (%) of complexes **6a-f** and **9a-d** at different concentration*

4- Conclusion and outlook

Motivated by the intent to find new metal-based fluorophores, whose properties are suitable for the use as near-infrared probe in cellular imaging, in this master thesis five new heteroleptic and one new homoleptic bis(dipyrrinato) Zn (II) complexes were successful synthesised. These complexes are characterized by peculiar and appealing properties.

All complexes emit in the deep-red and near-infrared region ($\lambda > 690$ nm), with local maxima between 680 and 690 nm. Photophysical investigations confirm that the emissive state of both homoleptic and heteroleptic complexes is ligand centred. In homoleptic complexes however, the population of a charge-transfer state might reduce drastically the luminescence in polar solvents. This is not the case for heteroleptic complexes, and this difference results in a highlighted fluorescence also in polar solvents.

Despite the introduction of the tri(ethylene)glycol chain in some complexes, the relative zinc complexes did not show total water-solubility, but suspensions have been mostly observed. Definitely, water-solubility must be improved with the introduction of other groups and therefore functionalizing simple dipyrrins in different way and different positions.

It would be extremely intriguing also introducing specific groups, which can react into the cells, since all complexes show a very good biocompatibility and therefore low cytotoxicity, after 72 hours of incubation with Hela cells (survival rate of more than 70% for 2.5 μM concentration). Further studies will be needed in order to see the localization of these complexes inside the cell.

Even if the new complexes show good stability in cellular environment, it would be interesting test the possibility of a cation exchange in Zn-complexes and pave the way for the synthesis of bis(dipyrrinato)Mg complexes.

5-Experimental section

4.1-Materials and Methods

Analytical Resources and Apparatus

Nuclear Magnetic Resonance Spectroscopy (NMR)

The NMR spectra of compounds described herein were recorded by a Bruker Avance 300 NMR instrument at 300 MHz for ^{1}H NMR and 75 MHz for ^{13}C NMR, a Bruker Avance 500 NMR instrument at 500 MHz for ^{1}H NMR, 125 MHz for ^{13}C NMR.
The NMR spectra were recorded at room temperature in deuterated chloroform commercially available. The reference, used for an easy identification of the peaks, is a table of known impurities in a large number of common deuterated solvents, heavily employed in organometallic laboratories.[154] The chemical shift is displayed in parts per million [ppm], all the following compounds were analysed in deuterated chloroform and the references used were 7.26 ppm for ^{1}H and 77.0 ppm for ^{13}C.
Evaluation of the signals was done according to first order spectra. When describing couplings, the following abbreviations were used: s = singlet, d = doublet, t = triplet, m = multiplet, dd = doublet of doublet, ddd = doublet of doublet of doublet. Coupling constants "*J*" are given in Hertz [Hz] with the largest value first. Couplings are given with their respective number of bindings and binding partners, as far as they could be determined, written as index of the coupling constants.

Mass Spectrometry (MS)

The method used for the measurements was a MALDI -ToF System.
As equipment was employed *Shimadzu Biotech Axima Canfidence* (2.9.3.20110624) (80 mJ, 100 Profiles, 10 shots per profile). The tuning mode was reflectron with a restering of 600 µm of width and 600 µm of high). The matrices employed were: α-Cyano-4-hydroxycinnamic acid (αCHCA), Ferulic acid (FA) and 6-Aza-2-thiothymine (ATT).
For characterisation, the mass to charge ratio (m/z) is plotted against the relative intensity, with the base peak set to "100%".

Photophysics

The absorption spectra were recorded with a *PerkinElmer Lambda* 750 double-beam UV/Vis-NIR spectrometer. The measurements were performed at 20 °C. A correction of spectra was made automatically by the instrument with the absorption of the pure solvent (blank).

Fluorescence was measured with a Jobin-Yvon Fluoromax 4 fluorimeter with a step width of 1 nm. All measurements were performed in quartz cuvettes with septum from Hellma.

Dichlorometane solvent for spectroscopic measurements was supplied by Merck (Uvasol). Photoluminescence quantum yields were determined utilizing as reference $Ru(bpy)_3Cl_2(\cdot 6\ H_2O)$ in air-equilibrated water solution. Lifetime measurements were performed by time-correlated single photon counting method (TCSPC) with a DeltaTime kit for DeltaDiode source on FluoroMax systems, including DeltaHub and DeltaDiode controller. The light sources were NanoLED sources (456 or 570 nm).

MTT [3-(4,5-dimethylthiazol-2-yl)-2,5-diphenyltetrazolium bromide] assay

The cell viability was tested with MTT assay. HeLa cells were seeded in the 96 well plates at the density of $1x10^4$ cells/well in DMEM (Dulbecco's Modified Eagle Medium) supplemented with 10% FCS (Fetal Calf Serum) and 1% penicillin/streptomycin. After 24 h of incubation at 37°C, 5% CO_2, the medium was removed and the cells were treated with various concentrations of the compounds and incubated for 72 h at 37°C, 5% CO_2. Thereafter, 15 µl of the MTT reagent were given in each well. For a positive control, Triton X-100 (1%) was added in some wells before treating them with the MTT reagent. After 3 h of incubation the cells were lysed using the Stop Solution to release the blue-purple formazan. The cell viability was determined by measuring the absorbance of the resulting formazan at 595 nm using a multi-well plate reader.

Chemicals: DMEM cell culture medium, DPBS (Dubecco's Phosphate Buffered Saline, FCS, Penicillin/Streptomycin, Trypsin-EDTA 0.25% acquired from Gilbco Life Technologies. MTT dye and stop solution (Promega), Triton X-100 (Serva).

Devices: Incubator c200 (37 °C, 5% CO_2) (Labotect), Microscope (Leica), Microplate Reader ELx808in (Bio-Tek instruments), Multichannel pipette (Eppendorf), Pipetboy (Brand), Pipettes 200-1000 µL, 50-200 µL, 0.1-10 µL (Eppendorf, Pipetman), Cell culture hood ESCO class II BSC (Biomedis).
Other materials: 96-Well Plates (Cellstar), Eppendorf tubes1,5, 2 mL (Eppendorf), Falcon tubes 15, 50 mL (Cellstar), Cell culture Flasks 250 mL (Cellstar).
Organisms: Hela human cervix carcinom cells.

Solvents and Chemicals

Solvents of p.a. quality (per analysis) were commercially acquired from Sigma Aldrich, Carl Roth or Acros Fisher Scientific and, unless otherwise stated, used without previous purification. Absolutized solvents were either purchased from Carl Roth, Acros or Sigma Aldrich (< 50 ppm H_2O over molecular sieve). All reagents were commercially purchased (from ABCR, Acros, Alfa Aesar or Sigma Aldrich). Unless otherwise stated, they were used without further purification.
Dry solvents were provided from an automatic solvent purification system (SPS) model 800 manuals of MBRAUN.

Preparative Work

Air- and moisture-sensitive reactions were carried out under argon atmosphere in previously baked out apparatuses with standard Schlenk techniques. Liquid reagents and solvents were injected with syringes and stainless-steel cannula of different sizes.

Product Purification

Reaction mixtures were purified by flash chromatography. For the stationary phase of the column, silica gel, produced by Merck (silica gel 60, 0.040 × 0.063 mm, 260 – 400 mesh ASTM), aluminium oxide (neutral), 50-200 µm, 60A, from Acros Organics and sea sand by Riedel de Haën (baked out and washed with hydrochloric acid) were used.

Solvents used were commercially acquired in HPLC-grade and individually measured volumetrically before mixing.

4.2 -Commercially available starting materials

4.2.1- 1H-Pyrrole ***(1)***

The 1*H*-pyrrole chosen for the preparation of the dipyrrins investigated in this thesis was the 2,4-dimethyl-1*H*-pyrrole, supplied by Sigma Aldrich.

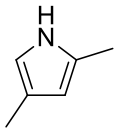

^{1}H-NMR (300 MHz, $CDCl_3$) δ/ppm: 7.62 (1H, s, pyrrole N-H), 6.52 (1H, s, pyrrole H), 6.00 (1H, s, pyrrole H), 2.45 (3 H, s, CH_3), 2.35 (3H, s, CH_3).

4.2.2- Aldehydes

Hereafter the commercially available aldehydes that were used in this thesis are reported. Several other aldehydes were synthesised in the laboratory and their syntheses are described in paragraph 4.3.

Commercially available aldehydes used in this thesis:

- *Mesitylaldehyde* ***(2a)***

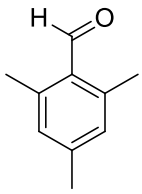

Mesitylaldehyde **(2a)**

^{1}H-NMR (300 MHz, $CDCl_3$) δ/ppm: 9.90 (1H, s, CHO), 7.02 (2H, s,C_{Ar}H), 2.41 (6H, s, -CH_3), 2.35 (3H, s, -CH_3).

- *4-Bromobenzaldehyde* ***(2b)***

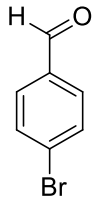

4-Bromobenzaldehyde **(2b)**

^{1}H-NMR (300 MHz, $CDCl_3$) δ/ppm: 9.95 (1H, s, CHO), 7.52 (2H, d,$C_{Ar}H$), 7.15 (2H, d, $C_{Ar}H$)

- *4-Methoxybenzaldehyde* ***(2d)***

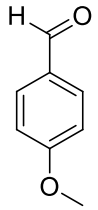

4-Methoxybenzaldehyde **(2d)**

^{1}H-NMR (300 MHz, $CDCl_3$) δ/ppm: 10.02 (1H, s, CHO), 7.54 (2 H, s, $C_{Ar}H$), 7.02 (2H, s,$C_{Ar}H$), 3.81 (3H,s,-OCH_3),

- *2-Naphtaldehyde* ***(2e)***

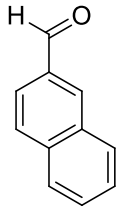

2-Naphthaldehyde **(2e)**

^{1}H-NMR (300 MHz, $CDCl_3$) δ/ppm: 9.95 (1H, s, CHO) 7.95 (2H, m,$C_{Ar}H$), 7.85 (1H, m,$C_{Ar}H$), 7.83 (2H, m,$C_{Ar}H$), 7.53 (2H, s,$C_{Ar}H$),

4.3 -Synthesis of precursors and intermediates.

Synthesized aldehydes:

- *(rac)-4-Formyl [2.2] paracylophane* ***(2c)***

To a solution of [2.2]paracyclophane (14.6 g, 70.0 mmol, 1.00 equiv.) in 600 mL of dichloromethane at 0 °C was added 15.4 mL of titanium tetrachloride (26.6 g, 140 mmol, 2.00 equiv.) followed 6.42 mL of 11-dichloromethylether (8.16 g, 71.0 mmol, 1.05 equiv.). After stirring for 15 min at 0 °C, the mixture was stirred for 16 h at room temperature. The mixture changes colour from clear to yellow to black. The black reaction mixture was poured on ice and stirred for 2 h again changing its colour to yellow. The organic layer was extracted with dichloromethane (3 x 200 mL). The combined organic layers were washed with brine (300 mL), dried over Na_2SO_4 and the solvent was removed under reduce pressure. The crude compound was filtered (silica, dichloromethane) to remove residual titanium salts and recrystallized from *n*-hexane to yield 14.8 g of **2c** (62.8 mmol, 90%) as a white solid.

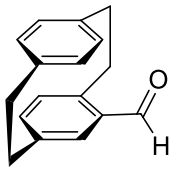

2c

^{1}H-NMR (400 MHz, $CDCl_3$) δ/ppm: 9.95 (1H, s, CHO), 7.02 (1 H, d, J=1.9 Hz), 6.73 (1H, dd, J=7.8, 1.8 Hz), 6.61-6.55 (2 H, m), 6.50 (1 H, dd, J=7.8, 1.9 Hz), 6.43 (1H, dd, J=7.8, 1.8 Hz), 6.38 (1 H, dd, J= 7.8, 1.8 Hz), 4.11 (1 H, ddd, J= 13.0, 9.9, 1.7 Hz), 3.35-3.14 (3 H, m), 3.14-2.89 (4 H, m).

^{13}C-NMR (101 MHz, $CDCl_3$) δ/ppm: 192.02 (CHO), 143.30 (C_{quat}), 140.73 (C_{quat}), 139.57 (C_{quat}), 139.52 (C_{quat}), 138.16 (+,C_{Ar}H), 136.64 (C_{quat}), 136.43 (+,C_{Ar}H), 136.20 (+,C_{Ar}H), 133.34 (+,C_{Ar}H), 133.00 (+,C_{Ar}H), 132.44 (+,C_{Ar}H), 132.23 (+,C_{A}rH), 35.34 (-,CH_2), 35.23 (-,CH_2), 35.06 (-,CH_2), 33.71 (-, CH_2).

- *4- (2´phenyl-ethynyl)-benzaldehyde* ***(2g)***

In a three-neck flask, were solved ethynylbenzene (1.08 g, 1.16 mL, 11 mmol, 1.30 equiv.) and 4-bromobenzaldehyde **(2a)** (1.50 g, 8.1 mmol, 1.00 equiv.) in *N*-propan-2-ylpropan-2-amine (DIPA) (25.0 mL), The reaction was carried out under argon atmosphere at room temperature for 12 hours and then was heated at 80 °C for 9 hours. As catalyst was used Pd $(PPh_3)_2Cl_2$ (285 mg, 405 µmol, 0.0500 equiv.) and as co-catalyst CuI (309 mg, 1.6 mmol, 0.200 equiv.). The progress of the reaction was checked with TLC using as eluent dichloromethane and cyclohexane (70:30). The solvent was removed under reduce pressure. The crude residue was purified *via* column chromatography, packed with silica, using as eluent mixture dichloromethane:cyclohexane (70:30). The target compound **(2g)** was isolated as a light brown solid (4-(2-phenylethynyl) benzaldehyde with a yield of 47 % ,787 mg (3.8 mmol).

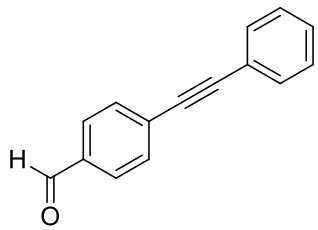

^{1}H-NMR (300 MHz, $CDCl_3$) δ/ppm: 9.85 (1H, s, CHO), 7.75 (2 H, d, $C_{Ar}H$), 7.55 (2H, d, $C_{Ar}H$), 7.45(2 H, d, $C_{Ar}H$), 7.28 (2 H, d, $C_{Ar}H$).

- *2,6-dimethyl-4-bromobenzaldehyde*

In a three-neck flask, 5-bromo-2-iodo-1,3-dimethylbenzene (2.00 g, 6.4 mmol, 1.00 equiv.) was solved in 10 ml of dry THF. The reaction was conducted in dry glassware under inert atmosphere (Ar). The solution was cooled down to -15 °C, then Isopropylmagnesium Chloride (992 mg, 4.82 mL, 9.6 mmol, 1.50 equiv.) was added and the reaction was left stirring for 1.5 hours. Afterwards, Dimethylformamide (1.41 g, 1.49 mL, 19 mmol, 3.00 equiv.) was added and the reaction was left stirring at -15 °C for additional 1.5 hours and then it was left stirring at room temperature overnight. The reaction mixture was poured into a separation funnel and the organic layer was washed successively with HCl 1 M, extracted with ethyl acetate, and washed with brine. The organic layers were collected and were dried over $MgSO_4$.The mixture was filtered through a glass funnel and the solvent was evaporated under reduced pressure. The crude residue was purified with a plug of silica, using dichloromethane as eluent. The target compound was isolated as a light orange solid in 54% yield.

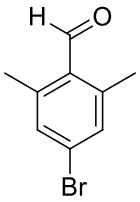

^{1}H-NMR (300 MHz, $CDCl_3$) δ/ppm: 10.5 (1H, s, CHO), 7.55 (2 H, d, $C_{Ar}H$), 2.52 (6H, s, $-CH_3$).

- 4-[4’-(2’’-(2’’’-methoxyethoxy) ethoxy) ethoxy phenyl] benzaldehyde **(2f).**

Into a dried round-bottom flask, the solvent mixture was placed, 1,4-dioxane (16.0 mL) and water (5.00 mL). To be sure that the solvents were perfectly degassed, xaborolan-2’’-yl 2’’’-[2’’’’-(2’’’’’-methoxyethoxy) ethoxy] ethyl ester **5d** (300 mg, 828 µmol, the "Freeze-pump thaw cycling" process was performed twice. Then 4-bromobenzaldehyde **2a** (153 mg, 828 µmol, 1.00 equiv.) and tetramethyl-1,3,2’-dio 1.00 equiv.) were solved into the solvent mixture. Afterwards, tetrakis(triphenylphosphine)palladium, Pd $(PPh_3)_2$ (47.8 mg, 41 µmol, 0.0500 equiv.) and Na_2CO_3 (132 mg, 1.2 mmol, 1.50 equiv.) were added and the reaction was refluxed for 6 hours at 80 °C and left stirring overnight at room temperature. After complete conversion of the starting materials, monitored by TLC, using dichloromethane as eluent, the reaction was quenched by addition of brine. The reaction mixture was poured into a separation funnel and the water phases was extracted with ethyl acetate. The organic phases were collected and were dried over $MgSO_4$. The mixture was filtered, and the solvent was evaporated under reduced pressure. The crude residue was purified *via* column chromatography, packed with silica, using a gradient eluent made of dichloromethane and 1% of methanol. The target compound **2f** (first fraction) was isolated as a yellow oil, with 87 % of yield.

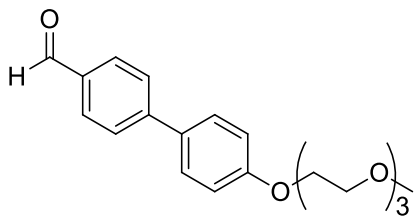

2f

^{1}H-NMR (300 MHz, $CDCl_3$) δ/ppm: 9.98 (1H, s, CHO), 7.85 (2 H, d, $C_{Ar}H$), 7.75 (2H, d, $C_{Ar}H$), 7.55 (2 H, d, $C_{Ar}H$), 7.35 (2 H, d, $C_{Ar}H$), 7.15 (2 H, d, $C_{Ar}H$), 3.99 (2H, m, -CH_2), 3.39, (2H, m, -CH_2), 3.3-3.2 (6H, m, -CH_2), 3.15 (2H, m, -CH_2),3.00 (3 H, s, -CH_3).

*- 2-[2'-(2''-methoxyethoxy)ethoxy]ethyl methanesulfonate **5b***

In a round bottom flask, under argon atmosphere and constant stirring, (5.00 g, 30 mmol, 1.00 equiv.) of 2-[2'-(2''-methoxyethoxy) ethoxy] ethanol **(5a)** was dissolved in dry dichloromethane (20.0 mL). After cooling down to 0 °C, Triethylamine (4.31 g, 5.91 mL, 43 mmol, 1.40 equiv.) was added, followed by methanesulfonyl chloride (3.49 g, 3.04 mL, 30 mmol, 1.00 equiv.). The solution was stirred at 0 °C for 5 minutes and at room temperature for 2 hours. The reaction mixture was washed with 15 mL of water, 20 ml of HCl 1 M, 25 ml of $NaHCO_3$-solution 10 % and 25 mL of brine. The organic phases were collected and were dried over $MgSO_4$. The mixture was filtered, and the solvent was evaporated under reduced pressure. The target compound **5b** was isolated as a light-yellow oil, with a yield of 78%, 5.73 g (24 mmol).

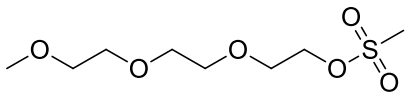

5b

.

^{1}H-NMR (300 MHz, $CDCl_3$) δ/ppm: 3.99 (2H, m, $-CH_2$), 3.39, (2H, m, $-CH_2$), 3.3-3.2 (6H, m, $-CH_2$), 3.15 (2H, m, $-CH_2$), 3.10 (3 H, s, $-CH_3$), 2.7 (3 H, s, $-CH_3$).

- *Tetramethyl-1,3,2-dioxaborolan-2'-yl 2''- [2'''-(2''''-methoxyethoxy) ethoxy] ethyl ester* ***5c***

In a three-neck flask, methanesulfonic acid 2-[2'-(2''-methoxyethoxy)ethoxy]ethyl ester **5b** (1.10 g, 4.5 mmol, 1.00 equiv.) and 4-(4',4'',5,5'-tetramethyl-1,3,2-dioxaborolan-2''-yl)phenol (1.00 g, 4.5 mmol, 1.00 equiv.) were solved into *N,N*-dimethylformamide (30.0 mL). Then was added potassium carbonate (11.3 g, 82 mmol, 18.0 equiv.) and heat the mixture until 100 °C. The reaction was refluxed for 8 hours and left stirring at room temperature over the weekend. The reaction was quenched with dichloromethane (10 mL) and the precipitate was filtered off. The filtrate was evaporated under reduce pressure and the obtained oil was purify with a plug of Silica, using dichloromethane as eluent. The target compound **5c** was isolated as a light orange oil in 46% yield.

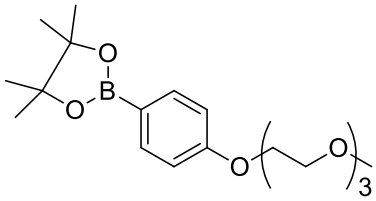

5c

^{1}H-NMR (300 MHz, $CDCl_3$) δ/ppm: 7.55 (2 H, d, $C_{Ar}H$), 7.35 (2 H, d, $C_{Ar}H$), 3.99 (2H, m, $-CH_2$), 3.39, (2H, m, $-CH_2$), 3.3-3.2 (6H, m, $-CH_2$), 3.15 (2H, m, $-CH_2$),3.00 (3 H, s, $-CH_3$), 1.45 (12 H, s, $-CH_3$).

4.4- Synthesis of plain dipyrrins.

The synthesis of the plain dipyrrins was performed following the procedure already described in the literature.[106]

- *Synthesis of (2Z)-2'-[(3,5-dimethyl-1H-pyrrol-2''-yl)-mesityl-methylene]-3',5''-dimethyl-pyrrole* ***(3a)****.*

In a round-bottom flask, under argon atmosphere and constant stirring, 2,4-dimethyl-1*H*-pyrrole **(1)** (1.93 g, 2.08 mL, 20 mmol, 2.50 equiv.) and 2,4,6-trimethylbenzaldehyde **(2a)** (1.20 g, 8.1 mmol, 1.00 equiv.) were dissolved in dichloromethane (15.0 mL), and hydrochloric acid 0,2 M (20.0 mL) was added. The reaction was carried out at room temperature, with constant stirring for 24 hours. After complete conversion of the starting material, monitored with TLC, using dichloromethane as eluent, 2,3,5,6-Tetrachlorocyclohexa-2,5-diene-1,4-dione (p-Chloranil) (2.19 g, 8.9 mmol, 1.10 equiv.) was added and the reaction was left stirring for additional 7 hours. The end of the reaction was checked *via* TLC analysis. The reaction mixture was quenched with 15 mL of water and washed with 10 mL of DCM; the organic layers were then washed with brine three times. The organic phases were collected, dried over $MgSO_4$ anhydrous, filtered and evaporated under vacuum.
The obtained crude product was purified *via* column chromatography, packed with alumina, using a gradient eluent made of dichloromethane methanol (1% MeOH).
The target compound **3a** was isolated as a black solid in 68% yield (1.75 g, 5.5 mmol).

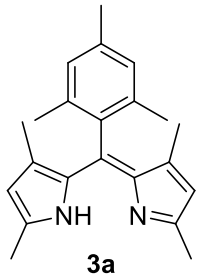

3a

Black powder

Yield: 68 %

^{1}H-NMR (300 MHz, $CDCl_3$) δ/ppm: 7.02 (2H, s,$C_{Ar}H$), 6.00 (2 H, s, H-pyrrole), 2.41 (6H, s, -CH_3), 2.35 (3H, s, -CH_3), 2.12 (6H, s, pyrrole-CH_3), 1.45 (6H, s, pyrrole-CH_3).

- *Synthesis of 2-[(3',5'-dimethyl-1'H-pyrrol-2'-yl)-(4''-bromophenyl)-methylene]-3,5-dimethylpyrrole* ***(3b).***

In a round bottom flask, under argon atmosphere and constant stirring, 2,4-dimethyl-1*H*-pyrrole **(1)** (1.29 g, 14 mmol, 2.50 equiv.) and 4-bromobenzaldehyde **(2b)** (1.00 g, 5.4 mmol, 1.00 equiv.) were dissolved in dichloromethane (15.0 mL), hydrochloric acid 0,2 M (20.0 mL) was added. The reaction was carried out at room temperature, with constant stirring for 24 hours. After complete conversion of the starting material, monitered with TLC, using as eluent dichloromethane, 2,3,5,6-Tetrachlorocyclohexa-2,5-diene-1,4-dione (p-Chloranil) (2.19 g, 8.9 mmol, 1.10 equiv.) was added and was left stirring for additional 7 hours. The end of the reaction was checked *via* TLC analysis. The reaction mixture was quenched with 15 mL of water and washed with 10 mL of DCM and the organic layers were then washed with brine three times. The organic phases were collected, dried over $MgSO_4$ anhydrous, filtered and evaporated under vacuum.

The obtained crude product was purified *via* column chromatography, packed with alumina, using gradient eluent made of dichloromethane methanol (1% MeOH).

The target compound **3b** was isolated as a black solid in 65% yield (1.25 g, 3.5 mmol).

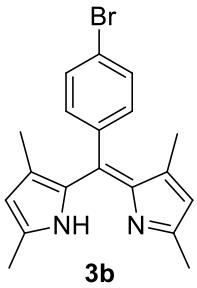

3b

Black powder
Yield 65%

^{1}H-NMR (300 MHz, $CDCl_3$) δ/ppm: 7.52 (2H, d,C_{Ar}H), 7.15 (2H, d, C_{Ar}H), 5.95 (2 H, s, H-pyrrole), 2.40 (6H, s, pyrrole-CH_3), 1.45 (6H, s, pyrrole-CH_3).

- *Synthesis of **3c***

In a round bottom flask, under argon atmosphere and constant stirring, 2,4-dimethyl-1H-pyrrole **(1)** (1.01 g, 11 mmol, 2.50 equiv.) and rac-4-Formyl[2.2]paracyclophane **(2c)** (1.00 g, 4.2 mmol, 1.00 equiv.), were solved in dichloromethane (15.0 mL), and was added hydrochloric acid 0,2 M (20.0 mL). The reaction was carried out at room temperature, with constant stirring for 48 hours. After complete conversion of the starting material, monitored with TLC, using as eluent Dichloromethane, was added 2,3,5,6-Tetrachlorocyclohexa-2,5-diene-1,4-dione (p-Chloranil) (2.19 g, 8.9 mmol, 1.10 equiv.) and was left stirring for 48 hours. The end of the reaction was checked via TLC analysis, using DCM as eluent. The reaction mixture was quenched with 15 mL of water and washed with 10 mL of DCM; the organic layers were then washed with BRINE three times. The organic phase was collected, dried over $MgSO_4$ anhydrous, filtered and evaporated under vacuum. The obtained crude product was purified *via* column chromatography, packed with alumina, using dichloromethane as eluent. The target compound was isolated as a black solid in 50% yield (0.858 g, 2.1 mmol).

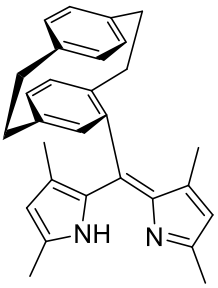

3c

Black powder
Yield: 50 %

The **^{1}H-NMR** spectra are very difficult to understand, and not so clear, because the multiplets are very bumpy. This is probably due to the presence of different diastereoisomers that were formed from the racemic mixture. Therefore, mass spectrometry was used to identify the target compound.

HRMS m/z ($C_{29}H_{30}N_2$): 407.24 (calculated), 407.91 (found).

- *Synthesis of **3d***

In a three-neck flask, (400 mg, 1.3 mmol, 1.00 equiv.) of (2Z)-2-[(3,5-dimethyl-1H-pyrrol-2-yl)-mesityl-methylene]-3,5-dimethyl-pyrrole **3a** were solved in a mixture of chloroform (30.0 mL) and methanol (30.0 mL). The reaction mixture was cooled until 0°C. Then, were added Iodine (638 mg, 2.5 mmol, 2.00 equiv.) and iodic acid (442 mg, 2.5 mmol, 2.00 equiv.) and was left stirring at 0°C for 1.5 hours. After complete conversion of the reagent, (two hours) checked with TLC, using dichloromethane as eluent, were added 50 ml of chloroform. The reaction mixture was poured into a separation funnel and the organic layer was washed successively with a saturated solution of Na_2SO_3 and 30 mL of water. The organic layers were collected and were dried by the addition of $MgSO_4$. The mixture was filtered through a glass funnel and the solvent was evaporated under reduced pressure. The crude residue was recrystallized from dichloromethane/methanol at -30 °C, using an ice/methanol (60:40) bath. The target compound **3d** was isolated as a dark red solid with 87 % of yield (624 mg, 1.1 mmol).

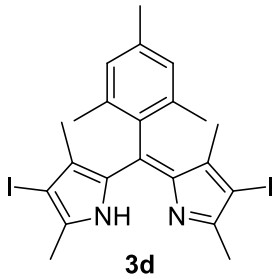

3d

Dark red powder

Yield: 87 %

^{1}H-NMR (300 MHz, $CDCl_3$) δ/ppm: 7.02 (2H, s,$C_{Ar}H$), 2.41 (6H, s, $-CH_3$), 2.35 (3H, s, $-CH_3$), 2.12 (6H, s, pyrrole-CH_3), 1.45 (6H, s, pyrrole-CH_3).

4.5-Synthesis of π-expanded dipyrrins.

The π-expansion of the dipyrrins was obtained *via* a Knoevenagel condensation using the general procedure found in literature.[106]

- *Synthesis of **4b***

In a dried three-neck flask, under argon atmosphere and constant stirring, (300 mg, 942 µmol, 1.00 equiv.) of (2Z)-2'-[(3,5-dimethyl-1*H*-pyrrol-2''-yl)-mesityl-methylene]-3',5'-dimethyl-pyrrole **3a** and (939 mg, 5.7 mmol, 6.00 equiv.) of 3,4-dimethoxybenzaldehyde **2d**, were solved in 10 mL of toluene. Then were added dropwise 500 µL of piperidine and 500 µL of glacial acetic acid. The reaction was carried out at 100 °C, (reflux), for 5 hours and was left stirring at room temperature overnight. The reaction mixture was poured into a separation funnel and the organic layer was washed successively with 10 mL of H_2O, 30 ml of DCM and brine. The organic phases were collected and were dried over of $MgSO_4$. The mixture was filtered, and the solvent was evaporated under reduced pressure. The crude residue was purified *via* column chromatography, packed with alumina, using dichloromethane and 2% of methanol as eluent. The target compound, **4b**, first fraction, was isolated as a violet powder, with 30 % of yield.

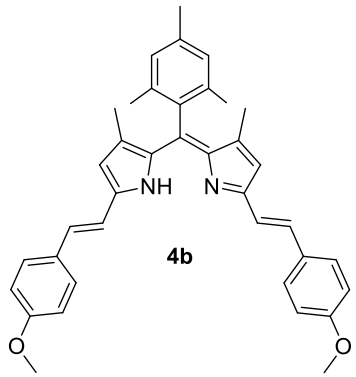

4b

Violet powder

Yield: 30%

^{1}H-NMR (300 MHz, $CDCl_3$) δ/ppm: 7.54 (4 H, m, $C_{Ar}H$), 7.02 (2H, s,$C_{Ar}H$), 6.95 (2 H, m, -CH), 6.78 (2H,m, -CH), 6.55 (4 H, m, $C_{Ar}H$), 6.00 (2 H, s, H-pyrrole), 3.85 (3H, s, --OCH_3), 3.81 (3H,s,-OCH_3), 2.41 (6H, s, -CH_3), 2.35 (3H, s, -CH_3), 1.45 (6H, s, pyrrole-CH_3).

- *Synthesis of **4d***

In a dried three-neck flask, 300 mg, 942 µmol, 1.00 equiv. of (2Z)-2'-[(3,5-dimethyl-1*H*-pyrrol-2''-yl)-(2''',4,6-trimethylphenyl)methylidene]-3',5'-dimethylpyrrole **3a** and (883 mg, 5.7 mmol, 6.00 equiv.) naphthalene-2-carbaldehyde **2e** were solved in 10 mL of toluene. Then, were added dropwise 500 µL of piperidine and 500 µL of acetic acid. The reaction was carried out at 100 °C, with reflux, for 8 hours and was left stirring overnight at room temperature. The reaction mixture was quenched with 10 ml of H_2O, then the solvent was evaporated under reduced pressure. The crude residue was purified *via* column chromatography, packed with alumina, using dichloromethane and cyclohexane (50:50) as eluent. The target compound **4d** was isolated as a violet powder with 40 % of yield.

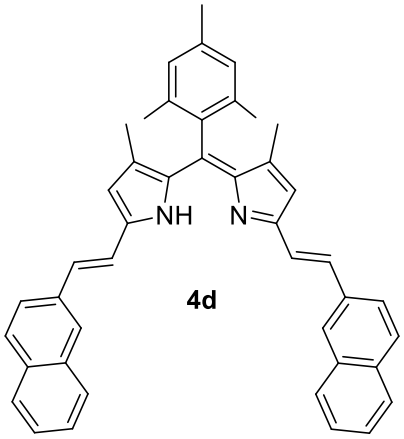

4d

^{1}H-NMR (300 MHz, $CDCl_3$) δ/ppm: 7.95 (4H, m,C_{Ar}H), 7.85 (4H, m,C_{Ar}H), 7.83 (2H, m,C_{Ar}H), 7.53 (2H, s,C_{Ar}H), 7.02 (2H, s,C_{Ar}H), 6.00 (2 H, s, H-pyrrole), 2.41 (6H, s, -CH_3), 2.35 (3H, s, -CH_3), 2.12 (6H, s, pyrrole-CH_3), 1.45 (6H, s, pyrrole-CH_3).

HRMS m/z: 594.79 (calculated), 593.87 (founded).

4.6- Synthesis of dipyrrins with glycolic chain

- *Synthesis of **4f***

Also in this case was performed a Knoevenagel condensation, according to general procedure found in literature.[106]

In a three-neck flask, under argon atmosphere, 400 mg (1.1 mmol, 1.00 equiv.) of (2Z)-2'-[(3,5-dimethyl-1*H*-pyrrol-2''-yl)-mesityl-methylene]-3',5'-dimethyl-pyrrole **3a** and 582 mg (1.7 mmol, 1.50 equiv.) of **2f** were solved in 10 mL of toluene. Then, were added dropwise, 500 µL of piperidine and 500 µL of glacial acetic acid.

The reaction was carried out at 80 °C, (at reflux), for 15 hours and at room temperature for 24 hours. The reaction mixture was poured into a separation funnel and the organic layer was washed with brine. The aqueous layers were recombined and extracted with DCM, meanwhile the organic phases were collected and dried over $MgSO_4$.The mixture was filtered, and the solvent was evaporated under reduced pressure. The crude residue was purified *via* column chromatography, using first cyclohexane/dichloromethane (60:40) as eluent mixture, then only dichloromethane, and at the end dichloromethane with 2% of methanol and 0.2 % of triethylamine. The target compound **2f** was obtained with 35 % of yield.

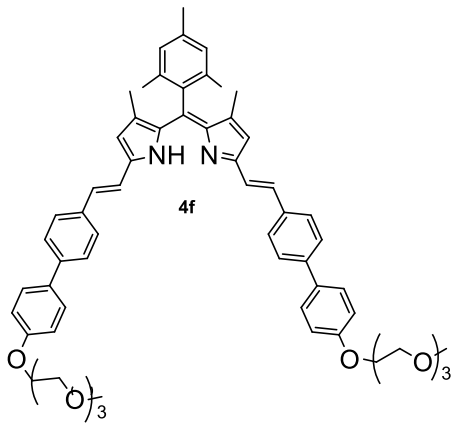

^{1}H-NMR (300 MHz, $CDCl_3$) δ/ppm: 7.85 (4 H, m, $C_{Ar}H$), 7.75 (4H, m, $C_{Ar}H$), 7.55 (4 H, m, $C_{Ar}H$), 7.52 (2H, d,$C_{Ar}H$), 7.35 (4 H, m, $C_{Ar}H$), 7.15 (2 H, d, $C_{Ar}H$), 7.10 (2H, d, $C_{Ar}H$), 6.98 (2 H, m, -CH), 6.88 (2H,m, -CH), 5.95 (2 H, s, H-pyrrole), 3.99 (2H, m, -CH_2), 3.39, (2H, m, -CH_2), 3.3-3.2 (6H, m, -CH_2), 3.15 (2H, m, -CH_2),3.00 (3 H, s, -OCH_3), 1.45 (6H, s, pyrrole-CH_3).

- *Synthesis of **4g***

In a round bottom flask, 523 mg (1.5 mmol, 1.00 equiv.) of **2f** and 361 mg (3.8 mmol, 2.50 equiv.) of 2,4-dimethyl-1*H*-pyrrole (**1)**, were solved into 15 mL of dichloromethane and then was added a solution of hydrogen chloride 0.02 M (20.0 mL). The reaction mixture was left stirring for 48 hours room temperature. After complete conversion of the starting material, checked with TLC, using DCM as eluent, was added 2,3,5,6-Tetrachlorocyclohexa-2,5-diene-1,4-dione (*p*-Chloranil) (410 mg, 1.7 mmol, 1.10 equiv.) and was left stirring for 24 hours at room temperature. The reaction mixture was poured into a separation funnel and the organic layer was washed with brine. The aqueous layers were recombined and extracted with DCM meanwhile the organic layers were collected and were dried over $MgSO_4$. The mixture was filtered, and the solvent was evaporated under reduced pressure. The crude residue was purified *via* column chromatography, using dichloromethane with 1% of methanol as eluent. The target compound **4g** was isolated as a black solid, with 45 % of yield, (349 mg, 679 µmol).

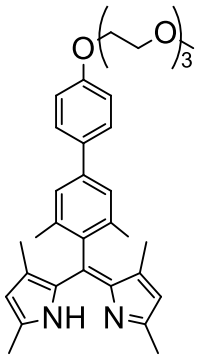

4g

^{1}H-NMR (300 MHz, $CDCl_3$) δ/ppm: 7.85 (2 H, m, $C_{Ar}H$), 7.75 (2H, m, $C_{Ar}H$), 7.55 (2 H, m, $C_{Ar}H$), 7.35 (2 H, m, $C_{Ar}H$), 7.15 (2 H, m, $C_{Ar}H$), 6.00 (2 H, s, H-pyrrole), 3.99 (2H, m, $-CH_2$), 3.39, (2H, m, $-CH_2$), 3.3-3.2 (6H, m, $-CH_2$), 3.15 (2H, m, $-CH_2$),3.00 (3 H, s, $-OCH_3$), 2.12 (6H, s, pyrrole-CH_3), 1.45 (6H, s, pyrrole-CH_3).

4.7- Synthesis of Zn-complexes

General procedure:[106]

In a round bottom flask, two different kind of functionalized dipyrrin (1 equiv. each), were dissolved in 10 mL of dichloromethane and 5 mL of methanol. Then zinc diacetate (1 equiv.) was added and the reaction was left stirring overnight at room temperature. The solvent was removed under reduce pressure and the crude residue was purified by flash chromatography on alumina, using dichloromethane as eluent.

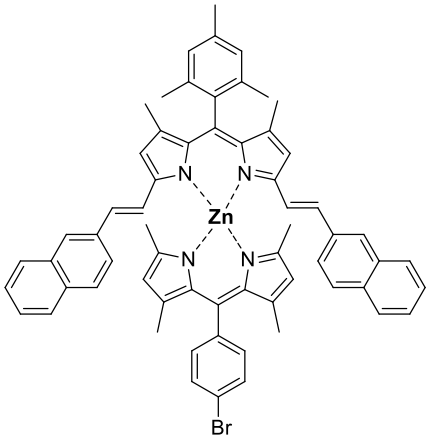

6a

^{1}H-NMR (300 MHz, $CDCl_3$) δ/ppm: 7.95 (4H, m,$C_{Ar}H$), 7.85 (4H, m,$C_{Ar}H$), 7.83 (2H, m,$C_{Ar}H$), 7.53 (2H, s,$C_{Ar}H$), 7.52 (2H, d,$C_{Ar}H$), 7.15 (2H, d, $C_{Ar}H$),7.02 (2H, s,$C_{Ar}H$), 6.00 (2 H, s, H-pyrrole), 5.95 (2 H, s, H-pyrrole) 2.45 (6H, s, -CH_3), 2.40 (6H, s, pyrrole-CH_3), 2.35 (3H, s, -CH_3), 2.12 (6H, s, pyrrole-CH_3), 1.40 (6H, s, pyrrole-CH_3), 1.45 (6H, s, pyrrole-CH_3).

^{13}C-NMR (300 MHz, $CDCl_3$) δ/ppm:148.00, 143.65, 141.80, 141.10, 140.40, 139.95, 137.80, 137.70, 135.90, 133.64, 133.35, 133.24, 132.00, 131.80, 128.60, 127.80, 127.50,127.10, 126.40, 126.10, 126.00,125.10, 124.50, 124.40, 122.80, 122.30, 117.8, 113.50, 108.10, 107.43, 21.90, 20.1, 15.78, 13.84, 13.71.

HRMS MALDI m/z: 1013.1500 (calculated), 1014.9022 (found).

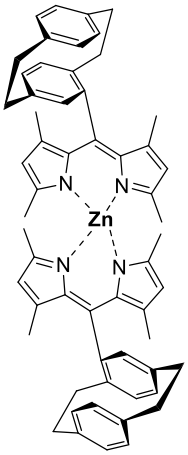

6b

HRMS m/z ($C_{51}H_{54}N_4Zn$): 876.51 (calculated), 883 (found).

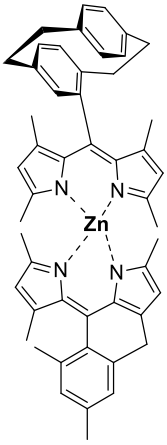

6c

HRMS m/z ($C_{51}H_{54}N_4Zn$): 788.40 (calculated), 787.44 (found).

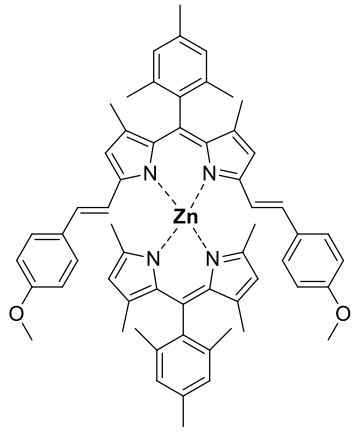

6d

^{1}H-NMR (300 MHz, $CDCl_3$) δ/ppm: 7.54 (4 H, m, $C_{Ar}H$), 7.02 (2H, s,$C_{Ar}H$), 6.95 (2 H, m, -CH), 6.78 (2H,m, -CH), 6.55 (4 H, m, $C_{Ar}H$), 6.00 (2 H, s, H-pyrrole), 5.95 (2 H, s, H-pyrrole ,3.85 (3H, s, --OCH_3), 3.81 (3H,s,-OCH_3), 2.45 (6H, s, -CH_3), 2.41 (6H, s, -CH_3), 2.35 (3H, s, -CH_3), 2.30 (3H, s, -CH_3), 2.25 (6H, s, pyrrole-CH_3), 2.12 (6H, s, pyrrole-CH_3), 1.45 (6H, s, pyrrole-CH_3).

^{13}C-NMR (300 MHz, $CDCl_3$) δ/ppm: 148.01, 143.64, 141.85, 140.24, 139.94, 137.88, 137.74, 137.41, 135.90, 130.25, 129.80, 127.81, 127.50, 124.40, 126.00, 125.50, 124.50, 124.30, 123.80, 121.50, 114.25, 113.54, 108.10, 107.41, 25.50, 25.41, 24.30, 22.20, 20.14, 19.35, 19.10.

HRMS MALDI m/z: 936.5645 (calculated), 936.4748 (found).

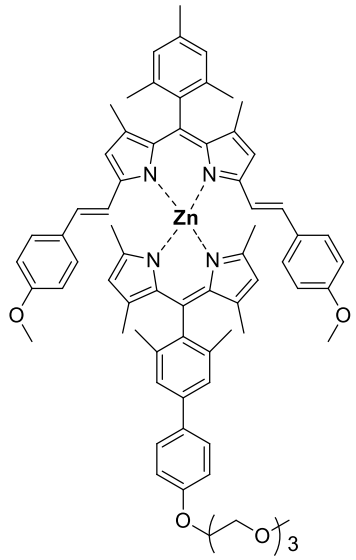

6e

^{1}H-NMR (300 MHz, $CDCl_3$) δ/ppm: 7.85 (2 H, m, $C_{Ar}H$), 7.75 (2H, m, $C_{Ar}H$), 7.55 (2 H, m, $C_{Ar}H$),7.54 (4 H, m, $C_{Ar}H$), 7.35 (2 H, m, $C_{Ar}H$), 7.02 (2H, s,$C_{Ar}H$), 6.95 (2 H, m, -CH), 6.78 (2H,m, -CH), 6.55 (4 H, m, $C_{Ar}H$), 6.00 (2 H, s, H-pyrrole), 5.95 (2 H, s, H-pyrrole), 3.99 (2H, m, $-CH_2$), 3.85 (6H, s, --OCH_3),), 3.39, (2H, m, $-CH_2$), 3.3-3.2 (6H, m, $-CH_2$), 3.15 (2H, m, $-CH_2$),3.0 (3 H, s, $-CH_3$), 2.41 (6H, s, $-CH_3$), 2.12 (6H, s, pyrrole-CH_3), 1.45 (6H, s, pyrrole-CH_3). 1.40 (6H, s, pyrrole-CH_3).

^{13}C-NMR (300 MHz, $CDCl_3$) δ/ppm: 148.20, 145.64, 144.65, 143.98, 143.84, 143.78, 141.47, 140.24, 139.94, 137.88, 137.74, 137.41, 135.90, 131.24, 129.80, 126.81, 126.50, 124.40, 126.00, 125.50, 124.50, 124.30, 123.74, 121.50,115.98, 115.20, 114.25, 113.54, 108.10, 107.41, 25.50, 25.41, 24.30, 22.20, 21.90,20.14, 19.35, 19.10.

HRMS MALDI m/z: 1132.7687 (calculated), 1331.8744 (found).

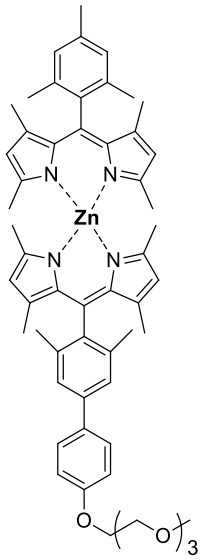

6f

^{1}H-NMR (300 MHz, $CDCl_3$) δ/ppm: 7.85 (2 H, m, $C_{Ar}H$), 7.75 (2H, m, $C_{Ar}H$), 7.55 (2 H, m, $C_{Ar}H$), 7.35 (2 H, m, $C_{Ar}H$), 7.02 (2 H, m, $C_{Ar}H$), 6.00 (2 H, s, H-pyrrole), 5.95 (2 H, s, H-pyrrole), 3.99 (2H, m, $-CH_2$), 3.39, (2H, m, $-CH_2$), 3.3-3.2 (6H, m, $-CH_2$), 3.15 (2H, m, $-CH_2$),3.00 (3 H, s, $-CH_3$), 2.41 (6 H, s, $-CH_3$), 2.25 (6H, s, pyrrole-CH_3), 2.12 (6H, s, pyrrole-CH_3), 1.55 (6H, s, pyrrole-CH_3), 1.45 (6H, s, pyrrole-CH_3).

^{13}C-NMR (300 MHz, $CDCl_3$) δ/ppm: 158.31, 148.00, 143.68, 142.87, 141.80, 140.45, 139.98, 137.44, 137.76, 136.54, 135.95, 132.44, 132.00, 129.81, 129.24, 127.81, 126.00, 124.44, 114.94, 113.15, 107.34, 105.25, 72.24, 69.41, 68.71, 67.77, 67.44, 59.3, 21.9, 19.3, 15.7, 13.8.

HRMS MALDI m/z ($C_{54}H_{62}N_4O_4Zn$): 896.4987 (calculated), 896.3345 (found).

6-Bibliography

(1)https://www.google.com/search?safe=strict&biw=1366&bih=625&tbm=isch&sxsrf==tumour+cells&gs_l=img.

(2) Passi, Aiom, A. *I*ntermedia, Ed.; 2018.

(3) Globacan.https://gco.iarc.fr/.

(4) AIRC https://www.iarc.fr/.

(5) worldometers.https://www.worldometers.info/it/.

(6) Mankoff, D. A. A Definition of Molecular Imaging. *J. Nucl. Med.* **2007**, *48* (6).

(7) Pysz, M. A.; Gambhir, S. S.; Willmann, J. K. Molecular Imaging: Current Status and Emerging Strategies. *Clin. Radiol.* **2010**, *65* (7), 500–516. https://doi.org/10.1016/j.crad.2010.03.011.

(8) Weissleder, R. Nbt0401_316. **2001**. https://doi.org/10.1038/86684.

(9) Alberti, C. From Molecular Imaging in Preclinical/Clinical Oncology to Theranostic Applications in Targeted Tumor Therapy. *Eur. Rev. Med. Pharmacol. Sci.* **2012**, *16* (14), 1925–1933.

(10) Kaplan, E.; Prashanth, A. K.; Brennan, C.; Sirovich, L. Optical Imaging: A Review. *Opt. Photonics News* **2000**, *11* (7), 26. https://doi.org/10.1364/opn.11.7.000026.

(11) S.L.Jacques, B.W. Pogue. Tutorial on Diffuse Light Transport. *J.Biomed.Opt.* **2008**, *13* (4).

(12)https://www.google.com/search?safe=strict&biw=1366&bih=625&tbm=isch&sxsrfuorescence+microscope++imaging+of+polmonar+arthery

(13) Policard A. Survey on the Aspects Offered by Experimental Tumors Examined in the Light of Wood. *C.R.Seances Soc.Biol.Fil.* **1924**, *91*, 1423–1424.

(14) Kosaka, N.; Ogawa, M.; Choyke, P. L.; Kobayashi, H. Clinical Implications of Near-Infrared Fluorescence Imaging in Cancer. *Futur. Oncol.* **2009**, *5* (9), 1501–1511. https://doi.org/10.2217/fon.09.109.

(15) Bernard Valeur. *Molecular Fluorescence: Principles and Applications*; 2001.

(16) Huang Z. A Review of Progress in Clinical Photodynamic Therapy. *Technol. Cancer Res* **2005**, *4* (3), 283–293.

(17) Calin, M. A.; Parasca, S. V. Photodynamic Therapy in Oncology. *J. Optoelectron. Adv. Mater.* **2006**, *8* (3), 1173–1179.

https://doi.org/10.1634/theoncologist.11-9-1034.

(18) Leblond, F.; Davis, S. C.; Valdés, P. A.; Pogue, B. W. Pre-Clinical Whole-Body Fluorescence Imaging: Review of Instruments, Methods and Applications. *J. Photochem. Photobiol. B Biol.* **2010**, *98* (1), 77–94. https://doi.org/10.1016/j.jphotobiol.2009.11.007.

(19) Ballou B., W. A. Fluorescence Imaging of Tumours in Vivo. *Curr. Med. Chem.* **2005**, *12* (7), 795–805.

(20) Yb, U. N.; Upconversion, E.; Wang, M.; Mi, C.; Wang, W.; Liu, C.; Wu, Y.; Xu, Z.; Mao, B.; Xu, S. Immunolabeling and NIR-Excited. *3* (6), 1580–1586.

(21) Plaetzer, K.; Krammer, B.; Berlanda, J.; Berr, F.; Kiesslich, T. Photophysics and Photochemistry of Photodynamic Therapy: Fundamental Aspects. *Lasers Med. Sci.* **2009**, *24* (2), 259–268. https://doi.org/10.1007/s10103-008-0539-1.

(22) Weissleder, R. N EWS AND V IEWS A Clearer Vision for in Vivo Imaging Progress Continues in the Development of Smaller , More Penetrable Probes for Biological Imaging . © 2001 Nature Publishing Group Http://Biotech.Nature.Com Toward the Phosphoproteome. **2001**.

(23) J. Swartling. Fluorescence Spectra Provide Information on the Depht of Fluorescent Lesions in Tissue. *Appl.Opt.* **2005**, *44* (10), 1934–1941.

(24) G.A. Wagnieres. In Vivo Fluorescence Spectroscopy and Imaging for Oncological Applications. *Photochem. Photobiol. Sci.* **1998**, *68* (5), 603–632.

(25) N. Billinton. Seeing the Wood through the Trees : A Review of Techniques for Distinguishing Green Fluorescent Protein from Endogenous Autofluorescence. *Anal.Biochem.* **2001**, *291*, 175–197.

(26) Hilderbrand, S. A.; Weissleder, R. Near-Infrared Fluorescence: Application to in Vivo Molecular Imaging. *Curr. Opin. Chem. Biol.* **2010**, *14* (1), 71–79. https://doi.org/10.1016/j.cbpa.2009.09.029.

(27) Ma, Q.; Su, X. Near-Infrared Quantum Dots: Synthesis, Functionalization and Analytical Applications. *Analyst* **2010**, *135* (8), 1867–1877. https://doi.org/10.1039/c0an00233j.

(28) Wang Y. Chen L. Quantum Dots, Lighting up the Research and Development of Nanomedicine. *Nanomed Nanoech Biol Med* **2011**.

(29) Janib SM. Imaging and Drug Delivery Theranostic Nanoparticles. *Adv Drug Deliv. Rev* **2010**, *62*, 152–1063.

(30) Liu, Y.; Song, N.; Li, Z.; Chen, L.; Xie, Z. Near-Infrared Nanoparticles Based on Aza-BDP for Photodynamic and Photothermal Therapy. *Dye. Pigment.* **2019**, *160* (May 2018), 71–78. https://doi.org/10.1016/j.dyepig.2018.07.034.

(31) Luo, S.; Zhang, E.; Su, Y.; Cheng, T.; Shi, C. A Review of NIR Dyes in Cancer Targeting and Imaging. *Biomaterials* **2011**, *32* (29), 7127–7138. https://doi.org/10.1016/j.biomaterials.2011.06.024.

(32) Mérian, J.; Gravier, J.; Navarro, F.; Texier, I. Fluorescent Nanoprobes Dedicated to in Vivo Imaging: From Preclinical Validations to Clinical Translation. *Molecules* **2012**, *17* (5), 5564–5591. https://doi.org/10.3390/molecules17055564.

(33) De Almeida, D. R. Q. *Quimica* **1999**, *73* (9).

(34) Williams D.J.*Angew.Chem.Int.Ed.Engl.* **1984**, *23* (690).

(35) Gomez-Hens, A. *Trends Anal.Chem.* **2004**, *23* (127).

(36) Patonay G., S. J. *Molecules* **2004**, *9* (40).

(37) Tung, C. H. *Biopolymers* **2004**, *76* (391).

(38) Goncalves, M. S. T. ChemInform Abstract: Fluorescent Labeling of Biomolecules with Organic Probes. *ChemInform* **2009**, *40* (19), 190–212. https://doi.org/10.1002/chin.200919277.

(39) Lavis L.D., R. R. T. Bright Ideas for Chemical Biology. *ACS Chem BIol* **2008**, *3* (3), 142–155.

(40) Gorecki T. Synthesis of Novel Near-Infrared Cyanine Dyes for Metal Ion Determination. *J.Heterocyclic Chem* **1996**, *33* (6), 1871–1876.

(41) Song.F., P. X. Synthesis, Spectral Properties and Photostabilities of Novel Water-Soluble near-Infrared Cyanine Dyes. *Photochem. Photobiol. Sci.* **2006**, *181* (1), 79–85.

(42) Zhou, Y. The Charge Transfer Mechanism and Spectral Properties of Near-Infrared Heptamethine Cyanine Dye in Alcoholic and Aprotic Solvents. *Photochem. Photobiol. Sci.* **2007**, *187* (2–3), 305–310.

(43) Braun, A. B.; Wehl, I.; Kölmel, D. K.; Schepers, U.; Bräse, S. New Polyfluorinated Cyanine Dyes for Selective NIR Staining of Mitochondria. *Chem. - A Eur. J.* **2019**, *25* (34), 7998–8002. https://doi.org/10.1002/chem.201900412.

(44) Oswald. Red Laser Induced Fluorescence Energy Transfer in Immunosystem.

Anal.Biochem. **2000**, *280* (2), 272–277.

(45) Gayathri Devi D. Squaraine: A Novel Candidate in Photodynamic Therapy for Skin Cancer Models in Vivo. *Photochem. Photobiol. Sci.* **2008**, *92* (3), 153–159.

(46) Dilek, G.; Akkaya, E. U. Novel Squaraine Signalling Zn(II) Ions: Three-State Fluorescence Response to a Single Input. *Tetrahedron Lett.* **2000**, *41* (19), 3721–3724. https://doi.org/10.1016/S0040-4039(00)00474-3.

(47) Lee, Heejin, M. J. C. Heptamine Cyanine Dyes with a Robus C-C Bond at the Central Position of the Chromophore. *Organometallics* **2006**, *71* (20), 7862–7865.

(48) Hilderbrand, S. A. Monofunctional Near-Infrared Fluorochromes for Imaging Applications. *Bioconjug. Chem.* **2005**, *165* (5), 1275–1281.

(49) Saxena V. Degradation Kinetics of Indocyanine Geen in Aqueous Solution. *Pharma Sci.* **2003**, *92* (10), 2090–2097.

(50) Suzuki K., C. D. Water-Soluble NIR Fluorescent Probes Based on Squaraine and Their Application for Protein Labelling. *Anal Sci* **2008**, *24* (2), 213–217.

(51) Nakazumi H., Ohta T., Etoh H. Near-Infrared Luminescent Bis-Squaraine Dyes Linked by a Tiophene or Pyrene Spacer for Noncovalent Protein Labelling. *Synth. Commun.* **2005**, *15* (1–3), 33–36.

(52) Gassensmith J:J:; Baumes J.M. Discovery and Early Development of Squaraine Rotaxanes. *Chem. Commun.* **2009**, *42*, 6329–6338.

(53) Chen Y, Liu X. High Performance Organic Field Effect Transistors Based on Amphiphilic Tris(Phtalocyaninato). *J. Am. Chem. Soc* **2005**, *127* (45), 15700–15701.

(54) De la Torre G., Torres T. Role of Structural Cactors in the Non Linear Optical Properties of Phtalocyanines and Related Compounds. *Chem. Rev.* **2004**, *4* (3), 283–293.

(55) Kralova J., Pouckova P. Novel Porphyrin Conjugates with a Potent Photodynamic Antitumor Effect: Differential Efficacy of Mono-and Bis-Beta Cyclodextrin Derivatives in Vitro and in Vivo. *Org. Biomol. Chem.* **2008**, *82* (2), 432–438.

(56) Tanaka Y., O. A. A Facile Synthesis of Large Mesopentafluorophenyl-Substituted Expanded Porphyrins. *European J. Org. Chem.* **2008**, *2008* (8),

1341–1349.

(57) Zhu, H.; Cheng, P.; Chen, P.; Pu, K. Recent Progress in the Development of Near-Infrared Organic Photothermal and Photodynamic Nanotherapeutics. *Biomater. Sci.* **2018**, *6* (4), 746–765. https://doi.org/10.1039/c7bm01210a.

(58) Dos Santos, A. F.; De Almeida, D. R. Q.; Terra, L. F.; Baptista, M. S.; Labriola, L. Photodynamic Therapy in Cancer Treatment - an Update Review. *J. Cancer Metastasis Treat.* **2019**, *2019*. https://doi.org/10.20517/2394-4722.2018.83.

(59) Pérez-Laguna, V.; Gilaberte, Y.; Millán-Lou, M. I.; Agut, M.; Nonell, S.; Rezusta, A.; Hamblin, M. R. A Combination of Photodynamic Therapy and Antimicrobial Compounds to Treat Skin and Mucosal Infections: A Systematic Review. *Photochem. Photobiol. Sci.* **2019**, *18* (5), 1020–1029. https://doi.org/10.1039/c8pp00534f.

(60) Treibs, A., Kreuzer, F.H. Lieb. *Liebigs Ann.Chem.* **1968**, *718* (203).

(61) Sakamoto, R.; Iwashima, T.; Kögel, J. F.; Kusaka, S.; Tsuchiya, M.; Kitagawa, Y.; Nishihara, H. Dissymmetric Bis(Dipyrrinato)Zinc(II) Complexes: Rich Variety and Bright Red to near-Infrared Luminescence with a Large Pseudo-Stokes Shift. *J. Am. Chem. Soc.* **2016**, *138* (17), 5666–5677. https://doi.org/10.1021/jacs.6b02128.

(62) Yu, M.; Wong, J. K. H.; Tang, C.; Turner, P.; Todd, M. H.; Rutledge, P. J. Efficient Deprotection of F-BODIPY Derivatives: Removal of BF2 Using Brønsted Acids. *Beilstein J. Org. Chem.* **2015**, *11* (Scheme 1), 37–41. https://doi.org/10.3762/bjoc.11.6.

(63) Xochitiotzi-Flores, E.; Islas-Mejía, A. A.; García-Ortega, H.; Romero-Ávila, M.; Mendez-Stivalet, J. M.; Carreón-Castro, M. D. P.; Santillan, R.; Maldonado-Domínguez, M.; Arcos-Ramos, R.; Farfán, N. On the Structure of Meso-Substituted F-BODIPYs and Their Assembly in Molecular Crystals: An Experimental-Theoretical Approach. *J. Organomet. Chem.* **2016**, *805*, 148–157. https://doi.org/10.1016/j.jorganchem.2016.01.021.

(64) Stoll, K. R.; Scholle, F.; Zhu, J.; Zhang, X.; Ghiladi, R. A. BODIPY-Embedded Electrospun Materials in Antimicrobial Photodynamic Inactivation. *Photochem. Photobiol. Sci.* **2019**. https://doi.org/10.1039/c9pp00103d.

(65) Ashokkumar, P.; Ashoka, A. H.; Collot, M.; Das, A.; Klymchenko, A. S. A Fluorogenic BODIPY Molecular Rotor as an Apoptosis Marker. *Chem.*

Commun. **2019**, *55* (48), 6902–6905. https://doi.org/10.1039/c9cc03242h.

(66) Awuah, S. G.; You, Y. Boron Dipyrromethene (BODIPY)-Based Photosensitizers for Photodynamic Therapy. *RSC Adv.* **2012**, *2* (30), 11169–11183. https://doi.org/10.1039/c2ra21404k.

(67) Li, L.; Nguyen, B.; Burgess, K. Functionalization of the 4,4-Difluoro-4-Bora-3a,4a-Diaza-s-Indacene (BODIPY) Core. *Bioorganic Med. Chem. Lett.* **2008**, *18* (10), 3112–3116. https://doi.org/10.1016/j.bmcl.2007.10.103.

(68) Grazon, C.; Si, Y.; Placial, J. P.; Rieger, J.; Méallet-Renault, R.; Clavier, G. Core-Shell Polymeric Nanoparticles Comprising BODIPY and Fluorescein as Ultra-Bright Ratiometric Fluorescent PH Sensors. *Photochem. Photobiol. Sci.* **2019**, *18* (5), 1156–1165. https://doi.org/10.1039/c8pp00457a.

(69) Tang, B.; Lv, F.; Chen, K.; Jiao, L.; Liu, Q.; Wang, H.; Hao, E. Development of BODIPY Dyes with Versatile Functional Groups at 3,5-Positions from Diacyl Peroxides via Cu(Ii)-Catalyzed Radical Alkylation. *Chem. Commun.* **2019**, *55* (32), 4691–4694. https://doi.org/10.1039/C9CC01602C.

(70) Zhang, X. X.; Wang, Z.; Yue, X.; Ma, Y.; Kiesewetter, D. O.; Chen, X. PH-Sensitive Fluorescent Dyes: Are They Really Ph-Sensitive in Cells? *Mol. Pharm.* **2013**, *10* (5), 1910–1917. https://doi.org/10.1021/mp3006903.

(71) Zhu, J.; Zou, J.; Zhang, J.; Sun, Y.; Dong, X.; Zhang, Q. An Anthracene Functionalized BODIPY Derivative with Singlet Oxygen Storage Ability for Photothermal and Continuous Photodynamic Synergistic Therapy. *J. Mater. Chem. B* **2019**, *7* (20), 3303–3309. https://doi.org/10.1039/c9tb00180h.

(72) Donoru VR, Zhu S. Near-Infrared Emissive BODIPY Polymeric and Copolymeric Dyes. *Polym. Chem.* **2010**, *51* (23), 5359–5368.

(73) Loudet, A. Bodipy Dyes and Their Derivatives: Syntheses and Spectroscopic Properties. *Chem. Rev.* **2007**, *107* (11), 4891–4932.

(74) Rurack K. A Highly Efficient Sensor Molecule Emitting in the Near-Infrared. *New J. Chem.* **2001**, *25* (2), 289–292.

(75) Burgess, Kevin, Burghart A. BODIPY Dyes: Synthesis, Spectroscopic, Electrochemical and Structural Properties. *J. Org. Chem.* **1999**, *64* (21), 7813–7819.

(76) Fischer, V. H.; Halbig, P. Ober Eine Neue Porphyrinsynthese, Oxydation von Porphyrinen. **1927**, *183* (1926).

(77) Dixon H.B., Liebecq C. No Title. *Pure Appl. Chem.* **1987**, *59* (779).

(78) Wood, T. E.; Thompson, A. Advances in the Chemistry of Dipyrrins and Their Complexes. *Chem. Rev.* **2007**, *107* (5), 1831–1861. https://doi.org/10.1021/cr050052c.

(79) Corwin A.H. *J. Am. Chem. Soc* **1955**, *53*, 5847.

(80) Motekaitis R.J. *Inorg. Chem.* **1970**, *9*, 1832.

(81) Muramaki Y., Sakata K., M. Y. *Bull.Chem.Soc.Jpn.* **1974**, *47*, 3021.

(82) Muramaki Y., Sakata K., M. Y. *Bull.Chem.Soc.Jpn.* **1974**, *47*, 458.

(83) Muramaki Y., Sakata K., M. Y. M. A. E. *Chem. Soc.Dalton.Trans.* **1973**, 1729.

(84) Johnson A.W. *J.Chem.Soc.* **1959**, 3416.

(85) Do L., Halper S. *Chem. Commun.* **2004**, 2662.

(86) Muramaki Y., Sakata K., M. Y. *Inorg. Chem.* **1971**, *10*, 1734.

(87) Porter C.R. *Chem.Soc.* **1938**, 368.

(88) Bruckner C., Rettig S.J. *Can. J. Chem.* **1996**, *74*, 2182.

(89) Yu, L.; Muthukumaran, K.; Sazanovich, I. V.; Kirmaier, C.; Hindin, E.; Diers, J. R.; Boyle, P. D.; Bocian, D. F.; Holten, D.; Lindsey, J. S. Excited-State Energy-Transfer Dynamics in Self-Assembled Triads Composed of Two Porphyrins and an Intervening Bis(Dipyrrinato)Metal Complex. *Inorg. Chem.* **2003**, *42* (21), 6629–6647. https://doi.org/10.1021/ic034559m.

(90) Lebedeva N.S., A. E.*Zh.Fiz.Khim.* **2000**, No. 74, 1165.

(91) Hill C.L., W. M. *Chem. Commun.* **1985**, No. 17, 1228.

(92) Fischer H., H. P. *Justus Liebigs Ann.Chem.* **1927**, No. 452, 268.

(93) Malachowski M.R. *Inorg. Chem.* **2004**, *43*, 1242.

(94) Bruniings K.J. *J. Am. Chem. Soc* **1944**, No. 66, 337.

(95) Halper S.R., C. S. *Angew. Chemie - Int. Ed.* **2004**, *43*, 2385.

(96) Jauma A., F. J. A. *Monatsch.Chem.* **1996**, *127*, 927.

(97) Guseva G.B., A. E. V. *Russ.J.Gen.Chem.* **2006**, *32*, 116.

(98) Lee, S.; Seok, C. H.; Park, Y.; Park, J. Synthesis and Electrochemical Properties of Bis(Dipyrrinato)Zinc Complex Derivatives. *Curr. Appl. Phys.* **2010**, *10* (4 SUPPL.), e131–e134. https://doi.org/10.1016/j.cap.2010.08.024.

(99) Lindsey J.S., S. I. V. No Title. *J. Am. Chem. Soc* **2004**, *126*, 2664.

(100) Sakamoto, R.; Iwashima, T.; Tsuchiya, M.; Toyoda, R.; Matsuoka, R.; Kögel, J. F.; Kusaka, S.; Hoshiko, K.; Yagi, T.; Nagayama, T.; et al. New Aspects in Bis

and Tris(Dipyrrinato)Metal Complexes: Bright Luminescence, Self-Assembled Nanoarchitectures, and Materials Applications. *J. Mater. Chem. A* **2015**, *3* (30), 15357–15371. https://doi.org/10.1039/c5ta02040a.

(101) Zander M. *Chem. Phys. Lett.* **1984**, *110* (602).

(102) Kang T.J. *Phys Chem.* **1988**, *92* (6800).

(103) Vauthey E. *Chem. Phys. Chem* **2012**, *13* (2001).

(104) Ge, Y.; O'Shea, D. F. Azadipyrromethenes: From Traditional Dye Chemistry to Leading Edge Applications. *Chem. Soc. Rev.* **2016**, *45* (14), 3846–3864. https://doi.org/10.1039/c6cs00200e.

(105) Tian, X.; Hussain, S.; de Pace, C.; Ruiz-Pérez, L.; Battaglia, G. Zn II Complexes for Bioimaging and Correlated Applications. *Chem. - An Asian J.* **2019**, *14* (4), 509–526. https://doi.org/10.1002/asia.201801437.

(106) Tungulin, D.; Leier, J.; Carter, A. B.; Powell, A. K.; Albuquerque, R. Q.; Unterreiner, A. N.; Bizzarri, C. Chasing BODIPY: Enhancement of Luminescence in Homoleptic Bis(Dipyrrinato) Zn II Complexes Utilizing Symmetric and Unsymmetrical Dipyrrins. *Chem. - A Eur. J.* **2019**, *25* (15), 3816–3827. https://doi.org/10.1002/chem.201806330.

(107) Verena Honn. Reseach Internship, 2018.

(108) Cucinotta, F.; Jarman, B. P.; Caplan, C.; Cooper, S. J.; Riggs, H. J.; Martinelli, J.; Djanashvili, K.; La Mazza, E.; Puntoriero, F. Light-Harvesting Antennae Using the Host-Guest Chemistry of Mesoporous Organosilica. *ChemPhotoChem* **2018**, *2* (3), 196–206. https://doi.org/10.1002/cptc.201700144.

(109) Arsenault, G. P.; Bullock, E.; MacDonald, S. F. Pyrromethanes and Porphyrins Therefrom. *J. Am. Chem. Soc.* **1960**, *82* (16), 4384–4389. https://doi.org/10.1021/ja01501a066.

(110) Dehaen, W.; Rohand, T.; Dolusic, E.; Ngo, T.; Maes, W. Efficient Synthesis of Aryldipyrromethanes in Water and Their Application in the Synthesis of Corroles and Dipyrromethenes. *Arkivoc* **2007**, *2007* (10), 307–324.

(111) Trinh, C.; Kirlikovali, K.; Das, S.; Ener, M. E.; Gray, H. B.; Djurovich, P.; Bradforth, S. E.; Thompson, M. E. Symmetry-Breaking Charge Transfer of Visible Light Absorbing Systems: Zinc Dipyrrins. *J. Phys. Chem. C* **2014**, *118* (38), 21834–21845. https://doi.org/10.1021/jp506855t.

(112) Ueura, K.; Satoh, T.; Miura, M. An Efficient Waste-Free Oxidative Coupling via Regioselective C-H Bond Cleavage: Rh/Cu-Catalyzed Reaction of Benzoic Acids with Alkynes and Acrylates under Air. *Org. Lett.* **2007**, *9* (7), 1407–1409. https://doi.org/10.1021/ol070406h.

(113) Tsuchiya, M.; Sakamoto, R.; Kusaka, S.; Kitagawa, Y.; Okumura, M.; Nishihara, H. Asymmetric Dinuclear Bis(Dipyrrinato)Zinc(Ii) Complexes: Broad Absorption and Unidirectional Quantitative Exciton Transmission. *Chem. Commun.* **2014**, *50* (44), 5881–5883. https://doi.org/10.1039/c4cc01573h.

(114) Tietze, L. F.; Brasche, G.; Gericke, K. M. Domino Reactions in Organic Synthesis. *Domino React. Org. Synth.* **2006**, 1–617. https://doi.org/10.1002/9783527609925.

(115) Khare, R.; Pandey, J.; Smriti, S.; Ruchi, R. The Importance and Applications of Knoevenagel Reaction (Brief Review). *Orient. J. Chem.* **2019**, *35* (1), 423–429. https://doi.org/10.13005/ojc/350154.

(116) Webster, G. K.; Bell, R. G.; Jackson, J. D. Poorly Soluble Drugs. *Poorly Soluble Drugs* **2017**, *6* (11). https://doi.org/10.1201/9781315364537.

(117) Dalessandro, E. V.; Collin, H. P.; Guimarães, L. G. L.; Valle, M. S.; Pliego, J. R. Mechanism of the Piperidine-Catalyzed Knoevenagel Condensation Reaction in Methanol: The Role of Iminium and Enolate Ions. *J. Phys. Chem. B* **2017**, *121* (20), 5300–5307. https://doi.org/10.1021/acs.jpcb.7b03191.

(118) Barder, T. E.; Walker, S. D.; Martinelli, J. R.; Buchwald, S. L. Catalysts for Suzuki-Miyaura Coupling Processes: Scope and Studies of the Effect of Ligand Structure. *J. Am. Chem. Soc.* **2005**, *127* (13), 4685–4696. https://doi.org/10.1021/ja042491j.

(119) Miyaura, N.; Suzuki, A. Palladium-Catalyzed Cross-Coupling Reactions of Organoboron Compounds. *Chem. Rev.* **1995**, *95* (7), 2457–2483. https://doi.org/10.1021/cr00039a007.

(120) Kumar, S.; Rao, G. K.; Kumar, A.; Singh, M. P.; Saleem, F.; Singh, A. K. Efficient Catalytic Activation of Suzuki-Miyaura C-C Coupling Reactions with Recyclable Palladium Nanoparticles Tailored with Sterically Demanding Di-n-Alkyl Sulfides. *RSC Adv.* **2015**, *5* (26), 20081–20089. https://doi.org/10.1039/c5ra00441a.

(121) Akira Suzuki. Recent Advances in the Cross-Coupling Reactions of

Organoboron Derivatives with Organic Electrophiles. *J. Organomet. Chem.* **1998**, *576*, 147–168. https://doi.org/S0022-328X(98)01055-9.

(122) Littke, A. F.; Dai, C.; Fu, G. C. Versatile Catalysts for the Suzuki Cross-Coupling of Arylboronic Acids with Aryl and Vinyl Halides and Triflates under Mild Conditions. *J. Am. Chem. Soc.* **2000**, *122* (17), 4020–4028. https://doi.org/10.1021/ja0002058.

(123) Penttala, V.; Al-Neshawy, F. Stress and Strain State of Concrete during Freezing and Thawing Cycles. *Cem. Concr. Res.* **2002**, *32* (9), 1407–1420. https://doi.org/10.1016/S0008-8846(02)00785-8.

(124) Agalave, S. G.; Maujan, S. R.; Pore, V. S. Click Chemistry: 1,2,3-Triazoles as Pharmacophores. *Chem. - An Asian J.* **2011**, *6* (10), 2696–2718. https://doi.org/10.1002/asia.201100432.

(125) Alvarez, R.; Velázquez, S.; San-Félix, A.; Aquaro, S.; De Clercq, E.; Perno, C. F.; Karlsson, A.; Balzarini, J.; Camarasa, M. J. 1,2,3-Triazole–[2′,5′-Bis-O-(Tert-Butyldimethylsilyl)-β-D-Ribofuranosyl]-3′-Spiro-5″-(4″-Amino-1″,2″-Oxathiole 2″,2″-Dioxide) (TSAO) Analogs: Synthesis and Anti-HIV-1 Activity. *J. Med. Chem.* **1994**, *37* (24), 4185–4194. https://doi.org/10.1021/jm00050a015.

(126) Flaxbart, D. Comprehensive Heterocyclic Chemistry II: A Review of the Literature 1982−1995. 12 Volume Set Editors-in-Chief: Alan R. Katritzky, Charles W. Rees, and Eric, F. V. Scriven. Elsevier (Pergamon): Oxford. 1997. 11 856 Pp. $6345.00. ISBN 0-08-042072-9. *J. Am. Chem. Soc.* **1997**, *119* (38), 9086–9086. https://doi.org/10.1021/ja975563y.

(127) Haldón, E.; Nicasio, M. C.; Pérez, P. J. Copper-Catalysed Azide-Alkyne Cycloadditions (CuAAC): An Update. *Org. Biomol. Chem.* **2015**, *13* (37), 9528–9550. https://doi.org/10.1039/c5ob01457c.

(128) Liang, L.; Astruc, D. The Copper(I)-Catalyzed Alkyne-Azide Cycloaddition (CuAAC) “Click” Reaction and Its Applications. An Overview. *Coord. Chem. Rev.* **2011**, *255* (23–24), 2933–2945. https://doi.org/10.1016/j.ccr.2011.06.028.

(129) Johansson, J. R.; Beke-Somfai, T.; Said Stålsmeden, A.; Kann, N. Ruthenium-Catalyzed Azide Alkyne Cycloaddition Reaction: Scope, Mechanism, and Applications. *Chem. Rev.* **2016**, *116* (23), 14726–14768. https://doi.org/10.1021/acs.chemrev.6b00466.

(130) Yamamoto, Y. Synthesis of Heterocycles via Transition-Metal-Catalyzed

Hydroarylation of Alkynes. *Chem. Soc. Rev.* **2014**, *43* (5), 1575–1600. https://doi.org/10.1039/c3cs60369e.

(131) Lee, H.; Lee, J. K.; Min, S. J.; Seo, H.; Lee, Y.; Rhee, H. Copper(I)-Catalyzed Synthesis of 1,4-Disubstituted 1,2,3-Triazoles from Azidoformates and Aryl Terminal Alkynes. *J. Org. Chem.* **2018**, *83* (8), 4805–4811. https://doi.org/10.1021/acs.joc.8b00022.

(132) Weusmann, J.; Mahmoodi, B.; Kordsmeyer, K.; Azaripour, A.; Walter, C.; Willershausen, B. Die Zahnärztliche Selektive Intensivprophylaxe in Rheinland-Pfalz: Untersuchungen an Erstklässlern Im Schuljahr 2013/2014. *Gesundheitswesen* **2017**, *79* (4), 247–251. https://doi.org/10.1055/s-0042-108582.

(133) Chinchilla, R.; Nájera, C. The Sonogashira Reaction: A Booming Methodology in Synthetic Organic Chemistry. *Chem. Rev.* **2007**, *107* (3), 874–922. https://doi.org/10.1021/cr050992x.

(134) Kusaka, S.; Sakamoto, R.; Kitagawa, Y.; Okumura, M.; Nishihara, H. An Extremely Bright Heteroleptic Bis(Dipyrrinato)Zinc(II) Complex. *Chem. - An Asian J.* **2012**, *7* (5), 907–910. https://doi.org/10.1002/asia.201200131.

(135) Tungulin, D. Research Internship, 2017.

(136) Sazanovich, I. V.; Kirmaier, C.; Hindin, E.; Yu, L.; Bocian, D. F.; Lindsey, J. S.; Holten, D. Structural Control of the Excited-State Dynamics of Bis(Dipyrrinato)Zinc Complexes: Self-Assembling Chromophores for Light-Harvesting Architectures. *J. Am. Chem. Soc.* **2004**, *126* (9), 2664–2665. https://doi.org/10.1021/ja038763k.

(137) Aslantürk, Ö. S. In Vitro Cytotoxicity and Cell Viability Assays: Principles, Advantages, and Disadvantages. *Genotoxicity - A Predict. Risk to Our Actual World* **2018**. https://doi.org/10.5772/intechopen.71923.

(138) Vistica, D. T.; Monks, A.; Pittman, A.; Boyd, M. R. Tetrazolium-Based Assays for Cellular Viability: A Critical Examination of Selected Parameters Affecting Formazan Production. *Cancer Res.* **1991**, *51* (10), 2515–2520.

(139) Tim Mossmann. Rapid Colorimetric Assay for Cellular Growth and Survival: Application to Proliferation and Cytotoxicity Assays. *J. Immunol. Methods* **1983**, *65*, 55–63.

(140) https://en.wikipedia.org/wiki/HeLa#/media/File:HeLa-III.jpg.

(141) Scudiero D.A., S. R. H. Evaluation of a Soluble Tetrazolium/Formazan Assay for Cell Growth and Drug Sensitivity in Culture Using Human and Other Tumour Cell Lines. *Cancer Res.* **1988**.

(142) Ishiyama M., Shiga M. A New Sulfonated Tetrazolium Salt That Produces a Highly Water-Soluble Formazan Dye. *Chem. Pharm. Bullettin* **1993**.

(143) Sakamoto K., T. H. A Water Soluble Tetrazolium Salt Useful for Colorimetric Cell Viability Assay. *Anal. Commun.* **1999**.

(144) Fotakis G., T. J. A. In Vitro Cytotoxicity Assays. *Toxicol. Lett.* **2006**.

(145) Repetto G., Z. J. L. A Simple Quantitative Procedure Using Monolayer Cultures for Cytotoxicuty. *Nat. Protoc.* **2008**.

(146) Borenfreud E., P. J. A. A Simple Quantitative Procedure Using Monolayer Cultures for Cytotocity Assays. *1984*.

(147) Thom S., H. R. Factors Affecting the Selection and Use of Tetrazolium Salts as Cytochemical Indicators of Microbial Viability and Activity. *J. Appl. Bacteriol* **1993**.

(148) Garn H., E. V. An Improved MTT Assay Using the Electron-Coupling Agent Menadione. *J. Immunol. Methods* **1994**.

(149) Berridge MV. Characterization of the Cellular Reduction of 3-(4,5-Dimethylthiazol-2-Yl)-2,5--Diphenyltetrazolium Bromide (MTT): Subcellular Localization. *Arch Biochem Biophys* **1993**.

(150) Berridge MV. Tetrazolium Dyes as Tools in Cell Biology: New Insights into Their Cellular Reduction. *Biotechnol Annu Rev* **2005**.

(151) https://abcnews.go.com/WN/womans-cells-changed-medicine/story?id=9712579.

(152) https://www.theguardian.com/world/2010/apr/04/henrietta-lacks-cancer-cells.

(153) https://www.microscopemaster.com/hela-cells.html.

(154) Fulmer, G. R.; Miller, A. J. M.; Sherden, N. H.; Gottlieb, H. E.; Nudelman, A.; Stoltz, B. M.; Bercaw, J. E.; Goldberg, K. I. NMR Chemical Shifts of Trace Impurities: Common Laboratory Solvents, Organics, and Gases in Deuterated Solvents Relevant to the Organometallic Chemist. *Organometallics* **2010**, *29* (9), 2176–2179. https://doi.org/10.1021/om100106e.